LARGE SCALE RESPONSE OF THE OCEAN TO SEA ICE FORMATION

by

Harold Solomon

B.S., Massachusetts Institute of Technology

(1963)

Submitted in partial fulfillment

of the requirement for the

Degree of Doctor of Philosophy

at the

MASSACHUSETTS INSTITUTE OF TECHNOLOGY

July 18, 1969

Signature of Author .....
Department of Meteorology, July 18, 1969

Certified by _____
Thesis Supervisor

Accepted by .....
Chairman, Departmental Committee on
Graduate Students

LARGE-SCALE RESPONSE OF THE OCEAN TO SEA ICE FORMATION

by

Harold Solomon

Submitted to the Department of Meteorology on 18 July 1969 in partial fulfillment of the requirement for the degree of Doctor of Philosophy.

ABSTRACT

When sea ice forms, salt is released by the freezing process, increasing the density of the water immediately under the ice. On the micro-scale, this produces unstable Rayleigh convection, but on the scale of oceanic circulations the effect of the local convection is to increase the density of the surface mixed layer, which appears to be uniform in Z and smoothly varying in X and t on this scale. Cooling and evaporation have the same effect, but the present study is limited to the case of ice formation.

There are many ways in which the effect of local mixing can be parameterized in the study of large-scale circulations. Two of the more important methods are considered here. The traditional method, published by Zubov and Defant, reduces the potential energy of a water column to the minimum that is consistent with the assumption of a surface mixed layer on top of an otherwise unchanged profile. The second method considered here, based on the work of Ball, and of Kraus and Turner, assumes that entrainment by penetrative convection conserves the potential energy and produces a very steep halocline below the mixed layer. The latter method gives results that are more consistent with oceanic data including data on the salinity of the mixed layer from Arctic drift stations and steep pycnoclines observed on S.T.D. profiles taken in the North Pacific Ocean in winter.

When ice forms on an ocean at a rate that varies horizontally, a large-scale density gradient is set up, producing a circulation. It is shown by the solution of both two-layer and continuously stratified numerical models that this circulation is always

weak; its vertical and ageostrophic components are strongly constrained by rotation. The motion is of little oceanographical importance. In particular, the outflow of bottom water from the Weddell Sea in winter cannot be driven by the seasonal formation of ice at the surface in a Hadley-type circulation (this does not mean that the bottom water cannot acquire its characteristic properties as a result of local convection).

The dynamical models presented here represent the first attempt to include a well-mixed layer in a numerical model. The mixing tends to generate spurious numerical oscillations in the continuously stratified model, in which the equations of motion must be used in their nongeostrophic form. A serious attempt to eliminate these oscillations is beyond the scope of the present work. The conclusions from this model are based on time-averaged, rather than instantaneous, velocites.

Thesis Supervisor: Norman A. Phillips
Professor of Meteorology

TABLE OF CONTENTS

Chapter 1

INTRODUCTION

A one to two meter thick layer of ice freezes and melts annually over the Arctic and Antarctic Oceans and subpolar seas such as the Bering Sea, Sea of Okhotsk, Greenland-Norwegian Sea and Baltic Sea. The consequences of this melting and freezing for the salinity distribution and haline circulation in the ocean are considerable but have received little theoretical attention. The effect of potentially greatest global importance is in the Weddell Sea of the Antarctic, where, according to one theory (Mosby, 1934), unstable convection due to the release of salt by freezing is believed to reach to the bottom and to be responsible for the renewal of most of the bottom water of the world's oceans. Approximately the same thickness of ice is formed in the polar and subpolar seas of the Northern Hemisphere, but the convection does not always reach to the bottom. In particular, in the deep central part of the Arctic Ocean the mixed layer is confined to the upper 50 to 100 meters, and it is believed that another explanation must be found for the renewal of Arctic bottom water (Kusunoki, 1962).

Surface cooling and heating, or for that matter rain and evaporation, produce effects which are similar to those of the freezing and melting of ice, except for a few specialized phenomena such as cabballing (the name of the process discussed by Fofonoff, 1956) which are not treated in the present work. One process had to be selected for the sake of definiteness. The freezing of ice was

chosen for several reasons. This work was originally motivated by an interest in the Arctic Ocean, so the freezing process seemed to be the most natural one to consider. More can be said about the nature of the mixing process because of the data available from Arctic drift stations, which move very slowly compared to boats. Heavy weather, and sometimes icebergs and scattered drift ice, make operation difficult in the regions of strongest cooling over open, or relatively open, water. The ocean is nearly isothermal in ice-covered regions, so that to a good approximation density is a function of only one variable. There is one disadvantage to the choice of freezing; the dynamical effects of the relative horizontal incompressibility of sea ice must be considered.

The melting of ice provides a source of low-density water at the top surface, leading to a very stable stratification, while the freezing process releases salt into the water, producing unstable stratification which causes a well-mixed surface layer to form. The difference between the two processes is so great that it is appropriate to treat them separately, at least until both are well-understood. Only the freezing process is considered in the present work primarily because the associated mixing process is easier to treat. Because the two processes are so different, it is likely that a mean nonzero steady state haline circulation is driven by the yearly cycle of melting and freezing. For the reader who is interested in pursuing the melting problem further, it is suggested that work on the seasonal thermocline (Turner and Kraus, 1967; Kraus and Turner, 1967) has some relevance to the local mixing process,

while the similarity analysis of the thermohaline circulation in the Red Sea by O. Phillips (1966) is one possible approach to the treatment of the dynamics.

When ice freezes on salt water, the salt is excluded from the crystal structure of the ice. Some of it will remain in the liquid water; some will be trapped within the ice in brine pockets. Varying amounts of brine may be trapped, depending on the salinity of the water and the rate of ice formation; an increase in either or both will increase the amount of salt that is trapped in the brine pockets. If the ice, including brine pockets, is melted, the water that is obtained will have a certain salinity, called the "salinity of the ice". The salinity of the ice is always less than the salinity of the water from which the ice formed. In sea water of about 30‰ it may vary from 3‰ to 25‰, depending on growth rate and other parameters (Untersteiner, 1968). The brine that remains in the ice gradually drains out into the water below by several processes discussed by Untersteiner (1968). Drinkable water has been obtained by melting ice from the top of a floe that is several years old. The study of sea ice is a complex field in itself; many aspects of it are covered in the book by Zubov (1944).

The present work will be restricted to the study of convection underneath ice which forms in water having an initial salinity greater than 24.7‰. In this range, the density of water increases monotonically as the temperature is decreased to the freezing point. The resulting unstable convection makes the water nearly isothermal for some distance below the ice when freezing starts.

When ice is formed on open water, the brine is released onto the top of a well-mixed isopycnal layer. Underneath perennial ice which has just completed the melting part of a yearly cycle, there may be some salinity stratification, but the really fresh water is confined to open leads above the level of the bottoms of adjacent floes (Little, personal communication, 1967), and quickly becomes saline (probably due to wind mixing) at the beginning of the Arctic winter. For our present purposes we can assume that the brine enters the liquid ocean on top of a layer which is isopycnal or nearly so, especially compared to the difference in density between the brine and the sea water that has not been modified by freezing.

The brine is then in a gravitationally unstable position, and mixes with the water below through Rayleigh convection. The micro-scale convection through which the brine initially mixes into the sea water is treated by Foster (1968). He finds that the mixing at the smallest scale, on which molecular coefficients of viscosity and diffusivity are appropriate, has a length scale of less than 1 centimeter and a time scale of a few (less than 5) minutes. This mixing produces a new instability, which mixes on a larger scale, with eddy mixing predominating. This mixing has a length scale on the order of tens of centimeters and a time scale between 5 and 10 minutes. Foster speculates that a heirarchy of larger and larger eddies may be formed in this way until the mixing is limited by the stratification of sea water. Other workers have suggested that the predominant scale of convection is determined by narrow open leads. This would imply length scales of tens, or at most hundreds, of meters. Stewart (1963) suggested that radiation pressure from wind

waves formed on open leads causes downward motion under the floes, with compensating upward motion under the leads. Coachman (1967) suggested that the downward motion is strongest under the leads because freezing is most rapid where the water is exposed directly to the cold air, expecially when the air temperature is well below zero. All of these proposals are speculation at this stage; much more experimental and observational work is needed to describe the convection adequately.

In the present work we are interested in length scales on the order of hundreds of kilometers, and time scales on the order of tens or hundreds of days. It obviously does not make sense to try to describe the micro-scale convection. All studies which have dealt with the time development of temperature, salinity and density profiles in regions of unstable surface convection in the real ocean have simply assumed the surface layer to be thoroughly mixed in the vertical, down to the depth where significant changes unrelated to the structure of convective cells or transient instabilities are first encountered. Practical forecasting of the onset of ice formation in the Arctic Ocean is carried out with this type of model (see, for example, Bulgakov, 1962). This practice will be followed here. The freezing of ice will be assumed to have the sole effect of instantaneously changing the salinity profile in a column directly beneath the point of freezing and extending to the bottom of the mixed layer. The profile may change in accordance with any one of a number of theories, which will be discussed in Chapter 2. It is further assumed that freezing takes place at a rate that is constant

in time and varies smoothly and gradually in space. This is the simplest possible assumption; available data does not warrant the introduction of further complications at this time.

This work deals not only with the effect of ice formation on the ocean due to local mixing, but also with the large-scale dynamical consequences of horizontal variations in the rate of freezing. The motion produced in this case contains both barotropic and baroclinic components. The barotropic mode is of some interest in connection with variations in sea level. The baroclinic modes contain vertical circulations that are potentially of major oceanographical importance on a variety of scales ranging from the renewal of bottom water in the largest oceans to density-driven outflow from smaller seas and bays.

The regions of strongest cooling and ice formation are usually presumed to be sinking regions in the ocean. The circulation in these regions is often thought of as being something like the cold end of a simple Hadley cell, with the large-scale sinking caused directly by the surface cooling. The theory of such a circulation is treated by Stommel (1962) and Stone (1968). Stommel predicts relatively small sinking regions, which agrees qualitatively with reality. According to Stone, the large-scale dynamics requires vertical velocities and horizontal diffusion to become large in a corner region where cooling is strongest. However, he does not find that sinking is confined to this region; he attributes the difference between his results and Stommel's to different boundary conditions.

There is little doubt that strong cooling and ice formation do tend to produce convective sinking. However, it is dangerous to

extend intuition gained from experience with laboratory models to large-scale circulations. The predominant scale of convection is generally small compared to the scale of interest. The large-scale motion is not necessarily a scaled-up replica of the smaller convective cells; it may have an entirely different character. In addition, rotation, stratification and the smallness of the aspect ratio all become important in large-scale problems. The danger of approaching a large-scale circulation as a simple analogue of micro-scale systems has been demonstrated by the experience of several workers with hurricane models, as summarized by Ooyama (1963a, 1963b, 1967). In early attempts to model hurricane dynamics numerically, the procedure used was to simply solve the Navier-Stokes equations, with coefficients of eddy (rather than molecular) viscosity in the frictional terms, with heat released by condensation of water vapor. The result was essentially a hurricane-sized cumulonimbus cloud, which grew in a matter of hours - a reasonable time scale for a cumulonimbus cloud, but a hurricane takes several days to develop. Ooyama (and others) recognized the problem as one of allowing for the fact that cumulus convection takes place in many small cells, and proceeded to formulate a model in which he parameterized the effect of the convection on the large-scale motion, rather than solving the equations for the convective motion explicitly. The result was substantially more reasonable than the earlier models. The reader is referred to Ooyama's papers for details.

A similar approach will be followed here. The equations will not simply be solved for a large-scale convective cell. Instead,

the effect of the small-scale convection on the large-scale motion is parameterized, in this case by incorporating a well-mixed surface layer into the model. The direct effect of the freezing is to produce an instantaneous change through the whole depth of the mixed layer. The macro-scale fields then adjust dynamically to the changed density distribution in the mixed layer. No salt flux is imposed on the large-scale equations; all they see is the instantaneous change in the mixed layer. No dramatic observational evidence analogous to the development time or other general features of a hurricane is available as yet to prove the correctness of this type of modelling in the case of the ocean. However, the existence of the mixed layer, which incidentally is not predicted by any of the Hadley-type convective models, is a well-known reality. It is reasonable to suppose that a dynamical model which incorporates this feature will give a more accurate picture of the large-scale circulation than one which does not.

Oceanographical Motivation for this Work

None of the models to be worked out here is meant to faithfully reproduce any specific situation in the ocean. Even the local mixing model, which is realistic enough to use actual data, is incomplete in several important respects. However, the ultimate motivation for these models is oceanographic, and the results do have a significant bearing on some oceanographic problems. A description of the specific oceanographic problems which serve as motivation is presented here.

1) The local time development of the mixed layer in regions of unstable density convection at the surface. Results obtained in the Arctic Ocean by Fujino (1967) indicate that the salt content of the mixed layer increases more in a season than can be explained by local ice formation. S.T.D. traces obtained by Reid (Scripps Institution of Oceanography, 1966) in the North Pacific Ocean show that there is often, although not always, a very sharp interface at the bottom of the mixed layer. We will see in Chapter 2 that these observations cannot be explained by the convection model of Zubov (1944) and Defant (1949), which has been in general use since its publication. It will be shown that a model incorporating turbulent entrainment, while still incomplete, provides a better fit to the observations.

2) The formation of bottom water through wintertime convection in the Antarctic. A good review of the descriptive features of the region and the proposed mechanism of bottom water formation is provided by Deacon (1963). Bottom water spreads northward into all three major ocean basins from all around the Antarctic Continent. This bottom water covers most of the deep ocean floor, and has been traced well north of the Equator. It is generally accepted that this water forms mainly in the southwestern part of the Weddell Sea, then spreads slowly and irregularly around Antarctica. According to Brennecke (1921) and Mosby (1934), seasonal convection produced by ice formation reaches the bottom of the continental shelf in late winter. Further convection produces an increase in density which causes this water to flow down the continental slope. As explained

by Deacon (1963), the effect of this convecting shelf water is to cool the warm (2°C) deep water, which already has a high salinity, in the deep part of the Weddell Sea. Cooling causes this water to become dense enough so that it forms a mixture with the shelf water that, according to Fofonoff (1956), is denser than either of its components, due to the nonlinear dependence of density on temperature and salinity. This dense mixture becomes the Antarctic bottom water. It has also been suggested (as reported by Foster, 1968) that perhaps thin filaments of salt reach to the bottom. In spite of the subtle differences in emphasis, a consistent theme runs through these hypotheses. This is that because the Antarctic is a region of strong cooling, water becomes denser there and flows out along the bottom. While the complexity of this problem makes it impossible to treat in its full generality here, one aspect of it can be understood from the results of the continuously stratified dynamical model. The magnitude of the circulation that develops will show clearly that the seasonal convection due to ice formation cannot by itself cause the outflow of the necessary quantity of bottom water; this says nothing about the formation of water with the desired characteristics. The significance of this result for the real ocean will be discussed in Chapter 4.

For completeness, it must be noted that other mechanisms for bottom water formation have been proposed. According to Arnold Gordon (personal communication, 1969) there are at least two other mechanisms by which significant amounts of bottom water formation takes place. Ice formation at the bottom of deep ice shelves is

relatively unaffected by seasonal climatic variations and produces bottom water all year. Very cold katabatic winds off of the Antarctic continent produce bottom water through intense cooling and evaporation in some regions, such as that off of the Adelie Coast south of Australia, which remain relatively ice-free in winter. V.G. Ledenyov (1966) reported evidence that bottom water forms all year in the interwater convergence zone all around the continent of Antarctica. However, according to Gordon, the best indications still point to the Weddell Sea as the most important source of Antarctic bottom water.

3) The seasonal oscillation in sea level. It has been shown for most oceans by Pattullo, Munk, Revelle and Strong (1955) and for the Arctic Ocean by Gudkovich (1962) and Beal (1968) that there is a seasonal component of the variations in sea level which can often, although not always, be explained with considerable accuracy by the seasonal variation in density of the water, with a small correction for the effect of atmospheric pressure changes. In a non-rotating system the variations in sea level would tend to equalize through long gravity waves. The two-layer dynamical model will help to determine the role of the geostrophic constraint in maintening differences in sea level set up by the seasonal density variation.

4) Many examples of density-driven circulations, while not directly related to the work presented here, can be investigated with the aid of similar dynamical models. These include, but are by no means limited to, the formation of bottom water in the Greenland-Norwegian Sea (Metcalf, 1960; Mosby, 1961 and 1967), outflow from the Aegean Sea in winter (Bruce and Charnock, 1965) and the circulation in the Adriatic Sea (Zore-Armanda, 1969). As in the case of the Antarctic, the roles of rotation and of the smallness of the predominant scale of convection have been largely neglected in these studies (rotation is probably not important in the long and narrow Adriatic).

The Theoretical Models

Three specific models will be formulated and solved here.

1) A one-dimensional model of the local mixing. This model is important both for its own contribution to an understanding of oceanic processes and to provide a realistic mixing model for use in the dynamical models.

2) A two-layer quasigeostrophic dynamical model. Since gravity waves are filtered out of the governing equations, it is computationally feasible to retain a free surface, so that the barotropic mode of motion is included in the solution. This is of interest in connection with the problem of variations in sea level. It will be seen in Chapter 2 that the convection in the mixed layer

tends to produce a sharp interface, or halocline, at the bottom of the mixed layer. Therefore, there is a significant two-layer component of the baroclinic motion. The two-layer model gives some indication of the nature of this response; in particular, it is the only model in which the height of the interface can be followed exactly. It must be noted that the particular two-layer model that is solved here has a lower layer of infinite depth. It will be seen that this requires the velocities to be zero, so that this model will not give any information about the motions below the interface.

3) A continuously stratified dynamical model. This model is necessary in order to study the general baroclinic motion and vertical circulation. The model is actually a many-layered finite difference approximation to a continuously stratified system. The initial density profile is based on observations in the Weddell Sea, so that this model has some relevance to the problem of bottom water outflow. This model retains the equations of motion in their hydrostatic but nongeostrophic form, and employs a rigid lid at the top surface to eliminate the computationally troublesome external gravity waves.

Chapter 2

THE LOCAL MIXING MODEL

This chapter is restricted to a study of convection in the mixed layer treated as a purely local phenomenon. The effects of such processes as horizontal advection and internal gravity waves, and irregularities associated with individual convective cells, are undoubtedly present and account for the irregularity observed in the data. However, it is believed that a significant degree of understanding of the seasonal variations in the surface layer has been obtained from consideration of the one-dimensional convective model alone.

It is assumed here that we are dealing with a horizontally infinite plane ocean, with no horizontal variations of properties. Rotation need not be considered in the study of local convection. Vertical mixing of salt is assumed to be complete in the mixed layer. Horizontal mixing is neglected. It is generally believed (Stewart, 1963) that unstable vertical convection weakens horizontal mixing because fluid particles find it easier to mix downward than to travel sideways.

The effect of temperature on density may be neglected because the thermal coefficient of expansion of water near its freezing point is small, and the water in the region of interest is nearly isothermal. In the Arctic Ocean in winter, water typically has a temperature of about $-1°C \pm 1°C$ and a salinity of

30‰ ± 2‰. Assuming a temperature of -1°C and a salinity of 30‰, then we find from the table on page 60 of Sverdrup, Johnson and Fleming (1942) that

$$\rho^{-1}\frac{\partial \rho^{-1}}{\partial T} = +10^{-5} \tag{1}$$

where ρ is density and T is temperature in degrees Centigrade. The relation between density and salinity at 0°C can be derived from formulas in the same book:

$$\rho = 1000 + 0.815S - 0.000482S^2 + 0.00000677S^3 - 0.093 \tag{2}$$

where S is in grams per kilogram of sea water (‰) and ρ is in kg/m^3. In the present work it is convenient and sufficient to put this in the form

$$\rho = 1000 + KS \tag{3}$$

which is valid in a restricted range of S. For S between 25‰ and 35‰ $K = 0.804$ is derived by eliminating ρ between (2) and (3) and substituting the desired values of S. We now find from (1) that a change of 1°C in temperature produces a change of 0.0102 kg/m^3 in the density, while a change of 1‰ in salinity changes the density by 0.804 kg/m^3. Therefore, the neglect of temperature variations is well justified. As additional evidence, it can be seen from observed vertical profiles such as those given by Kusunoki (1962) that the density in and above the main halocline in the Arctic Ocean depends almost entirely on salinity.

It is assumed that the expansion of water upon ice formation takes place entirely in the vertical direction. This is reasonable if the growth of ice crystals takes place by gradual accretion of molecules at the bottom of the ice rather than by the uniform freezing of a solid mass of water.

The Zubov-Defant Model

Zubov (1943) and Defant (1949) published what has until recently been the standard model for treating unstable surface convection. The two apparently worked independently; Zubov's book was only available in Russian at the time Defant published his paper. In this model the mixed layer always extends exactly to the depth at which its density equals the density of the undisturbed original profile. When salt is released by ice formation, it mixes uniformly throughout the depth of the mixed layer, increasing the salinity and (unless there is a sharp interface) the depth of the layer until a new equilibrium is reached (see Figure 1). The water below the bottom of the mixed layer is assumed to be completely undisturbed by the mixing. This model is easiest to visualize in its finite difference form (Figure 2). If an ocean is stably stratified into a number of layers, salt released by ice formation first increases the salinity of only the top layer. Vertical mixing is assumed to be complete within the top layer but stops at the interface between the first and second layers. When the

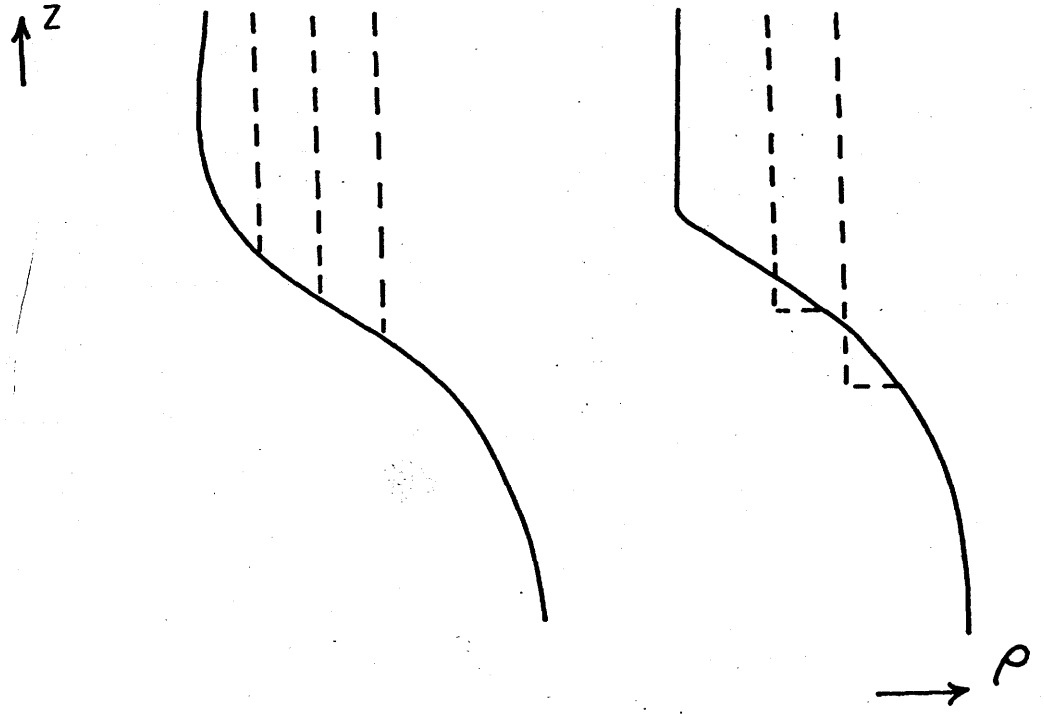

Figure 1 - Development of density profiles in a continuously stratified system according to the Zubov-Defant model (left) and the Kraus-Turner-Ball model (right). The solid line is the initial profile. Subsequent profiles, where different from the original, are shown by a dotted line.

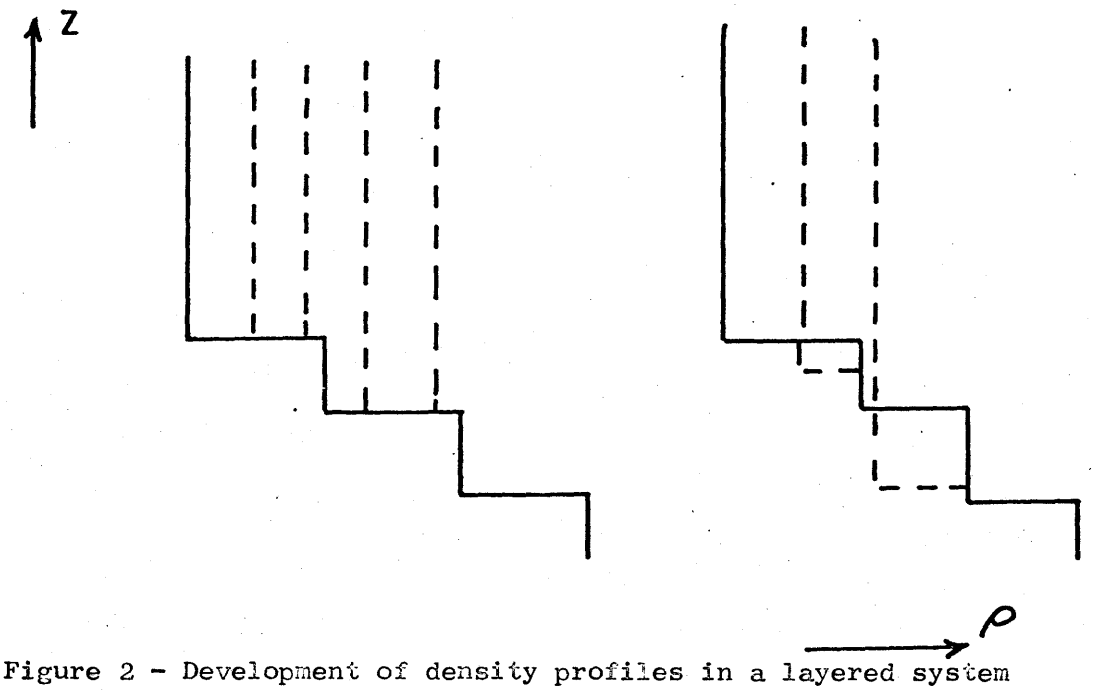

Figure 2 - Development of density profiles in a layered system according to the Zurov-Defant model (left) and the Kraus-Turner-Ball model (right).

density of the first layer becomes equal to the density of the second the two layers mix thoroughly, and become the new mixed layer. The process is then repeated until the density of the third layer is reached, and so on.

This process by itself cannot increase the density gradient, and in this sense* cannot play a role in the production of a halocline. The significance of this fact will become apparent later in this chapter.

Shortcomings of the Zubov-Defant Model

During the past several years, observational evidence which indicates that the Zubov-Defant model is not an accurate description of the surface mixing has begun to appear. Two examples of this observational evidence are described in this section. Still further evidence, in which the inadequacy of the Zubov-Defant model became evident as one result of the work reported here, will be presented later in this chapter.

1. Salt Balance in the Surface Layer of the Arctic Ocean

It has been known for some time that the surface layer of the Arctic Ocean becomes nearly fresh due to melting in summer

*Subsequent re-melting of the ice during the following summer can produce a halocline even though mixing during the freezing season takes place according to the Zubov-Defant model.

(in some locations) and that a mixed layer up to (rarely more than) 50 meters deep forms in winter. However, detailed observations of the surface layer taken for the purpose of studying seasonal convection have been scarce until recently. The study that is the most pertinent to the present discussion was carried out by Fujino (1966) on Ice Island Arlis II. In this study Fujino showed that the increase in salinity of the surface mixed layer, as calculated by the Zubov-Defant model, is more than can be accounted for by the observed amount of ice formation. Fujino's observations included points closely enough spaced in the vertical to have several within the mixed layer, with samples being taken about once every 10 days. Since Arlis II drifted into the East Greenland Current during the only full winter which Fujino spent on the island, he was forced to use an indirect argument based on observations taken from the end of one winter, through the summer, to the beginning of the next winter. Fujino's argument, slightly modified by the writer, is as follows.

Calculations based on the changes in the salinity of the upper mixed layer showed that a layer of fresh water about 1.4m thick must be supplied to account for the observed decrease in salinity in spring and summer. Of this, 0.35m must be supplied in early and mid-spring to account for a secondary peak in the curve of required fresh water supply vs. time. Since little melting was observed at this time and the air temperature was below freezing, it is assumed that this 0.35m of fresh water was supplied from

sources other than local melting. Fujino suggested advection from lower latitudes where melting begins earlier as one possibility; in any event, this leaves a maximum of 1.05m to be supplied by the excess of local melting and precipitation over evaporation. For an ice salinity of 5‰ (assumed by Fujino elsewhere in his paper, although he seems to have neglected this factor at this point, and based on his own measurements on Arlis II) and an ice density of 0.925 (Zubov, 1943), 1.3m of ice would be formed by the refreezing of this 1.05m of water into ice the following winter. The condition for maintaining a long-term steady state is that the amount of water that freezes into ice in winter must equal the amount of ice that melts in summer, so that 1.3m can be considered an upper bound to the amount of ice formation one would have to consider in a study of winter convection (if the summer studied by Fujino was typical). Since dilution by processes such as advection is believed to be taking place, the actual amount of ice formation is estimated by Fujino to be about 1 meter.

The application of the Zubov-Defant model to the observed profiles led Fujino to the conclusion that 2.1m of ice must form from a surface layer having the minimum salinity profile observed at the end of summer to reproduce the profile observed at the end of the previous winter. This corresponds to the freezing of about 1.9m of water, which is much more than the amount of fresh water mixed into the layer during the melting season. Some of the discrepancy may be due to the continuation of dilution by horizontal

advection during the winter, and possibly to the crude approximation of representing the entire mixed layer by a uniform "average" mixed layer. At any rate, there is a strong indication that the increase in salinity is more than can be accounted for by ice formation. Fujino attributes the difference to mixing between the surface layer and the more saline water in and just below the halocline. In this connection he points out that the decrease in vertical stability in winter makes such mixing easier in winter than in summer.

The present author believes that the assumption that as much ice must melt in summer as forms in winter requires further elaboration. It is known that a large quantity of ice floats out of the Arctic Ocean, mainly in the East Greenland Current, before melting in lower latitudes. Could it happen that much more ice forms in the Arctic than melts there, explaining the discrepancy found by Fujino?

Consider the cylindrical region $\mathcal{R}$ of the mixed surface layer, presumed to be somewhere in the central Arctic Ocean, shown in Fig. 3. It is bounded above by the lower surface of the ice and below by the halocline.

Let Φ_1 = the net yearly transport of water <u>into</u> $\mathcal{R}$ by horizontal advection.

Φ_2 = the net yearly transport of water <u>into</u> $\mathcal{R}$ by vertical advection across the halocline.

Φ_I = the net yearly transport of water (assumed fresh) <u>into</u> $\mathcal{R}$ due to ice freezing and melting. Precipitation is

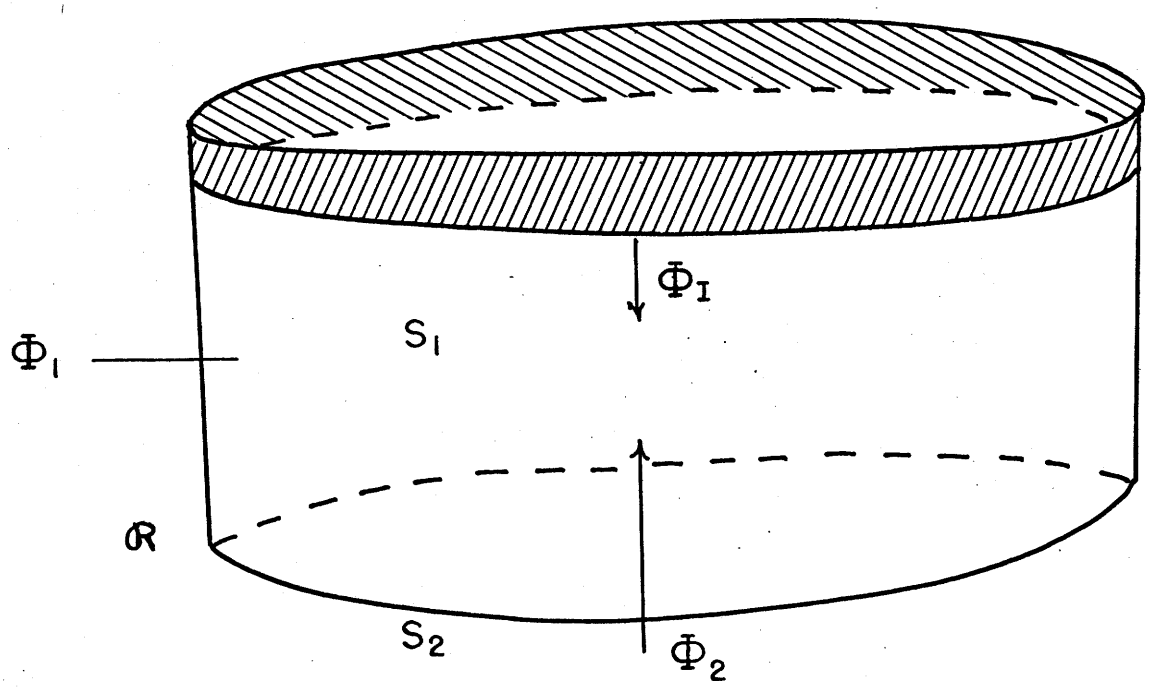

Figure 3 - Balance of mass flux into a region $\mathcal{R}$ of the surface layer of the Arctic Ocean. All fluxes are positive <u>into</u> $\mathcal{R}$. The shaded layer is the ice.

assumed to become part of the ice cover before reaching $\mathcal{R}$.

S_1 = the average salinity within the surface mixed layer.

S_2 = the average salinity within the halocline.

Conservation of mass in $\mathcal{R}$ requires that:

$$\Phi_1 + \Phi_2 + \Phi_I = 0 \tag{4}$$

Conservation of salt in $\mathcal{R}$ requires that:

$$\Phi_1 S_1 + \Phi_2 S_2 = 0 \tag{5}$$

Eliminating Φ_1, we obtain

$$\frac{S_2 - S_1}{S_2} \Phi_2 = \Phi_I \tag{6}$$

$S_2 > S_1$ is required for static stability. The crucial point of this argument is that the maintenance of a strong halocline probably implies the presence of an upward vertical velocity, just as upwelling is required to maintain the main thermocline in tropical and sub-tropical latitudes. Hence, $\Phi_2 > 0$, which, using (6) implies $\Phi_I > 0$; more fresh water is supplied to the surface layer than freezes out of it. The large volume of fresh water from rivers which empty into the Arctic basin is probably the major source of this fresh water.

2. Surface Profiles in the North Pacific Ocean in Winter

Many, although not all, of the S.T.D. profiles obtained by Reid (Scripps Institution of Oceanography, 1966) show a

nearly* well-mixed layer on top of an extremely steep pycnocline. We now recall the remark in the previous section that mixing according to the Zubov-Defant model cannot steepen a pycnocline. Another type of mixing, to be described in the next section, does form this kind of a profile.

Recent Advances in Mixing Theory

Recent discoveries about the nature of the mixing process, based on laboratory experiments and atmospheric observations, have made it apparent that the Zubov-Defant model may be oversimplified. These conclusions were reached independently of (and in most cases preceded) the oceanographical evidence presented in the preceding section.

Rouse and Dodu (1955) performed the first of a series of experiments on the behavior of a two-layer system in which turbulence is generated in one of the two layers. They found that the turbulent layer advances into the nonturbulent layer and the interface remains sharp as it advances. Fluid is entrained from the nonturbulent layer into the turbulent layer, into which it quickly becomes well-mixed, while the nonturbulent fluid which has not

*Reid (personal communication, 1969) insists that the surface layers in these profiles are not truly homogeneous, probably because of the trapping of rain water at the surface. However, they are very well-mixed compared to the stratification in and below the pycnocline; this is all that matters in the present work.

been reached by the interface remains practically undisturbed. This was a surprising result and is in contrast to the case in which turbulence is generated in both layers by shear at the interface; in the case of shear there is either little or no diffusion across the interface until the interface becomes unstable and gives way to a diffuse transition layer. Rouse and Dodu found an empirical relation for the diffusion rate in terms of a Froude number and a Reynolds number. They noted that the only relation that "can as yet be justified by simple reasoning" is based on the assumption that the rate of increase of potential energy due to entrainment is proportional to the rate of production of turbulent energy by mechanical agitation. This relation is similar to their empirical relation but involves a slightly different power of the Froude number.

Cromwell (1960) performed a similar experiment with a linear initial density gradient. He found that a strong pycnocline develops as a result of mechanical stirring.

Ball (1960) studied the diurnal variation of the height of a persistent atmospheric inversion over central Australia. He found that the kinetic energy of thermal turbulence which is generated in association with an upward convective heat flux near the ground cannot be destroyed by molecular or eddy viscosity if the mixed layer is sufficiently deep. Following the work of Rouse and Dodu, Ball showed that the turbulent energy is primarily destroyed by a downward heat flux and entrainment of warm air from above at

the top of the mixed layer rather than by viscous dissipation within the mixed layer. The implications of Ball's hypothesis in the case of turbulent cloud layers under an inversion are pursued further by Lilly (1968).

Turner and Kraus (1967), in an experimental study of the seasonal thermocline, accounted for the effect of heating and cooling by periodically adding sea water of varying density to the surface in addition to maintaining constant mechanical stirring. This experiment showed that it is reasonable to calculate the depth and density of the mixed layer on the basis of conservation of the potential energy in a fluid column plus the turbulent energy input due to mechanical stirring. In a companion paper (Kraus and Turner, 1967) a theory based on these results was shown to give a reasonable depth for the mixed layer at weather station P in the North Pacific Ocean during the summer heating season. The conclusion reached by Turner and Kraus has been questioned, at least for the case in which mechanical stirring is absent, by Deardorff, Willis and Lilly (1969), who did experiments with a stratified fluid heated from below. They found that most of the turbulent energy generated by the heat flux at the bottom was dissipated by molecular viscosity, and that very little entrainment took place. However, it must be noted that their experiments were performed on a laboratory scale, with much smaller Rayleigh numbers than are typical of the ocean, and do not necessarily affect the validity of the seasonal themocline model of Kraus and Turner in the ocean. The arguments used

by Ball to reach his conclusion, for example, fail if the depth of the mixed layer is too small.

A model incorporating entrainment due to penetrative convection will be used in addition to the Zubov-Defant model in the present work. This model will be referred to as the Kraus-Turner-Ball model since these authors have been primarily responsible for developing mixing models which employ the concept of potential energy conservation in a geophysical context. Its basic features can be given as a statement of the conservation of the total salt content,

$$(7)\quad \frac{\partial}{\partial t}\left(\int_{\text{WATER}} \rho S\,dz + \int_{\text{ICE}} \rho S\,dz\right) = 0$$

a statement of the conservation of the total mass,

$$(8)\quad \frac{\partial}{\partial t}\left(\int_{\text{WATER}} \rho\,dz + \int_{\text{ICE}} \rho\,dz\right) = 0$$

and a statement that the turbulent energy generated by the descent of salt released into the mixed layer (plus the energy generated by mechanical stirring when this is present) is recovered by the upward entrainment of heavier water into the mixed layer from below,

$$(9)\quad \Delta \int_{\substack{\text{WATER NOT}\\ \text{FROZEN IN } \Delta t}} \rho g z\,dz = 10^{-3}\rho(0)\left[S(0) - S_I\right] g D \propto \Delta I + E\,\Delta t$$

where $\propto \Delta I$ is the thickness of water that freezes in time Δt, D is the value of Z where it freezes and $10^{-3}\rho(0)\left[S(0) - S_I\right]$

is the density of the dissolved salt that is released by the freezing. E is the rate of energy input per unit of surface area due to mechanical stirring; α is the ratio of the density of sea ice to the density of sea water and has a numerical value of about 0.902. We neglect the change in potential energy due to the additional height by which the freezing water rises as it expands during the formation of ice crystals, along with whatever salt is trapped in the ice. This extra potential energy cannot play any part in salt convection since the ice would expand just as much even if the water were fresh. It must, of course, be accounted for in the total energy budget including the latent heat of freezing. Our approach is purely mechanical and is concerned only with the internal readjustment of the density field. In practice, it is sometimes simpler to approximate the actual condition by one which conserves the potential energy of the dissolved salt. This is permissible as long as the effect of temperature on density is not important. In any case, the salt that is retained in the ice must be omitted from the energy calculation.

The effect of the entrainment process on the development of salinity profiles due to ice formation can be compared with the pure Zubov-Defant model by studying the solutions for simple initial profiles that are given in the next section. Since the salinity of the mixed layer increases more rapidly than in the Zubov-Defant model, there is at least a possibility, which will be investigated later in this chapter, that entrainment can provide the

extra salt which Fujino found necessary to explain the Arlis II data. The increase in the steepness of the halocline, a result which applies to pycnoclines in general, can account for the formation of the very steep pycnoclines found by Reid. It is, in fact, already known that the seasonal thermocline becomes steeper during periods of wind mixing (Cromwell and Reid, 1956) and that it descends during storms (Francis and Stommel, 1953).

Solutions for Simple Initial Profiles

Analytical solutions for the salinity vs. depth profiles after a given amount of ice forms can be found for both the Zubov-Defant and Kraus-Turner-Ball models for some particularly simple initial distributions. These solutions help to illustrate the nature of the processes, and are valuable for later reference, such as when checking a procedure used to solve for more complicated initial profiles.

In the treatment of these models by analytical methods it is convenient to use the salt per unit of volume,

$$\sigma = \rho S \tag{10}$$

as a dependent variable in place of ρ and S separately, and, in the case of the Kraus-Turner-Ball model, to replace the exact energy condition in equation (9) by the approximate condition of conservation of the potential energy of dissolved salt in a water

column. Using (3), (10) can be inverted to give

$$(11) \qquad S = -621.89 + \sqrt{386747.85 + \frac{\sigma}{0.804}}$$

1. One-Layer Ocean (Fig. 4)

First consider the simplest possible case, a homogeneous one-layer ocean of water depth D and salt content per unit of volume σ. The initial values of D and σ are D_o and σ_o respectively. If a thickness I of ice forms from this layer and all salt is excluded from the ice, conservation of salt requires that

$$(12) \qquad \sigma D = \sigma_o D_o$$

We also have

$$(13) \qquad D + \alpha I = D_o$$

Since only the Zubov-Defant model applies here, (12) and (13) are the only equations that are needed. They are solved simply by finding D from (13), then substituting this value into (12) to find σ. If D_o = 50 meters and the initial salinity is S_o = 30‰ and one meter of ice is formed, the result is D = 49.08 meters and S = 30.55‰.

2. Two-Layer Ocean (Fig. 5)

The subscript 1 refers to the upper layer and 2 to the lower layer. Initial values in the upper layer have the subscript

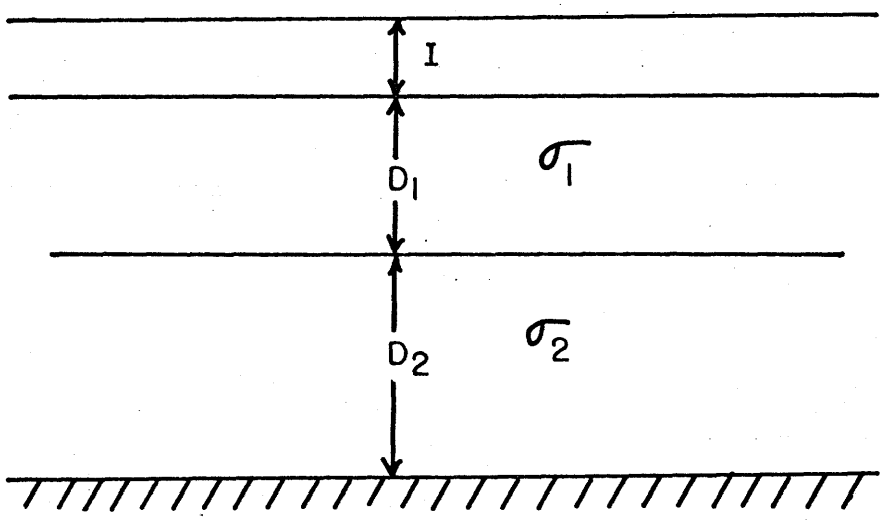

Figure 5 - Notation for the one-layer ocean model.

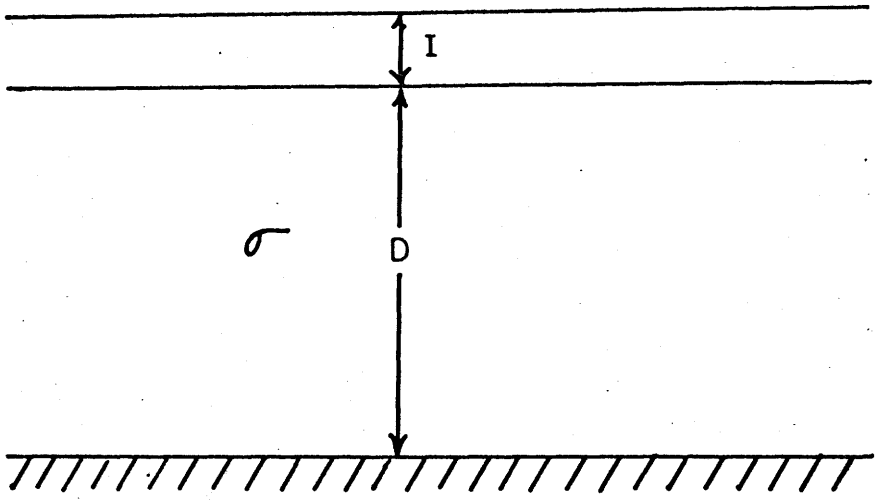

Figure 4 - Notation for the two-layer ocean model.

0; the initial total depth of the ocean is H.

The upper layer of a two-layer Zubov-Defant model has the same solution as a one-layer ocean until the density of the lower layer is reached, when the whole ocean becomes homogeneous.

The two-layer Kraus-Turner-Ball model, with full recovery of the potential energy of the salt released by freezing during entrainment but no mechanical energy input, is governed by the following equations:

$$\sigma_1 D_1 + \sigma_2 D_2 = \sigma_0 D_0 + \sigma_2 (H - D_0) \tag{12}$$

$$D_1 + D_2 + \alpha I = H \tag{13}$$

$$\int_0^{D_2} \sigma_2 z\,dz + \int_{D_2}^{D_1+D_2} \sigma_1 z\,dz = \int_0^{H-D_0} \sigma_2 z\,dz + \int_{H-D_0}^{H} \sigma_0 z\,dz \tag{14}$$

The solution* is

$$D_1 = \frac{(\sigma_2 - \sigma_0) D_0^2 - [2(\sigma_2 - \sigma_0) D_0 + \sigma_2 \alpha I] \alpha I}{(\sigma_2 - \sigma_0) D_0 - \sigma_2 \alpha I} \tag{15}$$

$$\sigma_1 = \frac{\sigma_0 (\sigma_2 - \sigma_0) D_0^2}{(\sigma_2 - \sigma_0) D_0^2 - [2(\sigma_2 - \sigma_0) D_0 + \sigma_2 \alpha I] \alpha I} \tag{16}$$

No terms are negligible. With S_0 = 30‰, D_0 = 50 meters and S_2

*For the reader who is interested in following the somewhat tedious algebra, it was found expedient to substitute for $\sigma_1 D_1$ into (14) from (12) and for D_1 from (13) and solve for D_2 first, then solve for σ_1 and D_1.

= 33‰, 1 meter of ice formation gives D_1 = 59.35 meters and S_1 = 31.32‰. Note that this is independent of H provided only that entrainment to the depth D_1 below the bottom of the ice does not reach the bottom of the ocean. It is instructive to compare this value of S_1 with the value of 30.55‰ obtained from the Zubov-Defant model.

3. Initial Profile Linear in σ (Fig. 6)

The salinity profile is slightly parabolic, according to (3) and (10). Note that σ_2 is a function of z. The initial profile is $\sigma_2(z) = \sigma_B(1-\Gamma z)$.

The equations which are common to both models are

$$(17)\quad \int_0^{D_2} \sigma_2\,dz + \sigma_1 D_1 = \int_0^H \sigma_2\,dz$$

and equation (13).

In the Zubov-Defant model we also have

$$(18)\quad \sigma_2(D_2) = \sigma_1$$

This leads to the solution

$$(19)\quad D_1 = \sqrt{2\frac{\alpha I}{\Gamma}(1-\Gamma H)+\alpha^2 I^2} \approx \sqrt{2\frac{\alpha I}{\Gamma}(1-\Gamma H)}$$

$$(20)\quad \sigma_1 = \sigma_B\left\{1-\Gamma[H-(D+\alpha I)]\right\}$$

In the Kraus-Turner-Ball model a discontinuity forms at the bottom of the mixed layer and (18) is replaced by conservation of the potential energy of the salt:

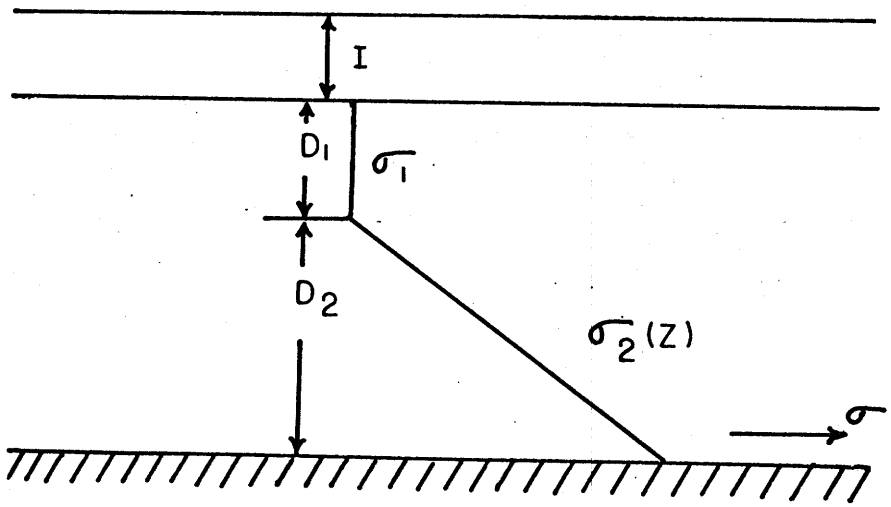

Figure 6 - Notation for the linear σ ocean model.

$$(21)\quad \int_0^{D_2} \sigma_2 z\,dz + \int_{D_2}^{D_1+D_2} \sigma_1 z\,dz = \int_0^{H} \sigma_2 z\,dz$$

The solution is

$$(22)\quad D_1 = \tfrac{1}{2}\alpha I + \tfrac{1}{2}\sqrt{24\tfrac{\alpha I}{\Gamma}(1-\Gamma H) + 9\alpha^2 I^2} \approx \sqrt{6\tfrac{\alpha I}{\Gamma}(1-\Gamma H)}$$

or $\sqrt{3}$ times the depth reached by convection in the Zubov-Defant model, and

$$(23)\quad \sigma_1 = \frac{D_1+\alpha I}{D_1}\sigma_B\left\{1-\Gamma\left[H_o-\tfrac{1}{2}(D_1+\alpha I)\right]\right\}$$

With H = 200 meters, an initial salinity at the bottom S_B = 34‰ and S = 30‰ at the top (typical values of salinity in the Arctic and Antarctic Oceans), 1 meter of ice formation gives D_1 = 55.26 meters and S_1 = 31.13‰ according to the Zubov-Defant model, and D_1 = 96.17 meters and S_1 = 32.67‰ according to the Kraus-Turner-Ball model.

The Numerical Model

In the analysis of actual data it is necessary to use a model that is suitable for calculating many small changes in a finite difference approximation to the true profile. The equations for calculating the change in a single step use the notation

in Fig. 7 and are:

$$(24)\quad \left[\rho_1 S_1 D_1 + \rho_I S_I I\right]_t^{t+\Delta t} = \int_{D_2(t+\Delta t)}^{D_2(t)} \rho_2 S_2 \, dz$$

$$(25)\quad \left[D_1 + D_2\right]_t^{t+\Delta t} = -\alpha \Delta I$$

$$(26)\quad \int_{D_2(t+\Delta t)}^{D_2(t)} \rho_2 z \, dz + \int_{D_2(t)}^{(D_1+D_2)(t+\Delta t)} \rho_1(t) z \, dz + \int_{(D_1+D_2)(t+\Delta t)}^{(D_1+D_2)(t)} 10^{-3} \rho_1(t)\left[S_1(t) - S_I\right] z \, dz$$

$$= \int_{D_2(t+\Delta t)}^{D_2(t)} \rho_1(t+\Delta t) z \, dz + E^*$$

where $E^* = \frac{E \Delta t}{g}$

Equation (3) is also part of the required system. The observed profiles were approximated by a series of homogeneous layers of 1 meter thickness for purposes of numerical calculation. Equations (24), (25) and (3) are sufficient for the calculation of successive profiles according to the Zubov-Defant model, since (26) is replaced by the condition of continuity of the profile at the bottom of the mixed layer. Salt is first added to the existing mixed layer and the resultant salinity calculated; if the resulting profile is unstable the process is repeated with the first layer below the old mixed layer assumed to be mixed into the new mixed layer. If the resulting profile is still unstable the process may be repeated as many times as necessary until a stable profile is achieved or convection reaches the bottom. The first

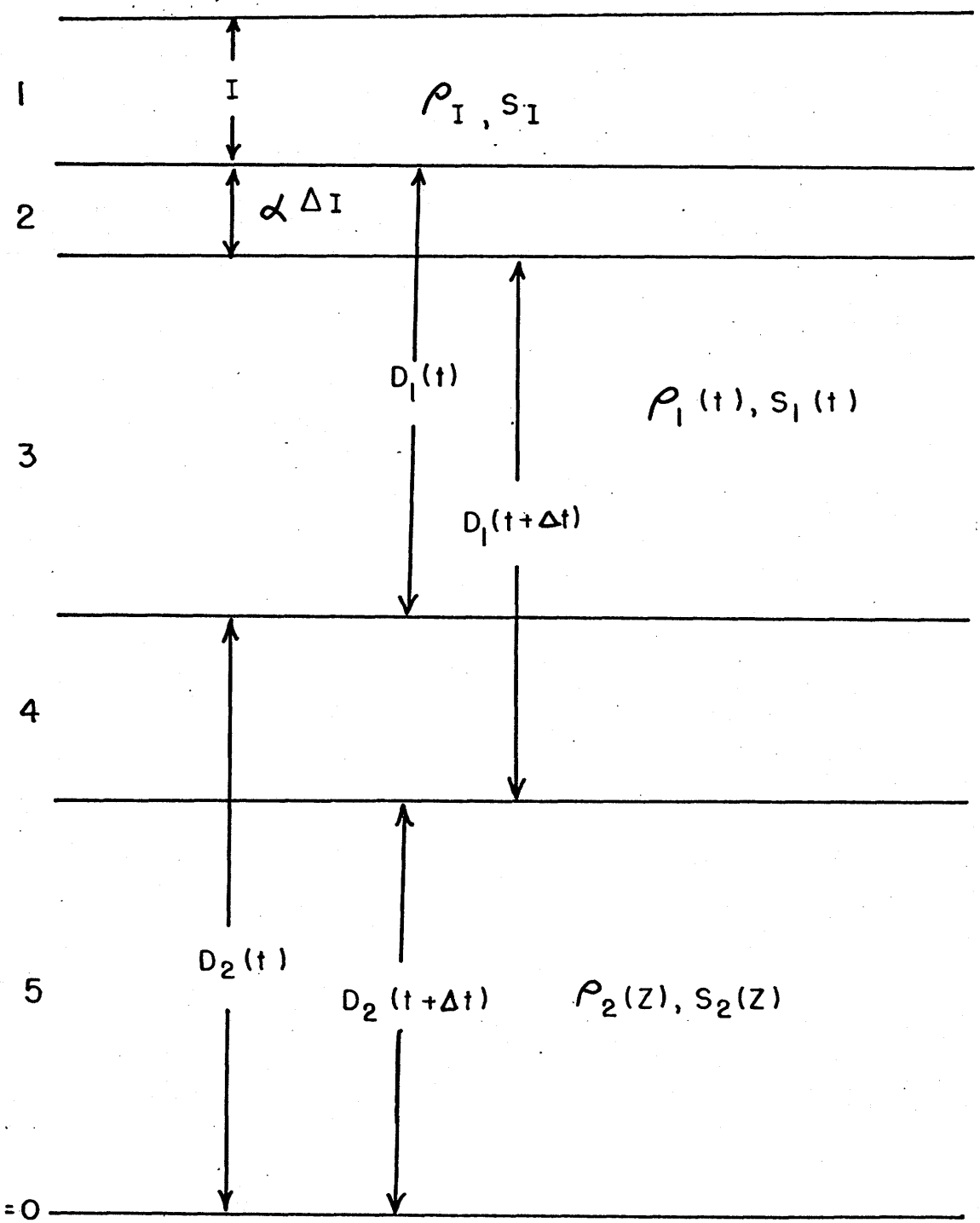

Figure 7 - Notation for the numerical calculation of successive profiles. the regions are: 1) ice already existing at time t; 2) water that freezes in the time Δt; 2U3 mixed layer at time t; 4) water that is entrained into the mixed layer in the time Δt; 3U4) mixed layer at time $t + \Delta t$; 5) nonturbulent water not reached by the convection. $z = 0$ at the ocean bottom or at a reference level below the deepest depth reached by the convection.

stable profile obtained in this way becomes the starting point for the next ice formation step. This procedure is shown in flow chart form in Fig. 8.

The full system including equation (25) must be used for the Kraus-Turner-Ball model. Two different procedures are possible in this case. The one which is the simplest conceptually is a purely trial-and-error calculation. First, the Zubov-Defant procedure is followed to give the profile of minimum energy, and the energy balance, which will always show a net loss during the mixing process, is calculated. Then additional layers are entrained, one at a time, and the energy balance for each resulting profile is calculated, until the profile which gives the closest possible fit to the desired energy balance is found. The desired energy balance may or may not include an added amount of energy from mechanical stirring. This procedure is shown in flow chart form in Fig. 9.

This procedure and the Zubov-Defant model were tested on a linear initial profile with S = 30‰ at the surface and S = 33‰ at a depth of 150 meters. The salinity and depth are compared with the analytical solutions found from the formulas in the preceding section. I is the amount of ice formed in meters; I = 0 initially.

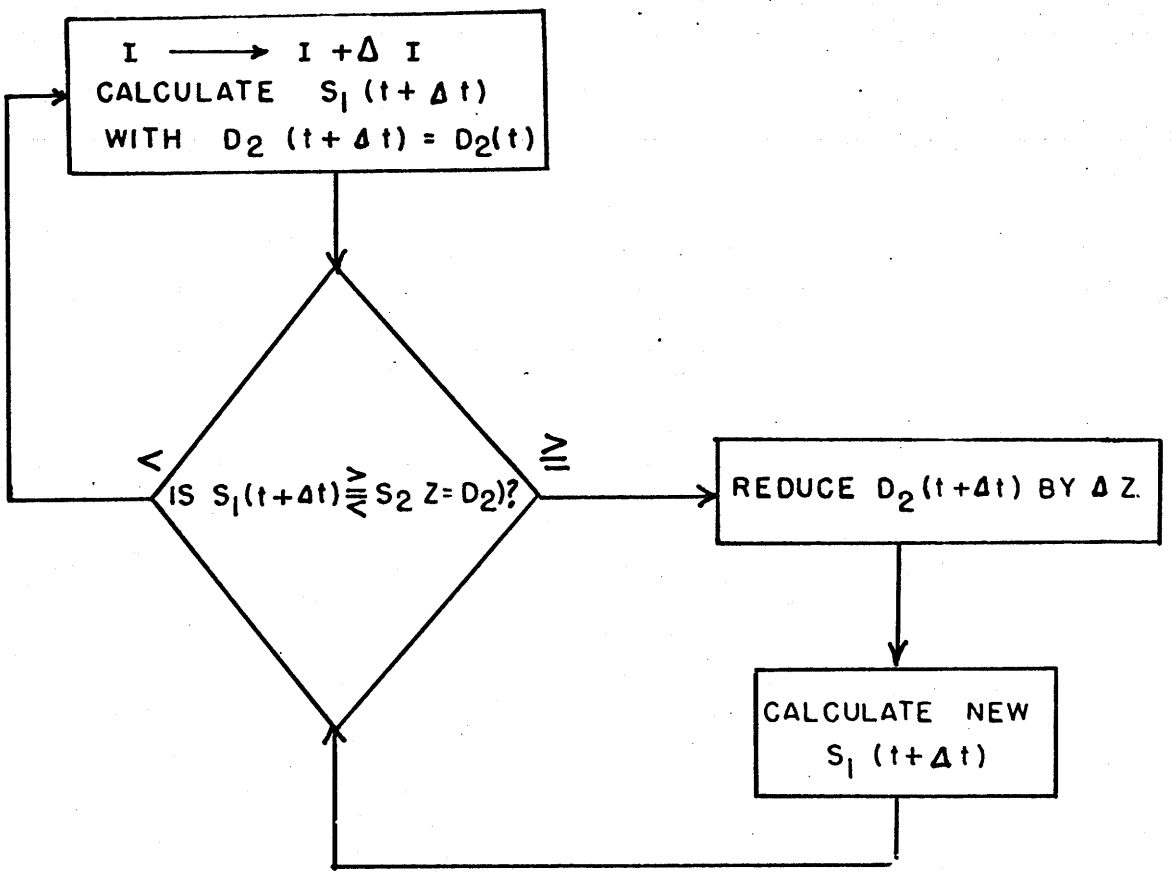

Figure 8 - Flow chart for the Zubov-Defant model. This is also the flow chart for the Kraus-Turner-Ball model with partial entrainment in the layer below the mixed layer if $S_1(t + \Delta t)$ and $S_2(D_2, t + \Delta t)$ are calculated according to equations (36) and (81).

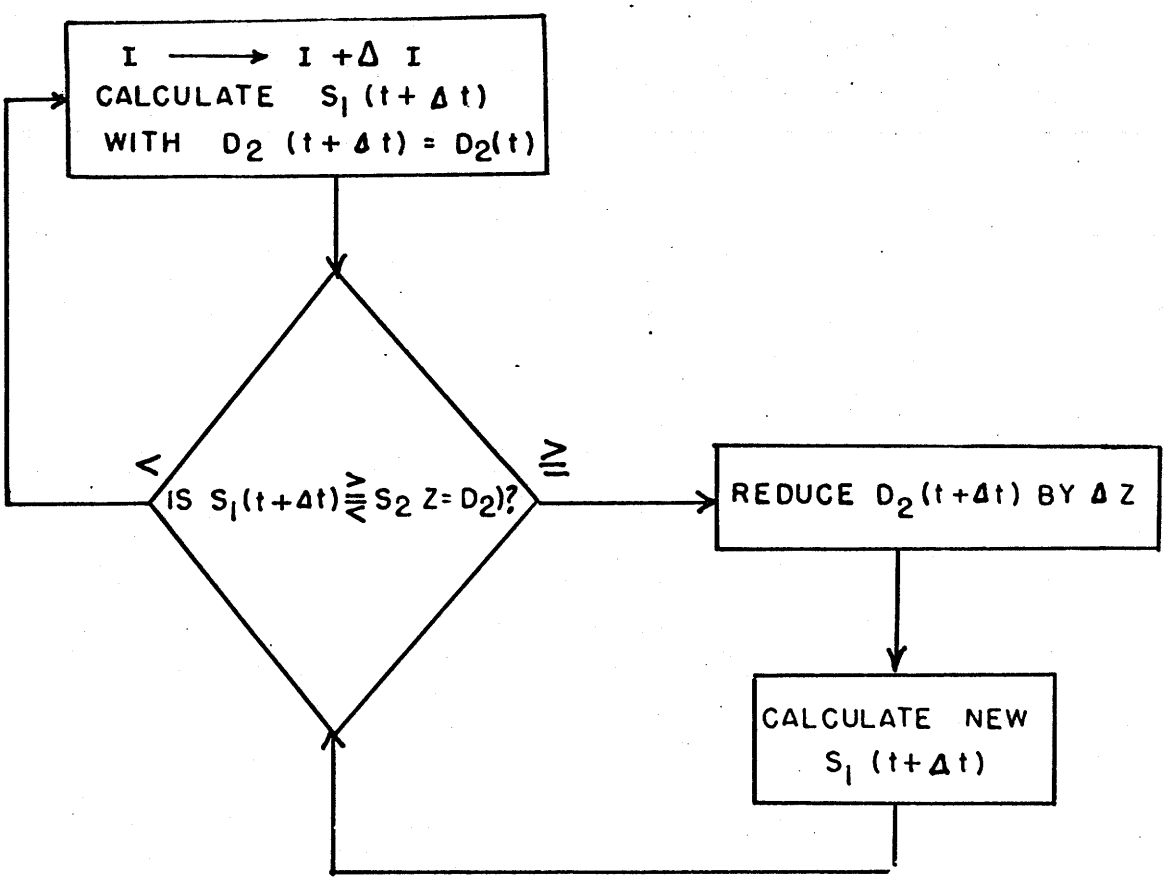

Figure 8 - Flow chart for the Zubov-Defant model. This is also the flow chart for the Kraus-Turner-Ball model with partial entrainment in the layer below the mixed layer if $S_1(t + \Delta t)$ and $S_2(D_2, t + \Delta t)$ are calculated according to equations (36) and (81).

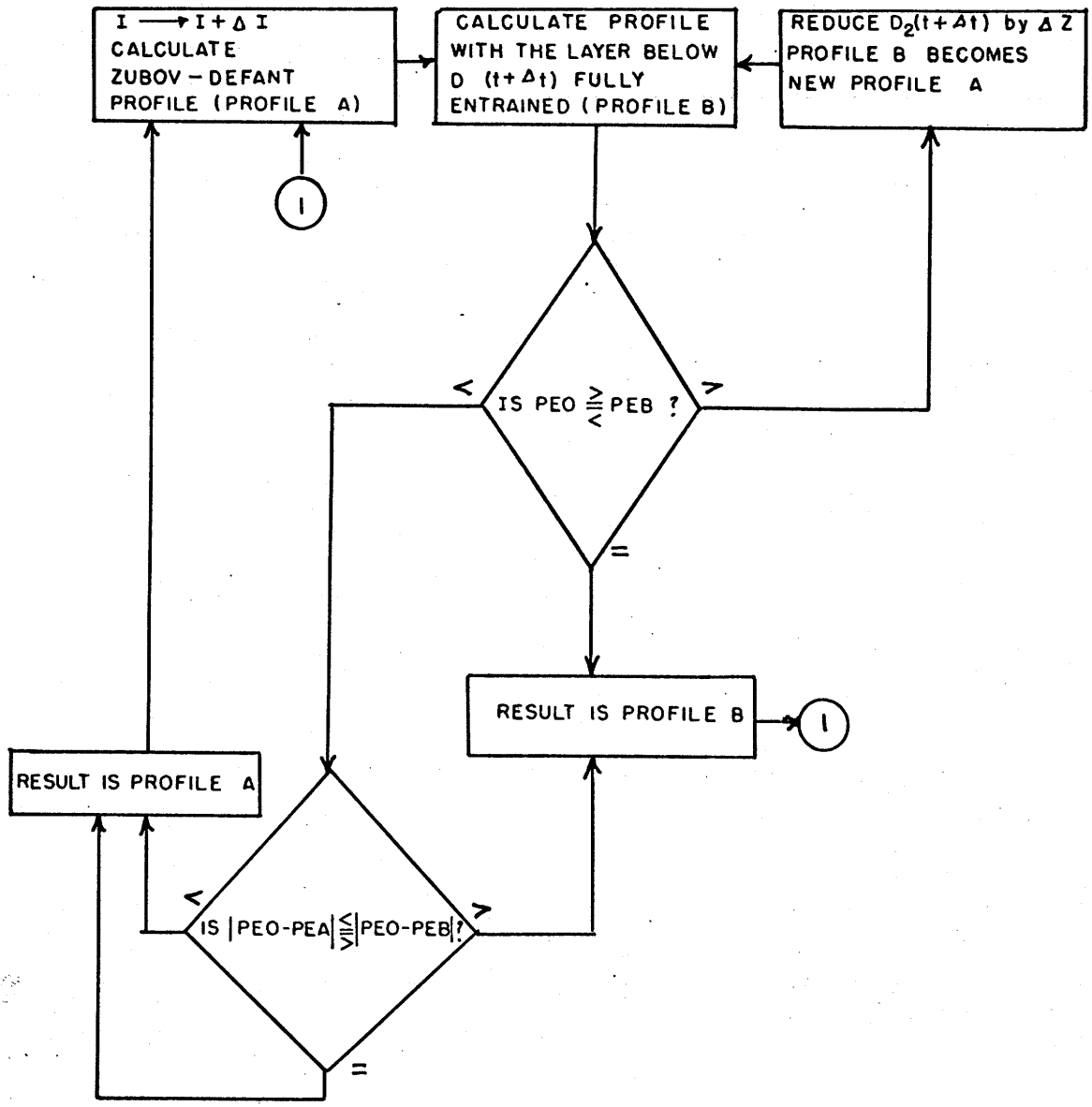

Figure 9 - Flow chart for the Kraus-Turner-Ball model calculated by a purely trail-and-error procedure. PEO is the potential energy of the "original" profile (at time t), with only the salt that is released by freezing included in the integral over region 2 in Figure 7. PEA is the potential energy of profile A, and PEB the potential energy of profile B, with region 2 omitted from the integral in both cases.

TABLE I

I	S (Analytical) in ‰	S (Computer) in ‰	D (Analytical) in meters	D (Computer) in meters
		Zubov-Defant Model		
0.01	30.11	30.100	5.2	5
0.10	30.33	30.306	16.5	15
0.20	30.47	30.431	23.3	22
0.30	30.57	30.527	28.3	26
0.50	30.74	30.680	36.8	34
		Kraus-Turner-Ball Model with Pure Trial-and-Error Numerical Procedure		
0.01	30.12	30.130	9.0	9
0.10	30.38	30.423	28.6	34
0.20	30.55	30.575	40.4	46
0.30	30.68	30.698	49.4	56
0.50	30.88	30.927	63.7	76

A shortcoming of this method became apparent when the local mixing model was incorporated into the continuously stratified dynamical model to be described in chapter 4. In the dynamical model it was not computationally feasible to use layers of only 1 meter thickness and it soon became obvious that the trial-and-error procedure in Fig. 9 would entrain much too slowly. The difficulty is that it takes so much energy to entrain a layer several meters thick that the procedure would usually stop with just the amount of mixing predicted by the Zubov-Defant model. The procedure does not "store" energy that is not used in such steps for entrainment in subsequent steps and can only give accurate

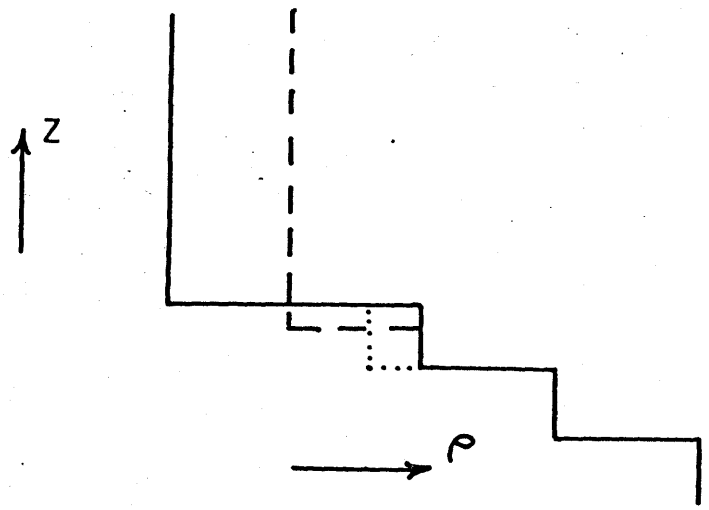

Figure 10.- Partial entrainment of the layer immediately below the mixed layer. The dashes show the actual profile that develops in a layered ocean; the dots show the representation in terms of a layer with fixed thickness but variable density.

results when the layers are thin enough so that the energy released in one ice formation step is usually enough to entrain a whole layer.

The response to this difficulty was to allow the nonturbulent layer immediately below the mixed layer to be partially entrained into the mixed layer during each ice formation step in a way that conserves potential energy exactly. This partially entrained layer is an averaged representation of a region into which the mixed layer has partially, but not completely, penetrated in the real ocean (Fig. 10). It is possible to start each step by finding the Zubov-Defant profile and then balance the energy by partial entrainment, and this is, in fact, the way in which the calculations were carried out in the continuously stratified dynamical model. However, it turns out to be simpler to calculate the entrainment directly, without a Zubov-Defant step. If this produces an instability, the "partially" entrained layer is assumed to be completely entrained into the mixed layer, and the procedure is repeated with the next layer down being partially entrained. The flow chart is essentially the same for this procedure as for the Zubov-Defant model.

The equations for this model, with the exact energy condition replaced by conservation of the potential energy of the dissolved salt, are:

$$D(t+\Delta t) = D(t) - \alpha \Delta I \tag{27}$$

From here on D_1 refers to $D_1(t + \Delta t)$.

$$(28)\quad \bar{\sigma}_2(t+\Delta t)\Delta z + \bar{\sigma}_1(t+\Delta t)D_1 = \bar{\sigma}_2(t)\Delta z + \bar{\sigma}_1(t)D_1 + \rho_I[S_1(t)-S_I]\,\Delta I$$

$$(29)\quad \int_0^{\Delta z} \bar{\sigma}_2(t+\Delta t)z\,dz + \int_{\Delta z}^{D_1+\Delta z} \bar{\sigma}_1(t+\Delta t)z\,dz = \int_0^{\Delta z} \bar{\sigma}_2(t)z\,dz + \int_{\Delta z}^{D_1+\Delta z} \bar{\sigma}_1(t)z\,dz + \int_{D_1+\Delta z}^{D_1+\Delta z+\alpha\Delta I} \rho_I[S_1(t)-S_I]z\,dz + E^*$$

where the subscript 1 refers to the mixed layer, 2 to the partially entrained layer and Δz is the thickness of the partially entrained layer.

The solution is (27) and:

$$(30)\quad \bar{\sigma}_2(t+\Delta t) = \frac{(D_1+\Delta z)\Delta z\,\bar{\sigma}_2(t) - (D_1+\alpha\Delta I)\Delta I\rho_I[S_1(t)-S_I] - 2E^*}{(D_1+\Delta z)\Delta z}$$

$$(31)\quad \bar{\sigma}_1(t+\Delta t) = \frac{D_1(D_1+\Delta z)\bar{\sigma}_1(t) + (2D_1+\Delta z+\alpha\Delta I)\Delta I\rho_I[S_1(t)-S_I] + 2E^*}{D_1(D_1+\Delta z)}$$

The ΔI's inside of the parentheses can usually be neglected to a good approximation.

In practice, the first procedure was used for the data analysis because it was the only procedure available when this work was performed. The second procedure was developed out of necessity for the dynamical model in chapter 4.

Forcing Functions

1. Ice Formation

In order to use the theory to analyze actual data, it is necessary to make some assumptions about the rate of ice formation and the salinity and density of the ice. Really adequate data on these quantities is simply not available. Ice formation takes place most rapidly in open leads, which are always opening up as a result of collisions between ice floes. Ice that is newly formed from open water traps large quantities of salty brine which drains out slowly as the season progresses (Zubov, 1943). The brine tends to collect in cells and drip through drainage channels (Lyon, personal communication, 1967; Untersteiner, 1968), leading to a distribution of salinity that is highly nonuniform in both the horizontal and vertical directions (Kusunoki, 1955). With present data, an accurate estimate of the effective salt source is impossible. Therefore, the simplest possible source function was taken as a crude estimate. For this purpose Fujino's observation that about 1 meter (perhaps slightly more) of ice formation from the saline upper layer of water must take place to compensate for the amount of fresh water mixed into this layer during the melting season (Fujino, 1966) was used. This freezing is assumed to take place over a period of about 200 days, so each 1 cm addition of ice (one step in the numerical calculation) is assumed to correspond to about 2 days of real time. This is crude but a more complicated function is not warranted by

the available data. From measurements by Fujino (1966) and data given by Zubov (1943) and Kusunoki (1955) 5‰ was chosen as a typical ice salinity. The density of the ice is then obtained from a table in Zubov's book as 925 kg/m^3.

2. Wind Mixing

A rough estimate of the energy input due to wind mixing can be obtained by the following variation of the argument used by Kraus and Turner (1967). Over open water, the mechanical energy input to the water is

$$E = \tau V_* \tag{32}$$

where V_* is the "friction velocity" of the water*.

Since the speeds of the water under the ice are observed to be about 1/10 of the speeds of water in the open ocean, the shielding effect of the ice will be roughly accounted for by introducing a factor of 0.1:

$$V_* = 0.1 V_{**} \tag{33}$$

and assuming that V_{**} can then be related to the "friction velocity" in the atmosphere as if the ice were not present.

$$E = 0.1 \tau V_{**} \tag{34}$$

It is shown by Kraus and Turner that

$$V_{**} = \sqrt{\frac{\rho_{AIR}}{\rho_{WATER}}}\, U_* \tag{35}$$

*U_* and V_* do not refer to velocity components in particular directions in this section.

and

$$(36)\quad \tau = \rho_{AIR}\, U_*^2$$

where U_* is the "friction velocity" in the atmosphere. (34), (35) and (36) can be combined to give:

$$(37)\quad E = 0.1\, \frac{\rho_{AIR}^{3/2}}{\rho_{WATER}^{1/2}}\, U_*^3$$

U_* is defined by $U_*^2 = C U_A^2$ where U_A is the wind speed at anemometer level. Sheppard (1958) gives the empirical relation

$$(38)\quad C = (0.80 + 0.114 U_A)\cdot 10^{-3}$$

where U is in m/sec. Wind data which accompanied some of the oceanographical data used in this study shows that typical winter wind speeds in the Arctic are on the order of 10 knots (5 m/sec) or less. This gives $C = 1.4 \cdot 10^{-3}$, and $U_* \approx 0.19$ m/sec; Using ρ_{air} = 1.247 kg/m^3 and ρ_{water} = 1025 kg/m^3, we find

$$E = 2.93 \cdot 10^{-5}\ \frac{\text{JOULES}}{M^2 - \text{SEC}}\ .$$

Over a two-day period, the energy input is

$$E\Delta t = 5.06\ \frac{\text{JOULES}}{M^2}$$

which gives

$$E^* = \frac{E\Delta t}{g} \approx 0.5\ \frac{KG}{M}$$

Substitution of this value into the calculations showed that it had little effect on the development of successive profiles. However, the dependence of E on the cube of the wind speed is well worth

noting. It will be found that wind mixing can become very important during prolonged periods of severe storms.

Analysis of Arctic Data

Data suitable for the study of the mixed layer is available from the Arctic Ocean, where drift stations have been operated for a number of years. All suitable free world (American and Japanese) data of which this author is aware, and which was available at the time this part of the work was performed (late 1967-early 1968) was obtained. One set of Soviet data was obtained from the report of the drift station "North Pole 2" (Gudkovich, 1954), which has been widely circulated in the United States. Much more data is known to have been taken by the Soviets - much more, in fact, than the amount of free world data - but regrettably has either been classified or received little or no distribution outside of the Soviet Union. Some recent unpublished University of Washington data from Ice Island T-3 was made available, a courtesy for which the author is grateful, but it was not used because it was taken on the Continental Shelf, where there is no halocline and convection reaches nearly to the bottom.

The data was first examined to find periods in which the general trend of the salinity in the surface layer showed a monotonic increase. A decrease of salinity must be explained by processes other than those being considered here. Some of the

series obtained in this way were later found to have salinity increases smaller than are predicted by the Zubov-Defant model, which gives the minimum possible salinity increase consistent with gravitational stability. They were discarded.

The mixed layers were not all perfectly uniform. Some of the data indicated the existence of small layers of gravitational instability and/or very slight stability, probably due to errors in measurement and such factors as irregularities associated with individual convective cells and the transient nature of the actual convection. For purposes of the present study it was necessary to assume the existence of a mixed layer without instabilities; it was sometimes, but not always, easy to define a layer in which the fluctuations were always much smaller than the differences between points in and out of the layer. Starting from the surface downward, the mixed layer was chosen so that it always included every point which had a salinity less than at least one of the points above it, and sometimes extended downward to include points which, although of higher salinity than all points above, varied from the points already included by not more than the variations among these points. The observed values at these points were then averaged to obtain the salinity of the mixed layer. Interpolation of the profiles below the mixed layer was done by computer, using the method of averaging two quadratic polynomial approximations (Rattray, 1962). This procedure occasionally gave an absurd section of profile, especially in the segment immediately

below the mixed layer, where the actual profile bends sharply. These short segments were discarded and interpolated by hand.

The theoretical model predicts entire profiles. However, it is obvious from even a superficial examination of the data that processes are always at work that tend to destroy the mixed layer. The actual mixed layer rarely reaches the depth predicted by the theory, especially the entrainment model. Therefore, the salinity of the mixed layer has been chosen as the most useful quantity for comparison between theory and observation.

Each series of data obtained in this way was assigned a number by the present author for use in this study, and the stations within each series were numbered successively. These numbers do not have any relation to the station numbers used by the original investigators. These series are listed on Table II (following this page).

The results of the calculations are shown in figures 11 through 18. One result that was obtained in every case is that mixing according to the Zubov-Defant model produces a smaller increase in salinity than is actually observed. The data can be divided into three groups, according to the results obtained from the Kraus-Turner-Ball model:

A - Series 2, 3, 6 and the first three stations of series 8. In these series the Kraus-Turner-Ball model provided a closer fit to the data than the Zubov-Defant model; in some cases the agreement with observations is quite good.

TABLE II

Data Series Number in Present Study	Number of Stations	Drift Station	Location	Dates	Author(s) and Institution
1	5	Arlis II*	85°49.6'N78°26.0'W to 86°29.5'N25°2.0'W	Aug. 1964 to Oct. 1964	Kusunoki, Minoda, Fujino, Kawamura Hokkaido University
2	4	Arlis II*	85°10.4'N15°47.0'W to 84°42.6'N17°53.0'W	Oct. 1964 to Nov. 1964	Kusunoki, Minoda, Fujino, Kawamura Hokkaido University
3	4	Arlis II*	84°35.2'N17°20.0'W to 82°7.4'N	Dec. 1964 to Jan. 1965	Kusunoki, Minoda, Fujino, Kawamura Hokkaido University
4	23	Arlis I	75°12'N140°49'W to 74°19'N153°39'W	Sept. 1960 to Nov. 1960	Brayton University of Washington
5	25	Arlis I	74°44'N161°10'W to 74°51'N167°7'W	Dec. 1960 to March 1961	Brayton University of Washington
6	4	Alpha	85°20'N172°40'W to 83°41.5'N164°40'W	Oct. 1957 to Dec. 1957	Farlow Woods Hole Oceanographic Institution
7	7	North Pole 2	78°53.4'N193°5'E to 81°28.2'N197°19'E	Sept. 1950 to April 1951	Gudkovich, Arctic and Antarctic Scientific Research Institute
8	4	T-3*	71°5'N145°5'W to 71°35'N149°59'W	Dec. 1959 to Feb. 1960	Kusunoki, Muguruma, Higuchi Hokkaido University

*indicates that the drift station was on an ice island or adjoining pack ice. The other drift stations were on open pack ice.

B - Series 1, 4, 5 and 7. In these series the salinity predicted by the Kraus-Turner-Ball model started to increase at a rate which, if continued, would provide a good fit to the data, but then leveled off, eventually reaching the same rate of increase predicted by the Zubov-Defant model. What happened in these cases was that the theoretically predicted profiles reached a depth at which the interface became so steep that the amount of energy released by the formation of 1 cm of ice was insufficient to entrain the much more saline layers below the interface. The reduction to the Zubov-Defant rate is undoubtedly due to the nature of the numerical procedure used, which requires sufficient energy to be available to entrain an entire layer before any entrainment can take place. If the procedure which allows partial entrainment of the layer immediately below the mixed layer had been used at least some entrainment would have continued. However, it is not certain which of these is a closer approximation to reality, since there have been indications (Lilly, personal communication, 1967) that the fraction of the turbulent energy recovered by entrainment decreases as the steepness of the pycnocline increases. The most convincing of this data is the data from Arlis I in series 4 and 5 (Brayton, 1961). It was taken from pack ice far removed from the possible disturbing effect of a deep ice island adjacent to the observing site (Coachman, personal communication, 1967). The data series are reasonably long, and contain many points closely

spaced in both time and depth. There are strong indications (for example, a large drop in salinity occurred between the two series) that the effect of horizontal advection and drift of the station was to reduce the salinity, so that the observed increase must have been entirely due to local mixing.

The theoretically predicted depth reached by the mixed layer at the time that the numerical model shows entrainment slowing to a standstill happens to be at about the depth of the steepest part of the halocline in the observed initial profile. This suggests that the type of penetrative convection described by the Kraus-Turner-Ball model has something to do with determining the depth of the steepest part of the halocline. The observed profiles at later times show that the depth of the mixed layer has increased little if at all, and that the salinity has increased by more than the predicted amount. These observations, as well as the salinity vs. time curves, can be explained if we assume that penetrative convection does extend to the theoretically predicted level, but other processes operate to continuously replenish the salt in the halocline. This salt is quickly mixed upward by the convection, increasing the salinity of the mixed layer by more than is predicted by theoretical calculations based on the original profile. Theoretical calculations based on observed profiles at later stations in each series show that the initial slope of the salinity vs. time curve predicted by the Kraus-Turner-Ball model is always such

that if this rate of increase were continued a reasonably good fit to later observations would be obtained.

The necessary upward salt transport can be accomplished either by upwelling ($w > 0$ on a large scale) or turbulent convection. Although some secondary mixing must take place to keep a sharp interface from developing, the absence of evidence of major penetration of surface properties into the intermediate layer of Atlantic water (below 200 to 250 meters) makes it seem likely that upwelling is an important mechanism by which upward salt transport takes place. The existence of upwelling is consistent with the notion, unproven but consistent with the little data that is available, that the inflow of Atlantic water into the Arctic Ocean, which occurs mostly at depths of several hundred meters, is largely compensated for by outflow closer to the surface in the East Greenland Current and between the islands of the Canadian Arctic Archipelago.

A rough estimate of the magnitude of upwelling required to produce the observed increase of salinity in the mixed layer can be obtained by approximating the actual profile by a two-layer system. If D is the depth of the upper layer, throughout which the salinity is increased by ΔS_1, S_2 is the salinity of the lower layer, and the water in a depth $w\Delta t$ passes from the lower layer into the upper layer in time Δt, we have approximately

$$(39) \qquad (w\Delta t)S_2 = D\Delta S_1$$

If D is assumed to be the depth of the mixed layer, and S_1 the salinity just below the steep part of the halocline, we have, using one set of numbers picked at random from the data in group B,

$D = 40$ meters

$\Delta S_1 = 1.1\%$

$S_2 = 31.3\%$

$\Delta t = 1.6 \ 10^{+7}$ seconds (200 days)

$w = 2.3 \cdot 10^{-7}$ m/sec $\sim$ 3 to 5 meters in 6 months

This is a reasonable rate of upwelling, less than the rate usually assumed to take place in the main thermocline in lower latitudes but it is doubtful if it is this strong so close to the surface, particularly in areas such as the Beaufort Sea where the surface flow is believed to be strongly convergent (Campbell, 1964 and 1965). Probably w is a maximum at the base of the halocline, 200 to 250 meters deep, and mixing becomes progressively more important above this level. The upwelling must be a steady state motion in order to avoid still further theoretical difficulties.

This theory leaves the actual depth of the mixed layer unexplained. The explanation is probably connected with the scale of turbulent eddies in the secondary mixing that takes place in the halocline.

C - The development of the profile between the third and fourth stations of series 8 was obviously determined primarily by

wind mixing. Three blizzards, two of them unusually intense, took place during the interval of time between these stations; for 6 of the 14 days, the ice drift speed varied from 30 to 40 cm/sec, or about 10 times the usual speed (Kusunoki, 1963). The numerical calculation (see Fig. 19) shows that the energy input due to wind mixing is on the order of $E^* = 800$ to 1000. Recalling our earlier calculation that $E^* = \mathcal{O}(1)$ most of the time, we see that if the wind speed is assumed to be roughly proportional to the speed of the ice drift, this is in rough agreement with the result of the Kraus-Turner theory that the energy input is proportional to the cube of the wind speed. The observed depth of the mixed layer after mixing was 175 meters, while the numerical calculation predicted 141 meters, again in rough order of magnitude agreement.

In Figures 11 through 18 triangles are observed points, dashed lines are salinity calculated by the Zubov-Defant model and solid lines are salinity calculated by the Kraus-Turner-Ball model.

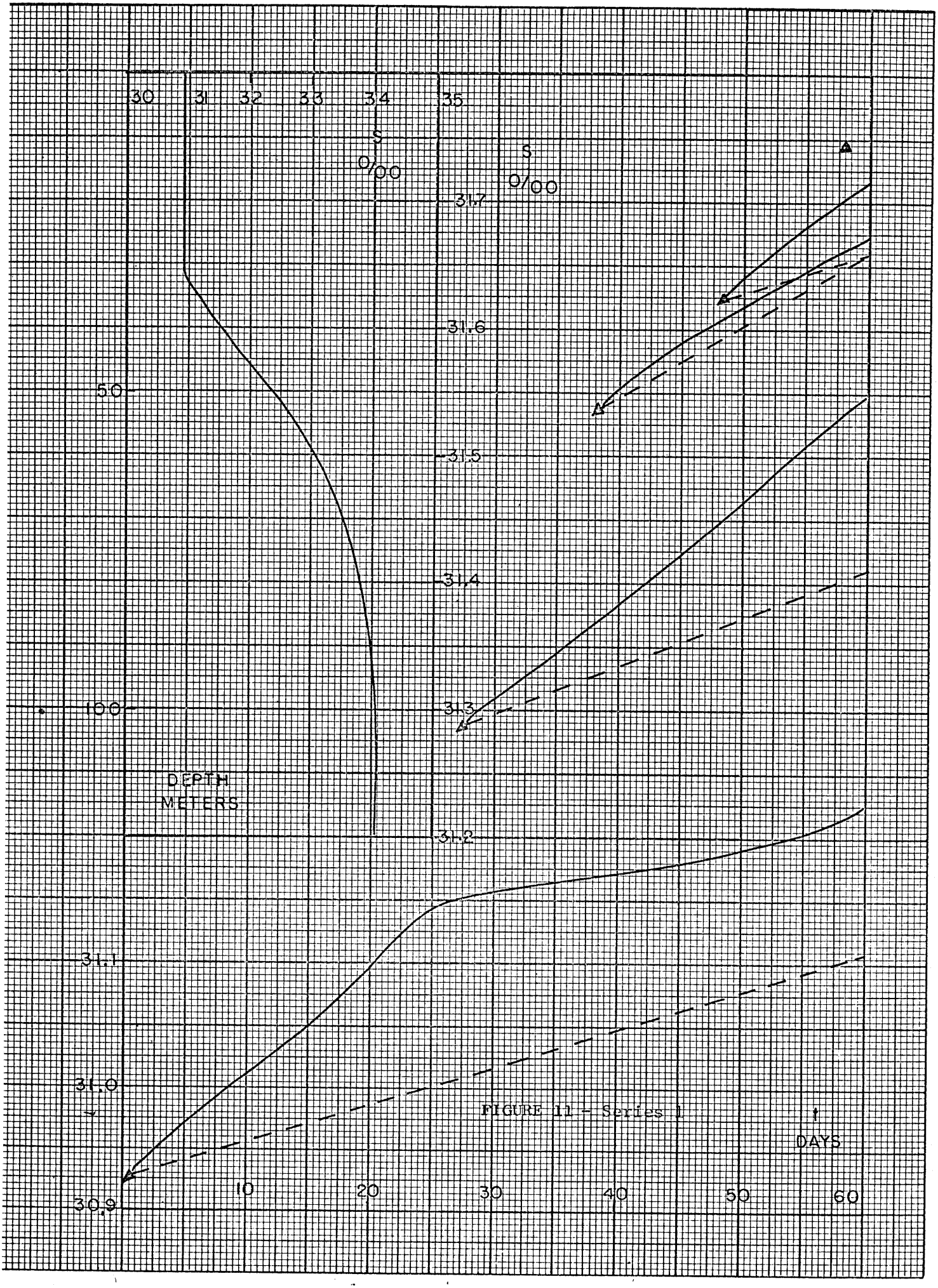

FIGURE 11 - Series I

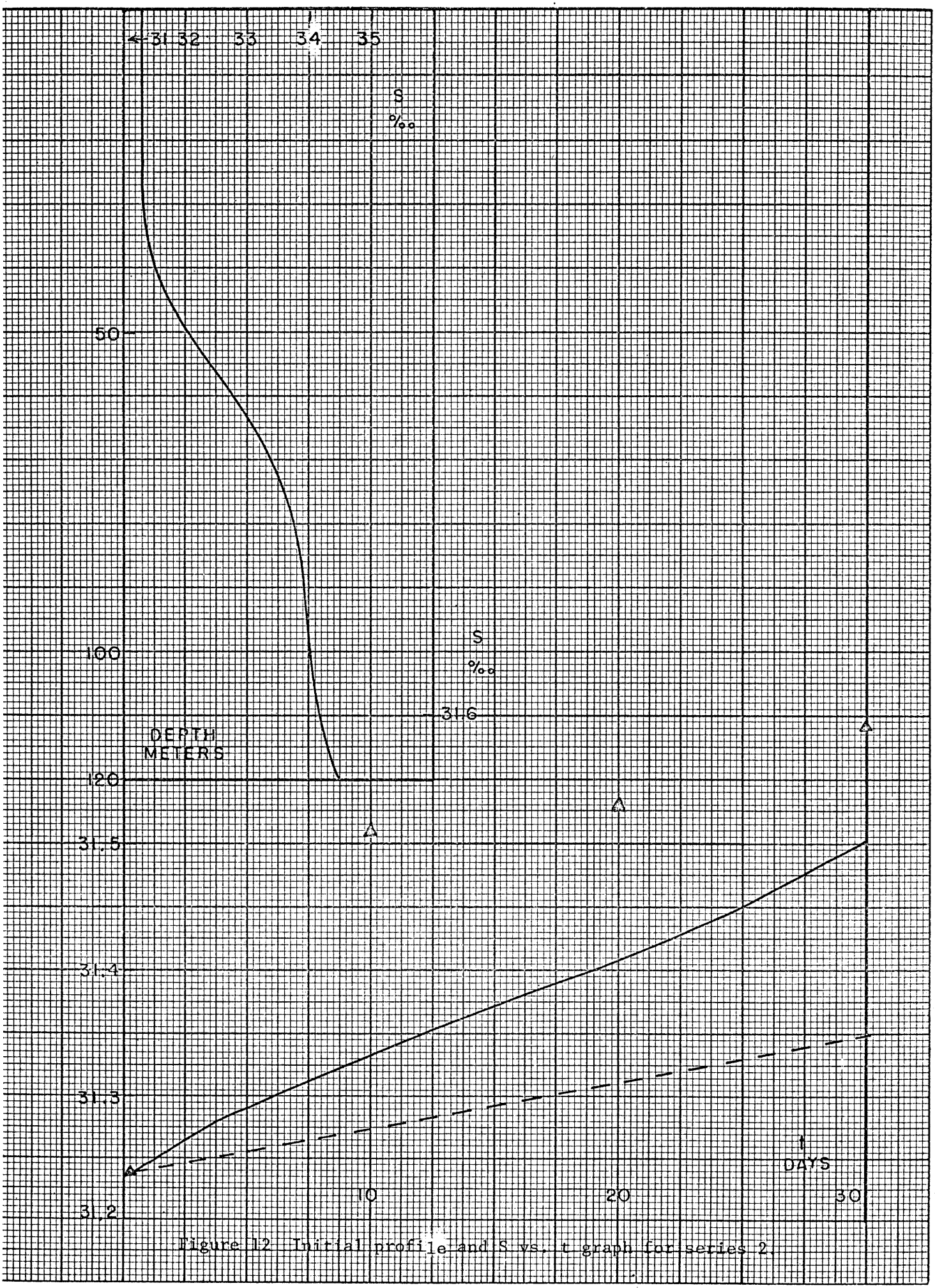

Figure 12 Initial profile and S vs. t graph for series 2

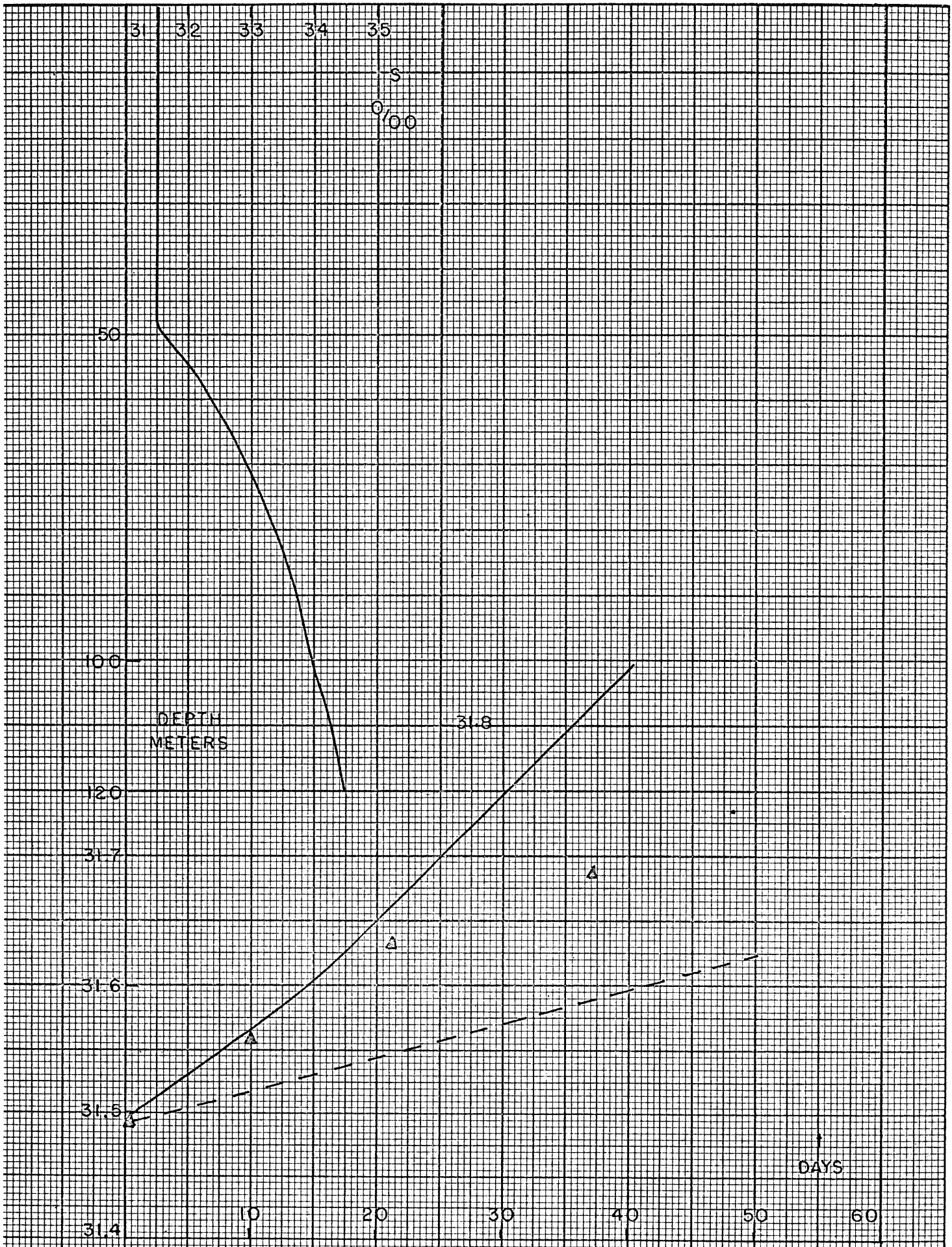

Figure 13. Initial profile and S vs t graph for series 3.

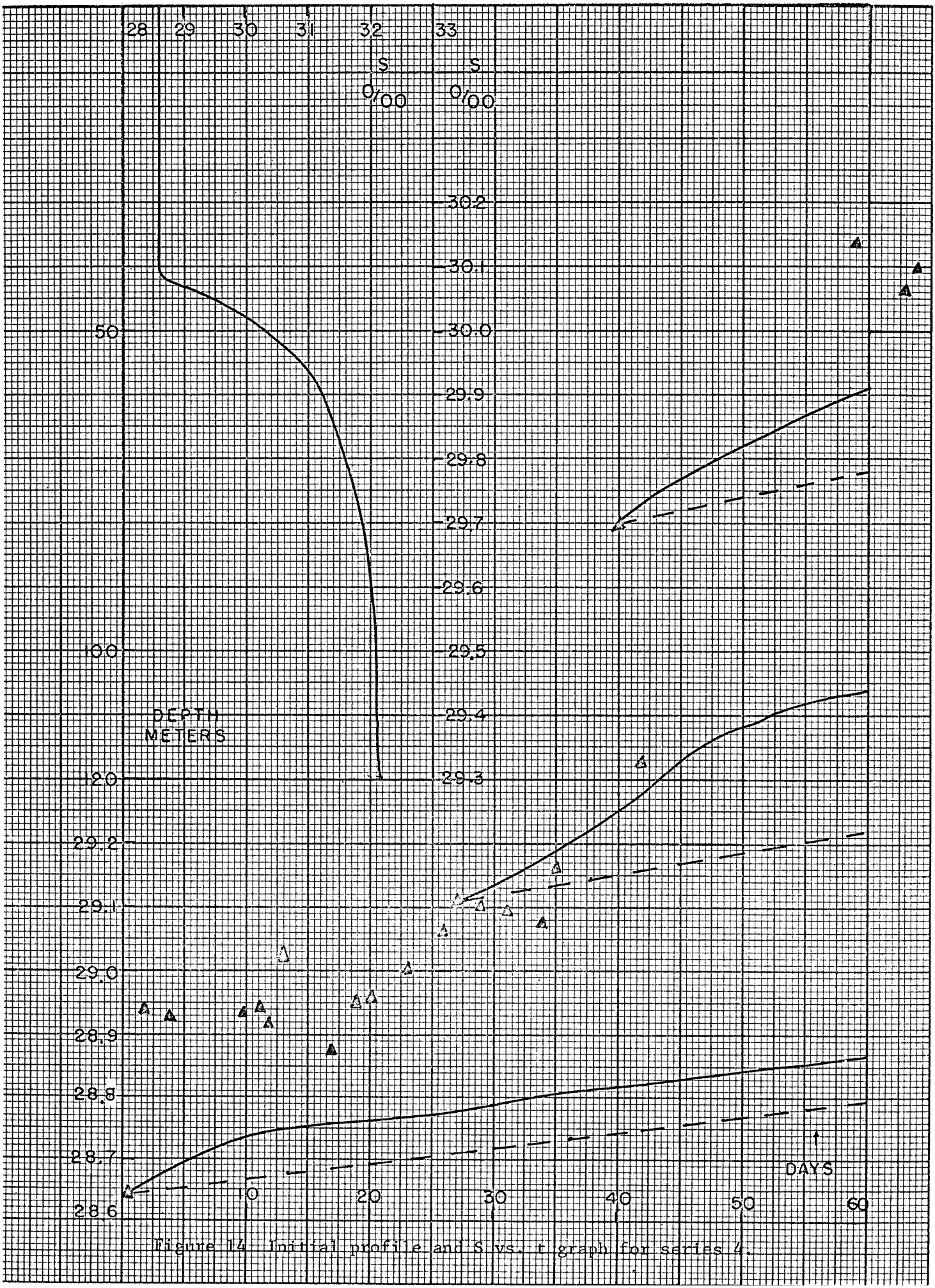

Figure 14 Initial profile and S vs. t graph for series 4.

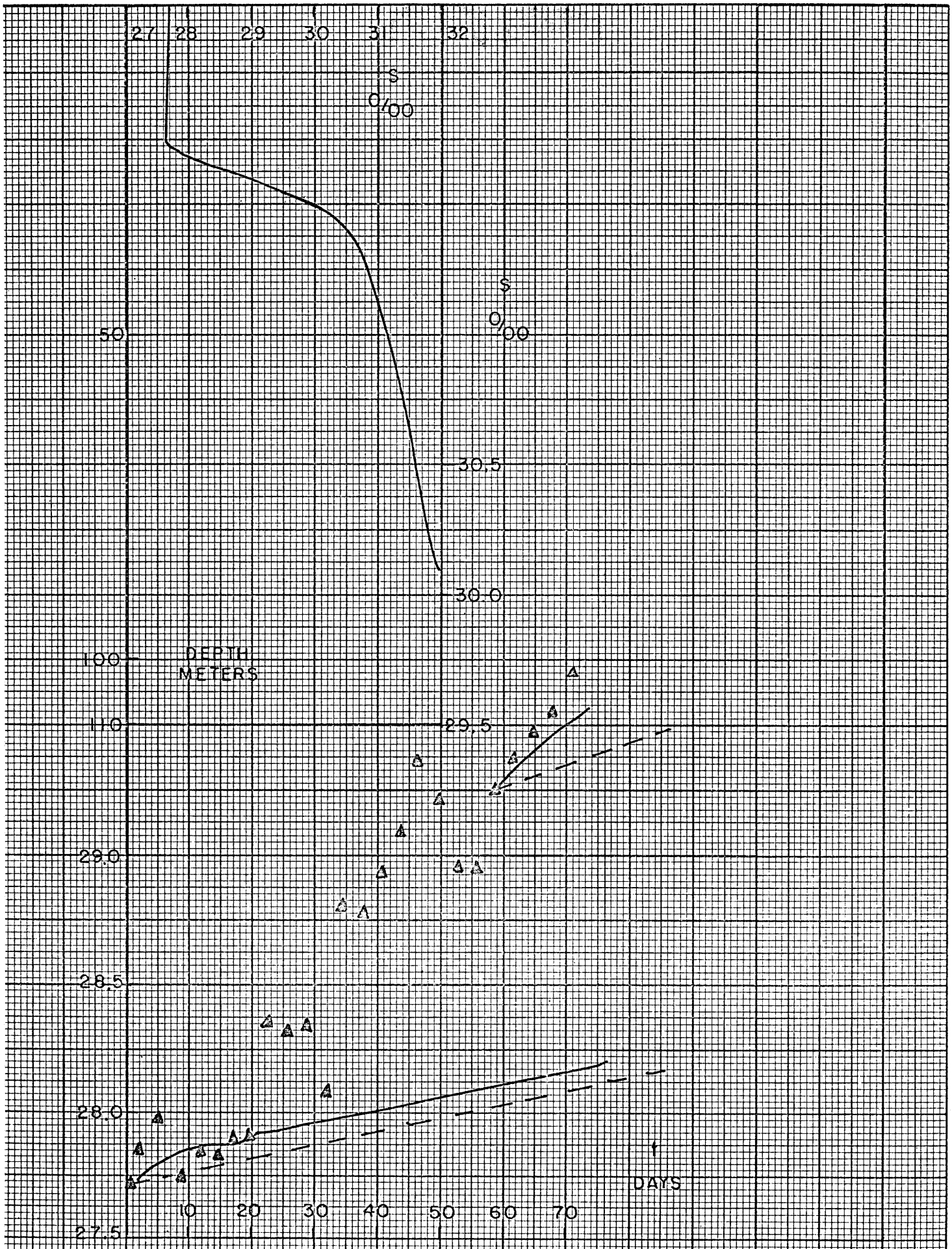

Figure 15 Initial profile and S vs. t graph for series 5.

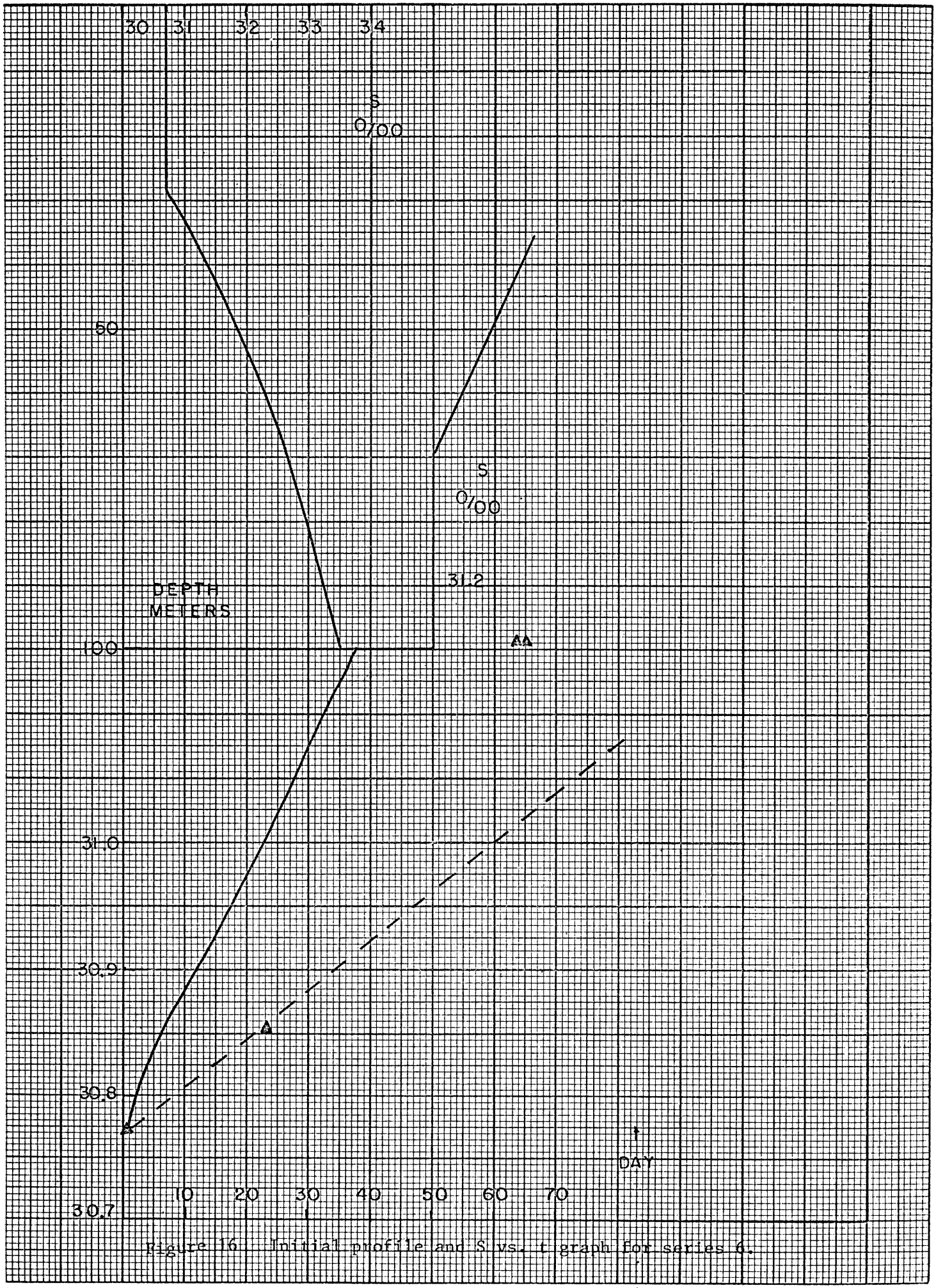

Figure 16. Initial profile and S vs. t graph for series 6.

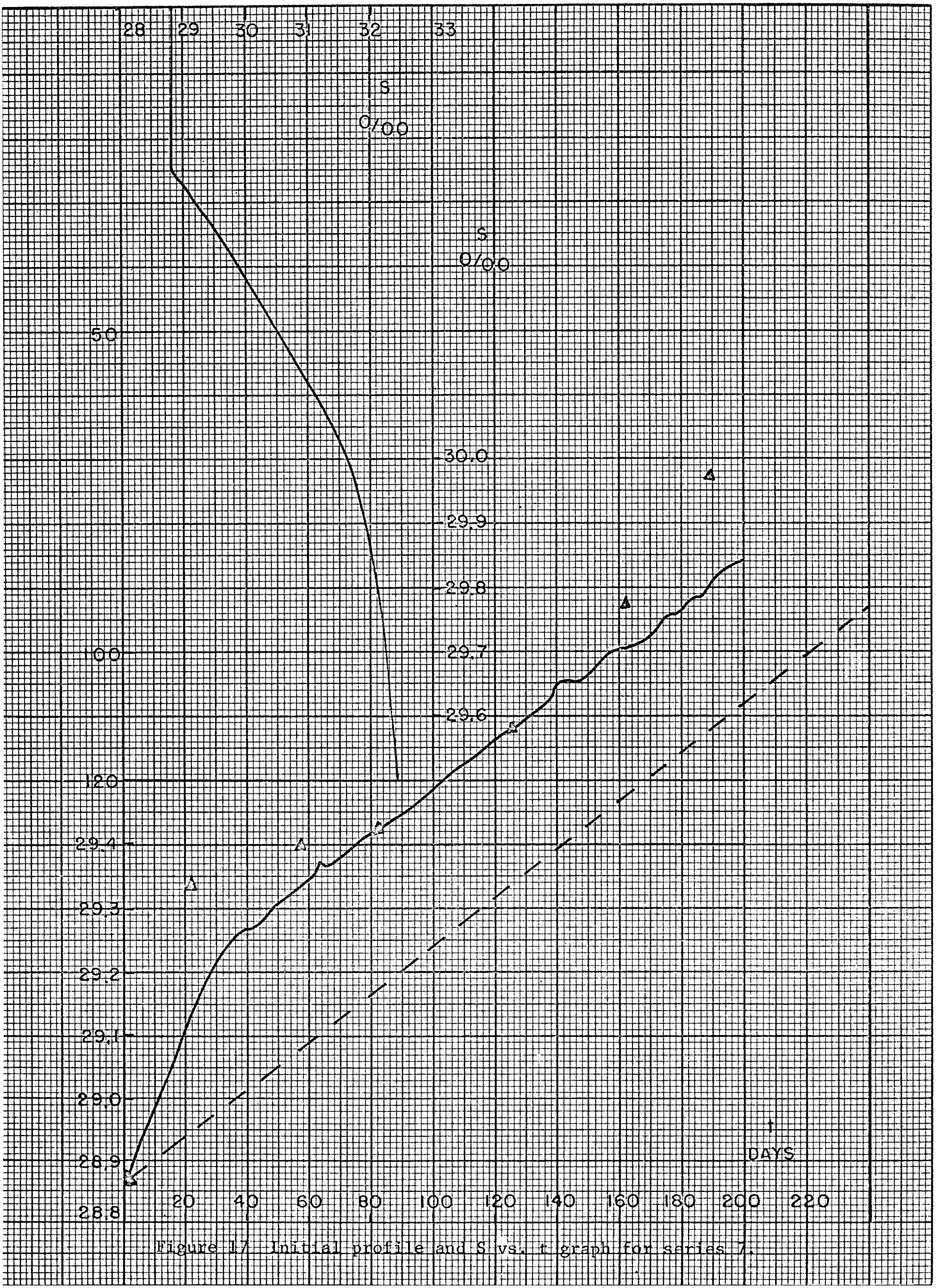

Figure 17 Initial profile and S vs. t graph for series 7.

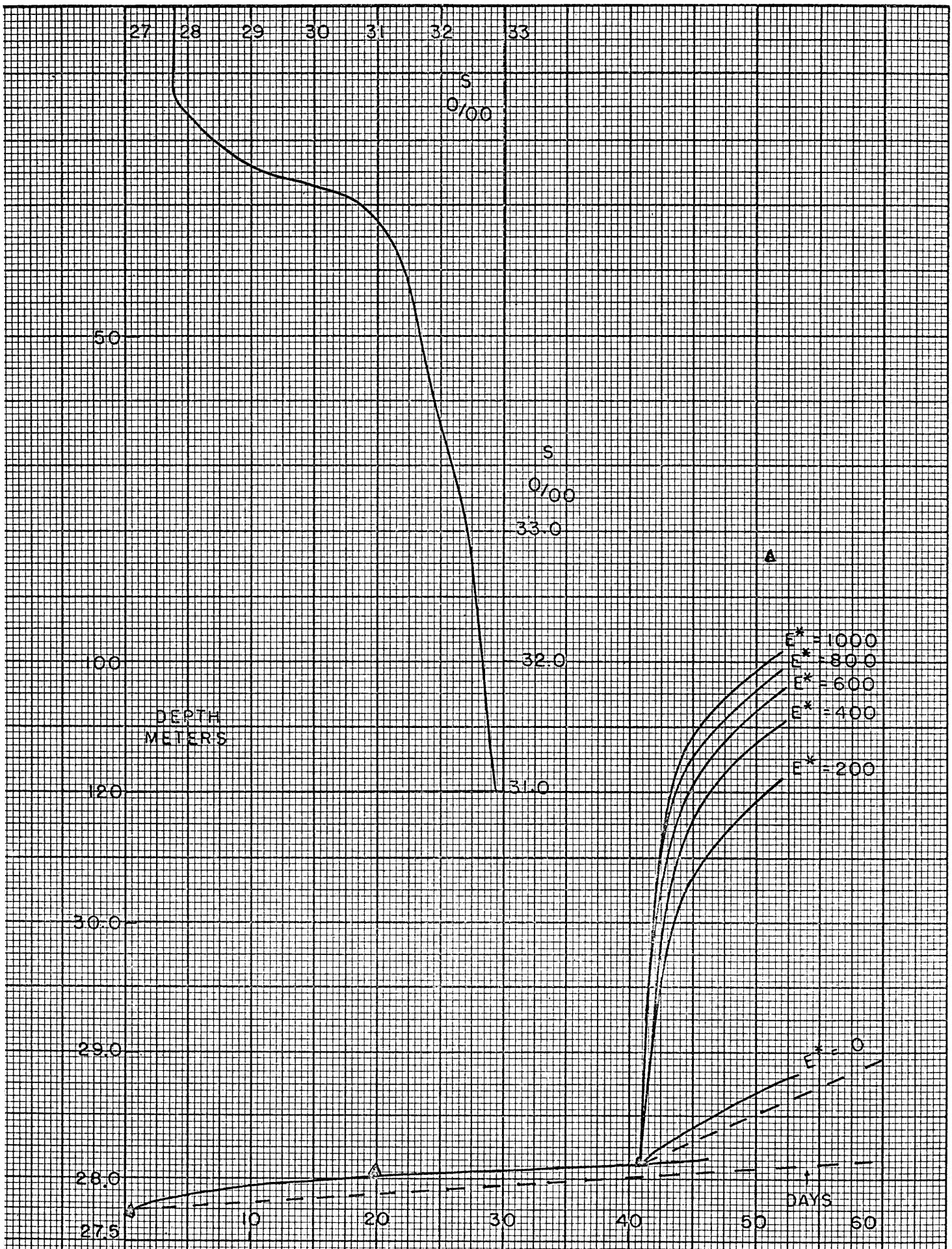

Figure 18. Initial profile and S vs. t graph for series 8. Note effect of wind mixing during the period of intense blizzards.

Chapter 3

THE TWO-LAYER MODEL

The basic dynamical model in this study is an ocean initially at rest with a stable density stratification that is horizontally uniform at $t = 0$, when ice starts to form at a horizontally varying rate. The ocean is assumed to lie on an f-plane; that is, on a plane surface in uniform rotation around a vertical axis with the centrifugal acceleration incorporated into the net local gravitational acceleration. For simplicity the ocean is assumed to be infinite in one horizontal direction, namely, the Y-direction. No variation of any of the dependent variables is permitted in the Y-direction, but there is a Y-component of velocity V. There is no forcing other than the variation of ice formation in the X-direction. The ocean is bounded by rigid frictionless vertical sidewalls at $X = 0$ and $X = L$, since finite boundaries are necessary for numerical computation.

The two-layer quasigeostrophic model is the simplest possible model which retains the essential features of the motions which we want to study. Since gravity waves are filtered out of the governing equation, it is computationally feasible to retain a free surface, so that the barotropic response of the system can be studied. This model also gives an estimate of the tendency of the interface at the bottom of the mixed layer to be deformed by dynamical motion (other than gravity waves) and of that part of

the baroclinic motion which is associated with this deformation. Further, it should be noted that there is often a steep halocline below the mixed layer, so that the response of a continuously stratified system can often be approximated by a two-layer model.

Horizontal momentum, as well as salt, is assumed to be rapidly and thoroughly mixed, with respect to the time scale of the seasonal forcing by the density-induced convection in the upper layer. Sverdrup used this assumption in his theory of the wind-driven ice drift even in the summer season, when it is less justified (because of the weaker vertical mixing) than in the winter problem being considered here. According to Rossby and Montgomery (1935) "the waters on the North-Siberian Shelf are characterized by a marked transition zone of great stability at a depth of 25 to 40m, separating an upper, lighter and practically homogeneous layer from a lower, heavier layer. The upper, homogeneous layer has, according to Sverdrup, a very high eddy-viscosity; he concludes that this water slides with the ice as a solid body over the lower, stable layer, there being practically no frictional stress in the transition zone." Rossby and Montgomery go on to question the validity of this assumption under certain conditions <u>in summer</u> but specifically exclude from their criticism the case when no shallow stable layer is present <u>immediately</u> below the ice, as is the case in winter and possibly part of the time even in summer. More recently Soviet Arctic oceanographers have reported observational evidence that the surface layer under the ice does in fact

move as a unit (Coachman and Barnes, 1961). Hunkins (personal communication, 1968) has also reported evidence of a relatively uniform horizontal velocity within the mixed layer, with strong shear immediately below the mixed layer.

For completeness it must be pointed out that mixed layers which are produced entirely by wind mixing in situations where the surface density flux tends to increase the stability do have velocity shear. It is known that the depth of the mixed layer equals the depth of the Ekman layer in this case (Rossby and Montgomery, 1935). Hence, it cannot be asserted that the existence of a layer well-mixed in temperature and salinity necessarily implies that momentum is well-mixed. This evidently depends on the relative strength of the vertical mixing and of the forces tending to create a velocity shear. In open water in the summertime the wind must do work against buoyancy forces to keep the mixed layer well-mixed; meanwhile, it provides a strong stress at the sea surface which tends to produce a velocity shear. Under winter conditions, the surface density flux adds to the wind mixing in keeping the ocean stirred up. In addition, when ice cover is present the wind is not nearly as effective in driving the sea surface. The observational evidence, together with Sverdrup's success in calculating ice drift using the "solid block" assumption, seems to indicate that momentum in the mixed layer is very strongly mixed, if not completely; at least, the assumption of complete mixing is a better approximation than the only other alternative of equivalent computational

simplicity, which is to neglect momentum mixing entirely. Even if we were to accept the computational complication of a vertical eddy viscosity, our observational knowledge of the mixing process is not adequate to permit us to achieve a demonstrably higher degree of accuracy than is obtained with the simpler assumption of complete mixing. In the case of the idealized models considered here, there is the additional factor that wind stress is neglected, and the only forcing is that due to the density distirbution (which itself is vertically well-mixed), so that the impulse is distributed much more evenly with depth than when there is a strong surface wind stress for the large-scale motions. The vertical momentum mixing is not so strong as to upset hydrostatic equilibrium.

Equations for the Two-Layer Model

The derivation of the equations for the two-layer model is considerably simplified if we assume from the beginning that the ice formation and the dynamical adjustment to the resulting density field are to be carried out separately, in alternating steps. This turns out to be necessary, or at least highly convenient, in any event. The strong vertical momentum mixing continues to operate during the dynamical steps. This makes it possible to use velocity components that are independent of z, in spite of the presence of a horizontal density gradient.

The basic dynamical equations arise from the require-

ments of conservation of mass and momentum in each of the layers. The ice will be assumed to constitute a separate layer in the initial derivation; suitable simplifications will subsequently be made. The notation for the two-layer model is given in Fig. 19.

1. Equations for the Ice Layer

Existing theoretical treatments of sea ice dynamics are extremely primitive. All models that have been published assume the ice to be a thin layer of fluid on top of the liquid ocean. The rationale for this is that the ice is broken up into many floes which are much smaller than the length scale of primary interest and are capable of independent motion, subject to interactions with each other which vaguely resemble the interactions between molecules in a fluid. The massed ice floes do behave somewhat differently than sea water, of course; this subject will be taken up in more detail when we come to the simplification of the basic equations. First, the equations will be derived in a more general form.

The equation of conservation of mass in the ice layer is:

$$\frac{\partial I}{\partial t} + \frac{\partial}{\partial x}(I u_I) = 0 \tag{40}$$

The equation for the conservation of the x-component of momentum involves pressure, of course. In applying the concept of pressure to the ice layer it is convenient to assume the existence

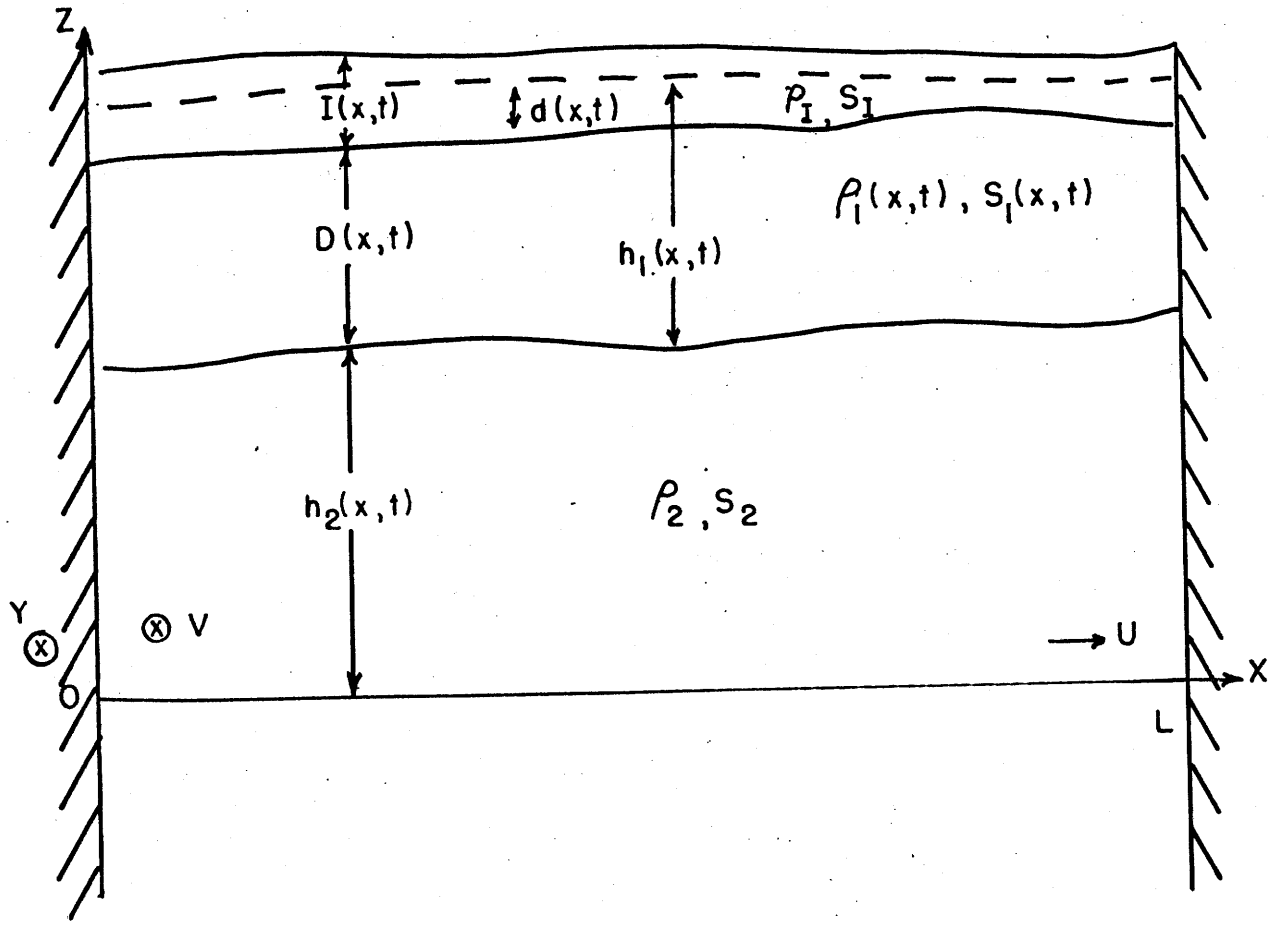

Figure 19 - Notation for the two-layer model. The horizontal solid lines are, from the top down, the top of the ice, the bottom of the ice, the interface between the turbulent and nonturbulent layers and the line Z = 0. Z = 0 is at the bottom if the depth of the ocean is finite; otherwise it is at an arbitrary reference level deep enough so that $h_2 > 0$ at all times. Rigid frictionless sidewalls are at X = 0 and X = L. The dotted line is the level of the free water surface in open leads in the ice.

of very narrow open leads at, say, X and $X+\Delta X$ (Fig. 20). The pressure force along the side of an adjacent ice floe is then the surface integral of the fluid pressure P_1 in the lead. The upper limit of integration is at the height $Z=h$, which is at the surface of the liquid water in the leads. h is determined by the requirement that the weight of a water column in the lead must equal the weight of an ice column in an adjacent ice floe. h is then given as

$$(41)\quad h=h_1+h_2=D+d+h_2=D+\alpha I+h_2$$

The pressure P_I should not be thought of as having any significance in terms of measurable forces within the solid ice. Suppose, for example, that a wedge-shaped block of ice is sitting on a table, as in Fig. 21. There is, of course, a pressure gradient $\frac{\partial P_*}{\partial X}$ within the ice, but the ice does not flow downhill. Therefore there must be a force F, equal and opposite to the force of the pressure gradient, which holds the ice in a rigid shape. Because of the presence of this force the actual pressure P_* within the solid ice does not have any significance in the calculation of oceanic motions. It is, in fact, entirely possible for $\frac{\partial P_I}{\partial X}$, which is determined by the slope of the surface of the ocean on which the ice floats, to have a direction opposite to $\frac{\partial P_*}{\partial X}$, which is determined by the thickness of the ice itself. It is obvious from Fig. 22 that the significance of $\frac{\partial h}{\partial X}$, which is related to $\frac{\partial P_I}{\partial X}$, is that the ice on the left, although thinner,

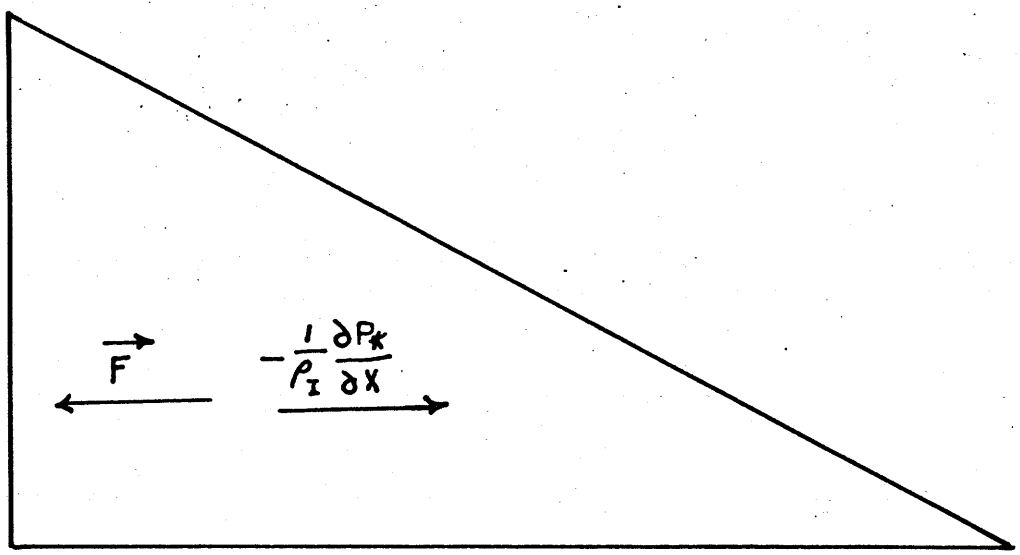

Figure 21 (see below).

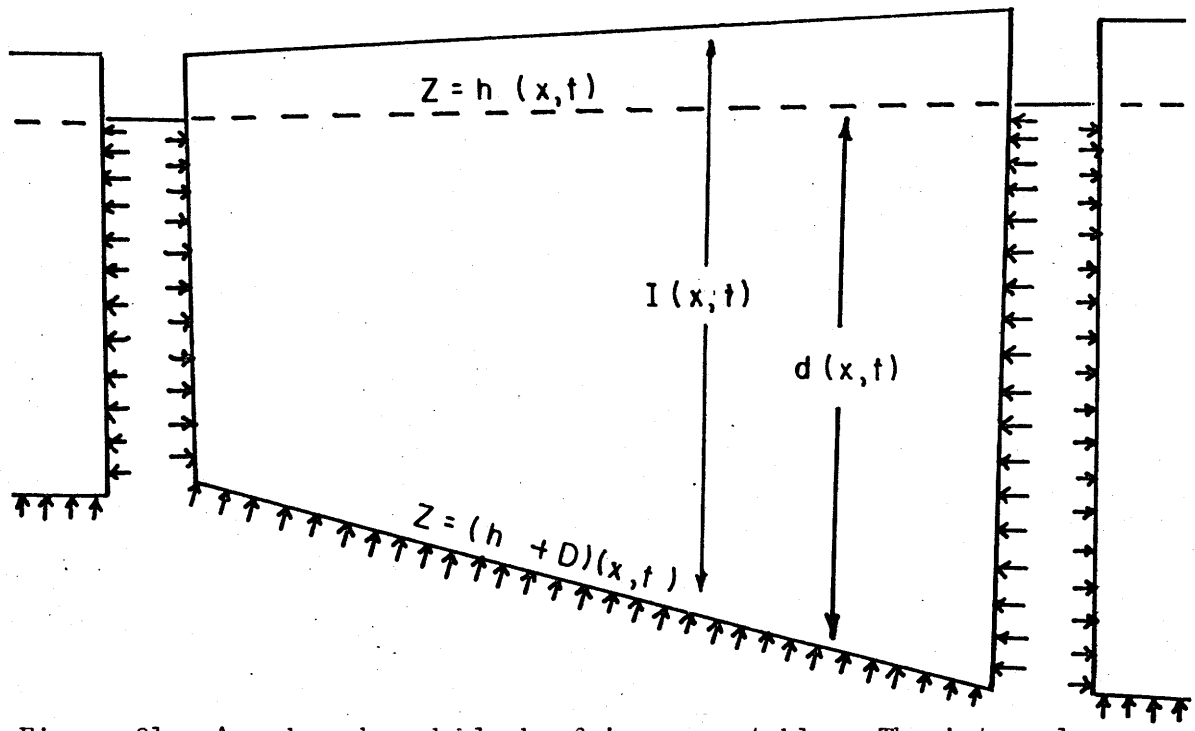

Figure 21 - A wedge-shaped block of ice on a table. The internal pressure gradient is balanced by a force F.

Figure 20 - The pressure on an ice floe.

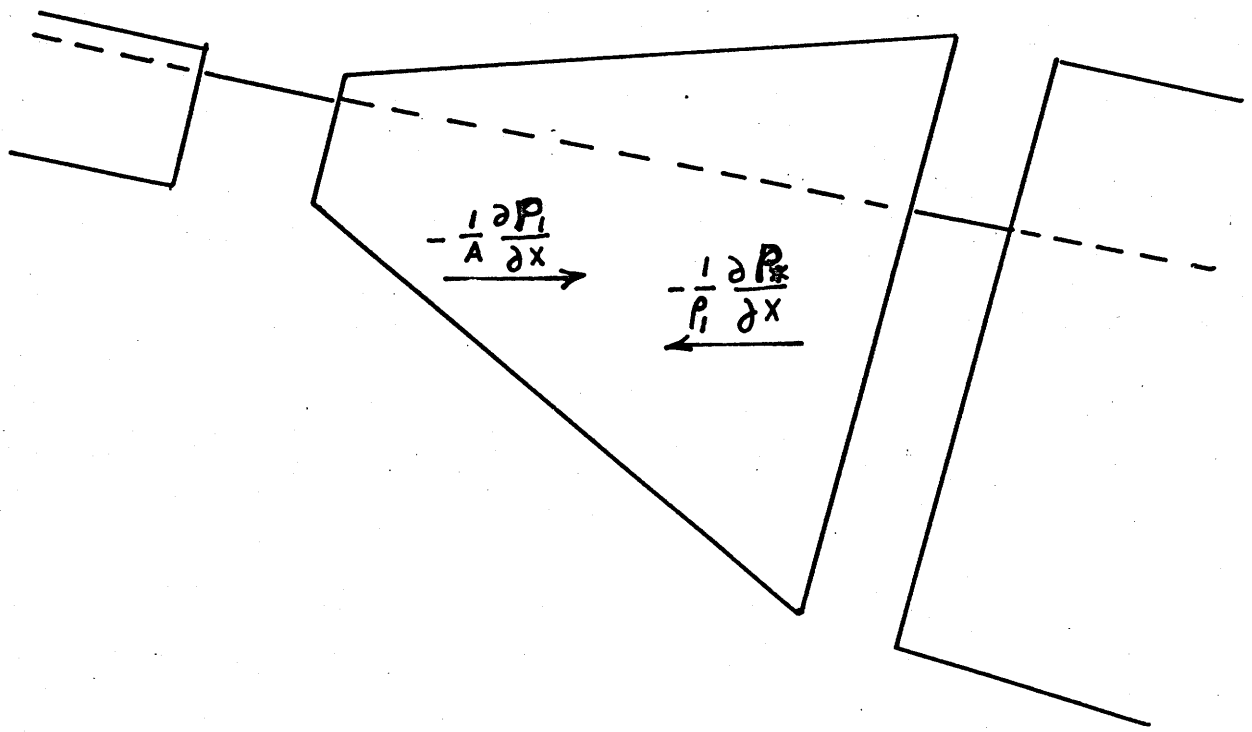

Figure 22 - Illustration of a case in which the fluid pressure P_I decreases to the right even though the internal ice pressure P_* increases.

floats higher than the ice on the right because the water level is higher. Therefore the pressure P_I at a fixed height Z will be higher even though the ice is thinner. It is this pressure that determines the geostrophic current in the thin layer of fluid which is being used to model the ice. (Fig. 22 is drawn with an exaggerated scale; actually, 90% of the ice should be below the water level.)

With the aid of Fig. 20, assuming the open leads to be at X and $X+\Delta X$; we can write the equation for the conservation of the X-component of momentum in difference form as

$$(42)\quad \left[\rho_I I U_I \Delta X\right]_t^{t+\Delta t} + \left[\rho_I I U_I^2 \Delta t\right]_X^{X+\Delta X} = -\left[\int_{h_2+D}^{h} P_I dz\, \Delta t\right]_X^{X+\Delta X} - P_I(D)\frac{\partial(h_2+D)}{\partial X}\Delta X \Delta t + \rho_I f I V_I \Delta X \Delta t$$

$P_1(D) = P_I(D)$ since both are given by the hydrostatic pressure of the ice. Using this, and adding $P_I(h)\frac{\partial h}{\partial X}\Delta X \Delta t$ (which is identically zero) to the right-hand side of (42), we obtain the differential form of the equation:

$$(43)\quad \rho_I \frac{\partial}{\partial t}(I U_I) + \rho_I \frac{\partial}{\partial X}(I U_I^2) = -\int_{h_2+D}^{h} \frac{\partial P_I}{\partial X} dz + \rho_I f I V_I$$

(ρ_I is a constant.) Using the hydrostatic equation,

$$(44)\quad P_I = \rho_1 g (h - z)$$

this becomes

$$(45)\quad \rho_I \frac{\partial}{\partial t}(IU_I) + \rho_I \frac{\partial}{\partial x}(IU_I^2) = -\left(\rho_1 g d \frac{\partial h}{\partial x} + \frac{1}{2} g d^2 \frac{\partial \rho_1}{\partial x}\right) + \rho_I f I V_I$$

The equation expressing conservation of the Y-component of momentum is analogous except that the pressure gradient terms are absent because the model ocean is uniform in the Y-direction.

$$(46)\quad \frac{\partial}{\partial t}(IV_I) + \frac{\partial}{\partial x}(IU_I V_I) = -f I U_I$$

2. Equations for the Mixed Layer

ρ_1, U_1 and V_1 are independent of Z because of the strong vertical mixing. The equations for the mixed layer are derived in an analogous way to the equations for the ice layer.

Conservation of mass:

$$(47)\quad \frac{\partial}{\partial t}(\rho_1 D) + \frac{\partial}{\partial x}(\rho_1 D U_1) = 0$$

Conservation of the X-component of momentum:

$$(48)\quad \frac{\partial}{\partial t}(\rho_1 D U_1) + \frac{\partial}{\partial x}(\rho_1 D U_1^2) = -\int_{h_2}^{h_2+D} \frac{\partial P_1}{\partial x} dz + \rho_1 f D_1 V_1$$

Using the hydrostatic equation,

$$(49)\quad P_1 = \rho_1 g (h - z)$$

we obtain

$$(50)\ \frac{\partial}{\partial t}(\rho_1 D U_1)+\frac{\partial}{\partial x}(\rho_1 D U_1^2)=-\left[\rho_1 g D\frac{\partial I}{\partial x}+\rho_1 g D\frac{\partial h_2}{\partial x}+g\frac{\partial}{\partial x}\left(\tfrac{1}{2}\rho_1 D^2\right)\right]+\rho_1 f D V_1$$

Conservation of the Y-component of momentum:

$$(51)\ \frac{\partial}{\partial t}(\rho_1 D V_1)+\frac{\partial}{\partial x}(\rho_1 D U_1 V_1)=-\rho_1 f D U_1$$

3. Equations for the Lower Layer

For a lower layer of finite depth, the derivations proceed in a manner similar to the derivations for the other layers. U_2 and V_2 are independent of Z because of the absence of a density gradient in the lower layer (in this model).

Conservation of mass:

$$(52)\ \frac{\partial h_2}{\partial t}+\frac{\partial}{\partial x}(h_2 U_2)=0$$

Conservation of the X-component of momentum:

$$(53)\ \rho_2\frac{\partial}{\partial t}(h_2 U_2)+\rho_2\frac{\partial}{\partial x}(h_2 U_2^2)=-\int_0^{h_2}\frac{\partial p_2}{\partial x}dx+\rho_2 f h_2 V_2$$

The hydrostatic equation is

$$(54)\ p_2=\rho_1 g h_1+\rho_2 g(h_2-z)$$

which leads to:

$$(55)\ \rho_2\frac{\partial}{\partial t}(h_2 U_2)+\rho_2\frac{\partial}{\partial x}(h_2 U_2^2)=-g\frac{\partial}{\partial x}(\rho_1 h_1+\rho_2 h_2)+\rho_2 f h_2 V_2$$

Conservation of the Y-component of momentum:

$$(56)\quad \frac{\partial}{\partial t}(h_2 v_2) + \frac{\partial}{\partial x}(h_2 u_2 v_2) = -f h_2 u_2$$

If the lower layer is of infinite depth, the velocity must be zero, because it is independent of depth, so that the system would have to have infinite energy to maintain a nonzero velocity. Zero velocity implies that there are no accelerations to balance the pressure gradient, which must therefore also be zero. The equations are

$$(57)\quad u_2 = 0$$

$$(58)\quad v_2 = 0$$

$$(59)\quad \frac{\partial}{\partial x}(\rho_1 h_1 + \rho_2 h_2) = 0$$

where h_2 is measured from an arbitrary reference level. These equations, together with the equations for the mixed layer and the ice layer, are sufficient to determine $\frac{\partial h_2}{\partial x}$, but to find h_2 itself, it is necessary to add the condition that the total mass above the reference level $Z = 0$ is conserved:

$$(60)\quad \frac{\partial}{\partial t}\int_0^L (\rho_1 h_1 + \rho_2 h_2)\, dx = 0$$

The Freezing Steps

Ice formation takes place in steps that are alternated

with the dynamical steps during the actual calculation. The changes in the salinity and depth of the mixed layer can be found from the equations for a two-layer ocean in chapter 2. Once these are found, the transfer of momentum from one layer to another by the freezing and mixing processes must be taken into account. Using primes to denote quantities at the end of the freezing step, we have, for the increase in momentum of the ice layer due to the acquisition of moving water by freezing,

$$(61)\quad \rho_I I' U_I' = \rho_I I U_I + \rho_1 \left[1 - 10^{-3}(S_1 - S_I)\right] \Delta I U_1$$

or

$$(62)\quad U_I' = \frac{I}{I'} U_I + \alpha \left[1 - 10^{-3}(S_1 - S_I)\right] \frac{\Delta I}{I'} U_1 \,.$$

All quantities on the right are known from the basic mixing calculation. ΔI is the increment of ice due to freezing only; changes due to dynamical motions do not enter into this calculation. In an exactly analogous way we obtain

$$(63)\quad V_I' = \frac{I}{I'} V_I + \alpha \left[1 - 10^{-3}(S_1 - S_I)\right] \frac{\Delta I}{I'} U_1 \,.$$

The salinity terms will make a difference of not over about 3% in the result, and can be neglected if this degree of accuracy is not required.

The transfer of momentum from the mixed layer to the ice layer by freezing does not change the velocities in the mixed layer. However, if the Kraus-Turner-Ball theory is used for mixing,

the entrainment of momentum from the lower layer into the upper layer must be accounted for according to

$$(64) \quad D'U_1' = DU_1 + \rho_2 U_2 \Delta h_2$$

where Δh_2 is the change in the height of the interface due to salt convection alone. Similarly,

$$(65) \quad D'V_1' = DV_1 + \rho_2 V_2 \Delta h_2$$

Dynamics of the Ice Layer

The outstanding difference between the dynamical behavior of an aggregate of ice floes and that of liquid sea water is the fact that ice resists horizontal convergence more than horizontal divergence, and the strength of this resistance. The pressure ridges and hummocks which are so familiar in photographs of the Arctic and the constant cracking of the thick ice floes are evidence of the large amount of energy that is dissipated by what is called "internal ice resistance" in macroscale dynamical problems. This effect must be taken into account in the equations for the ice layer.

The general form of the equation of motion for a layer of sea ice, as written by Campbell (1964, 1965), is:

$$(66) \quad \rho_i h \frac{d\vec{V}_i}{dt} = \vec{\tau}_A + \vec{\tau}_w + \vec{D} + \vec{G} + \vec{R}$$

The notation, which is taken directly from Campbell and does not have any relation to the use of the same symbols elsewhere in the present report, is as follows:

ρ = density of sea ice.

h = thickness of the ice

$\vec{V}_i$ = horizontal vector velocity of the ice.

$\vec{\tau}_A$ = wind stress at the air-sea interface.

$\vec{\tau}_w$ = water stress at the ice-water interface.

$\vec{D}$ = Coriolis force.

$\vec{G}$ = pressure gradient force due to the tilting of the surface of the sea on which the ice floats.

$\vec{R}$ = internal ice stress.

All models published to date have been concerned with equilibrium ice drift, with $\frac{d\vec{V}_i}{dt} = 0$. The chief differences between the models have been in which of the other terms are retained in the balance of forces, in the form of the ice resistance terms, and in the form of the stress terms. Most of the models (Sverdrup, 1928; Rossby and Montgomery, 1935; Shuleikin, 1938; Felzenbaum, 1958) have used an ice resistance term which is analogous to the representation of friction by a simple force proportional and opposite to the velocity. Such models have, with the proper "fudge factors", given more or less reasonable results for the problem of calculating the drift of single ice floes from a given wind stress. In the most recent and most sophisticated model, Campbell (1964, 1965) used a horizontal eddy viscosity, with a very

high Austausch coefficient, in a numerical model of the steady state wind-driven circulation of the entire Arctic Ocean. The results were reasonably good for some values of the eddy viscosity, but it is probable (Untersteiner, personal communication, 1967) that the eddy viscosity is not a good model in areas where the motion of the ice is divergent.

In the present work, with wind driving neglected, there isn't any need to attempt any degree of sophistication in modeling the internal ice resistance. The motions that can be expected to be generated by purely haline driving are rather weak, so that no significant differences in the result are likely to be produced by varying some parameter in any expression for the ice resistance. However, it is still necessary to model this effect in some way. This will be done in the simplest way possible - by taking the two extremes. The ice will either be assumed to not have any internal resistance at all, and to move as an integral part of the mixed layer, or it will be assumed to be completely unable to converge. Equations are derived for both cases, but only the former case was actually solved numerically.

1. Equations for the Case with No Internal Ice Resistance

Since the motion of the ice is frictionally coupled to that of the mixed layer, we have:

$$u_I = u_1 \tag{67}$$

$$v_I = v_1 \tag{68}$$

Substituting (67) and (68) into (40), (45) and (46) and then combining these with (47), (50) and (51), together with (41), gives the equations for an "equivalent" upper layer of ice and water:

$$(69)\quad \frac{\partial}{\partial t}(\rho_1 h_1) + \frac{\partial}{\partial x}(\rho_1 h_1 u_1) = 0$$

$$(70)\quad \frac{\partial}{\partial t}(\rho_1 h_1 u_1) + \frac{\partial}{\partial x}(\rho_1 h_1 u_1^2) = -\rho_1 g h_1 \frac{\partial h}{\partial x} - \frac{1}{2} g h_1^2 \frac{\partial \rho_1}{\partial x} + \rho_1 h f v_1$$

$$(71)\quad \frac{\partial}{\partial t}(\rho_1 h_1 v_1) + \frac{\partial}{\partial x}(\rho_1 h_1 u_1 v_1) = -\rho_1 f h_1 u_1$$

(40) must be retained in the system of equations if it is desired to calculate the dynamical effect on the thickness of the ice.

2. Equations for the Case when the Ice is Unable to Converge

This case was not solved numerically, and the following discussion is presented only for completeness. The inability of the ice to converge can be expressed mathematically as

$$(72)\quad \frac{\partial u_I}{\partial x} \geq 0$$

We will simplify the model at this point by restricting our consideration to cases in which ice is formed everywhere between rigid sidewalls. Then

$$(73)\quad \int_0^L \frac{\partial u_I}{\partial x}\, dx = u_I(L) - u_I(0) = 0$$

From (73), if $\frac{\partial U_I}{\partial x} > 0$ anywhere, it is necessary to have $\frac{\partial U_I}{\partial x} < 0$ somewhere else, but this would contradict (72), so that

$$\frac{\partial U_I}{\partial x} = 0 \tag{74}$$

(74), together with the boundary condition $U_I = 0$ at $X = 0$ and $X = L$, implies that

$$U_I = 0 \tag{75}$$

Then (40) implies (in the dynamical step)

$$\frac{\partial I}{\partial t} = 0 \tag{76}$$

The depth of the ice at each point is determined only by the amount of freezing that has taken place at that point since $t = 0$ (if we start with an ice-free ocean), and (46) implies that

$$\frac{\partial V_I}{\partial t} = 0 \tag{77}$$

$V_I = 0$ at $t = 0$, so this gives

$$V_I = 0 \tag{78}$$

Then (45) becomes

$$\rho_1 \frac{\partial h}{\partial x} + \frac{1}{2} d \frac{\partial \rho_1}{\partial x} = 0 \tag{79}$$

ρ_1 is determined during the freezing step, so that $\frac{\partial h}{\partial x}$ can be calculated directly from (79).

At this point it must be noted that if the frictional coupling of the ice to the mixed layer were to hold we would also

have $U_1 = 0$ and $V_1 = 0$, so that no motion could take place in the mixed layer. Although insufficient observational evidence is available to support any definite conclusions on this point, it is the opinion of the writer that some motion would probably take place in such a system. For purposes of the present model we may suppose that there is a thin boundary layer below the ice, below which the mixed layer behaves essentially as described by these equations. In actual practice the boundary layer is probably thickened somewhat by the strong vertical convection, so that there is some vertical velocity variation within the mixed layer. What is virtually certain is that because of the strong vertical mixing the motion will be weaker than in the case with no internal ice resistance.

The rest of this chapter deals exclusively with the case of no internal ice resistance.

Scale Analysis of the Equations

The equations will now be simplified by restricting them to quasigeostrophic motions and by making further use of the smallness of the percentage change in density (already partially accounted for in the equation of state). The subscript S will be used to denote scale factors where there is a possibility of confusion with actual physical variables.

ρ_S = a typical density of sea water at T = 0°C and S = 25‰

to 35‰.

$\Delta\rho_s$ = a typical yearly maximum value of the horizontal difference in the density of the mixed layer, from one side of the model ocean to the other. Since the upper layer is initially homogeneous, and the rate of freezing is zero at one side of the ocean, this is also the order of magnitude of the time difference of density in the mixed layer.

H_s = a typical thickness of the mixed layer.

ΔH_s = a typical space and time variation of the height of the interface.

L = the horizontal width of the channel. The driving will have a wavelength of $2L$, so L can be taken as an appropriate geometrical length scale.

U_s = a typical magnitude of the (ageostrophic) component of velocity. Since U = 0 at t = 0 for all x, and U = 0 at $x = 0$ and $x = L$ for all t, U can also be used to scale the space and time differences of U.

V_s = a typical magnitude of the (geostrophic) component of velocity and its space and time differences.

ω = the angular frequency corresponding to the seasonal time scale.

h_s = a typical space and time variation of the free surface height.

First consider the equation obtained by subtracting (69)

from (71). Replacing each variable by its scale factor and dividing through by the common factor $\rho_s H_s$ gives

$$(80) \quad O(\omega V_s) + O\left(\frac{U_s V_s}{L}\right) = O(fU_s)$$

L and ω are fixed, so in order to have the two terms on the left be of equal magnitude we would need to have

$$(81) \quad U_s = \omega L = \frac{2\pi}{180\ \text{DAYS}} \cdot 2000\ \text{KM} = 0.8 \frac{\text{M}}{\text{SEC}}$$

Speeds on this order are not observed in ice-covered regions, even in the presence of wind driving which is much stronger than the haline driving in this model. Therefore, it is consistent with observations to assume that

$$(82) \quad \frac{U_s}{L} < \omega$$

The balance in (80) then becomes

$$(83) \quad O(\omega V_s) = O(fU_s) \ .$$

or

$$(84) \quad \frac{U_s}{V_s} = \frac{\omega}{f}$$

The ratio $\frac{\omega}{f}$ is a type of Rossby number (evidently first used by Kibel.)

This result will now be used to scale (70) [after subtraction of (69)]. The order of magnitude balance is

$$(85) \quad O(\omega \rho_s U_s) + O\left(\rho_s \frac{U_s^2}{L}\right) = O\left(\frac{\rho_s g h_s}{L}\right) + O\left(\frac{g H_s \Delta\rho_s}{L}\right) + O(\rho_s f V_s)$$

Using (82), (84) and the fact that $\omega << f$, (85) reduces to the geostrophic balance:

$$(86)\quad O\left(\frac{\rho_s g h_s}{L}\right) + O\left(\frac{g H_s \Delta\rho_s}{L}\right) + O(\rho_s f v_s) = 0$$

A similar scale analysis holds for all of the equations which express conservation of the X-component of momentum. (70) becomes:

$$(87)\quad \rho_1 g \frac{\partial h}{\partial x} + \frac{1}{2} g h_1 \frac{\partial \rho_1}{\partial x} - \rho_1 f v_1 = 0$$

(55) becomes:

$$(88)\quad g \frac{\partial}{\partial x}(\rho_1 h_1 + \rho_2 h_2) - \rho_2 f h_2 v_2 = 0$$

(50) becomes:

$$(89)\quad \rho_1 g D \frac{\partial I}{\partial x} + \rho_1 g D \frac{\partial h_2}{\partial x} + g \frac{\partial}{\partial x}\left(\frac{1}{2}\rho_1 D^2\right) - \rho_1 f D v_1 = 0$$

(59) and (79) remain unchanged.

The equations will now be examined to see where the density can be taken outside of derivatives. Since the density change is the entire driving for the system, it can be expected that the changes in other dependent variables (especially the depths) are, in some sense, on the same order as the density change. Therefore, it is necessary to go through the scale analysis carefully.

First consider equation (71). The first term on the left-hand side can be expanded as:

$$(90)\quad \frac{\partial}{\partial t}(\rho_1 h_1 v_1) = \rho_1 h_1 \frac{\partial v_1}{\partial t} + \rho_1 v_1 \frac{\partial h_1}{\partial t} + h_1 v_1 \frac{\partial \rho_1}{\partial t}$$
$$\sim O(\rho_s \omega H_s v_s) + O(\rho_s \omega \Delta H_s v_s) + O(\Delta\rho_s \omega H_s v_s)$$

Since $\Delta\rho_s \ll \rho_s$, the third term in the expansion can be neglected compared to the first. Note that since the order of magnitude of ΔH_s is still unknown nothing can be said about the second term at this point, but at least the density can be taken outside of the derivative.

Now consider equation (69). The removal of ρ_1 from the derivative in the first term on the left is more difficult to justify than in the case of equation (71) because the velocity is missing, and the as yet unknown magnitude of ΔH_s becomes critical. We know from observational evidence that ΔH_s is not an order of magnitude larger than H_s ; it may be smaller or on the same order.

Let $R_o = \frac{\omega}{f}$ be the Rossby number associated with the local time derivative term.

$$R_o \approx \frac{1}{400} \text{ in numerical magnitude.}$$

Since $\omega L \approx 0.8$ m/sec, and $U_s \sim 0.05$ m/sec is a typical magnitude of current speeds in ice-covered regions, we have

$$(91)\quad \frac{U_s}{\omega L} \sim O(R_o^{1/2})$$

Note that this is a maximum; the value of U_s used here

is generated mainly by wind stress, which is absent from the present model.

The advective Rossby number is found from (84) and (91):

$$(92)\quad \frac{U_s}{fL} \sim O(R_o^{3/2})$$

$\frac{\Delta\rho_s}{\rho_s} \sim \frac{2}{1000}$ will be considered to be of $O(R_o)$.

Now expand (69) and substitute scale factors to obtain:

$$(93)\quad O(\omega\rho_s\Delta H_s) + O(\Delta\rho_s\omega H_s) + O\left(\frac{\rho_s H_s U_s}{L}\right) + O\left(\frac{\rho_s U_s \Delta H_s}{L}\right) + O\left(\frac{\Delta\rho H_s U_s}{L}\right) = 0$$

Dividing (93) through by $\omega\rho_s H_s$ and replacing known ratios by their Rossby number equivalents gives

$$(94)\quad O\left(\frac{\Delta H_s}{H_s}\right) + O(R_o) + O(R_o^{1/2}) + O\left(R_o^{1/2}\frac{\Delta H_s}{H_s}\right) + O(R_o^{3/2}) = 0$$

From (94) it is obvious that:

$$(95)\quad \frac{\Delta H_s}{H_s} \lesssim O(R_o^{1/2})$$

It is still not clear that $\frac{\Delta H_s}{H_s}$ is as large as $O(R_o^{1/2})$, but $h_1\frac{\partial\rho_1}{\partial t}$ can at least be neglected compared to $\rho_1 h_1 \frac{\partial u_1}{\partial x}$.

$\rho_1\frac{\partial h_1}{\partial t}$ must be retained in the equation in case $\frac{\Delta H_s}{H_s}$ is as large as $O(R_o^{1/2})$. (69) then becomes:

$$(96)\quad \frac{\partial h_1}{\partial t} + h_1\frac{\partial u_1}{\partial x} = 0$$

A similar Rossby number scaling can be applied to (71) to obtain:

$$(97)\quad \frac{\partial v_1}{\partial t} + fu_1 = 0$$

Care must be taken not to neglect the density derivatives arising from the pressure gradient terms. These provide the driving for the dynamical equations.

The System to be Solved Numerically

The system of dynamical equations that will actually be solved numerically is (96), (87), (97), (59) and (60) (plus the relation $h = h_1 + h_2$). The lower layer is assumed to be of infinite depth, and the Zubov-Defant model is used for the mixing in the freezing step. This gives us the simplest possible system which retains the essential features which we wish to study*.

(96), (87), (97) and (59) must be solved simultaneously, and will now be combined into a single equation. First $\frac{\partial h_2}{\partial x}$ is eliminated between (87) and (59), and the smallness of $\frac{\rho_2 - \rho_1}{\rho_1}$ used to obtain

$$(98)\quad (\rho_2 - \rho_1) g \frac{\partial h_1}{\partial x} - \frac{1}{2} g h_1 \frac{\partial \rho_1}{\partial x} - \rho_1 f v_1 = 0$$

(98) and (97) are then used to eliminate V_1. Using the smallness of percentage changes in ρ gives:

---

*Another factor in choosing the Zubov-Defant model is that at the time this work was performed the simplicity of the system when the freezing is assumed to be a separate step was not yet realized. The use of the Zubov-Defant model eliminated the entrainment terms, which at that time were included in the dynamical equations and were quite troublesome.

$$(99)\quad (\rho_2-\rho_1)\frac{g}{f}\frac{\partial^2 h_1}{\partial x\partial t}-\frac{1}{2}\frac{gh_1}{f}\frac{\partial^2\rho_1}{\partial x\partial t}+\rho_1 f v_1=0$$

$\frac{\partial u_1}{\partial x}$ is eliminated by differentiating (99) with respect to x, then using (96):

$$(100)\quad (\rho_2-\rho_1)\frac{gh_1}{f}\frac{\partial^3 h_1}{\partial x^2\partial t}-\frac{g}{2f}\frac{\partial^3\rho_1}{\partial x^2\partial t}h_1^2-\rho_1 f\frac{\partial h_1}{\partial t}=0$$

(100) is the governing equation for h_1. This can be recognized as a variant of the pressure tendency equation common to quasi-geostrophic theory, the last term representing the effect of divergence in changing the relative vorticity. The boundary condition on h_1 is obtained by setting $U_1 = 0$ in (99):

$$(101)\quad (\rho_2-\rho_1)\frac{\partial^2 h_1}{\partial x\partial t}-\frac{1}{2}h_1\frac{\partial^2\rho_1}{\partial x\partial t}=0 \quad \text{AT } x=0 \text{ AND } x=L.$$

When h_1 has been found, h_2 can be found from (59) and (60). Then U_1 can be found from (99), and V_1 from (98). The difference equations and numerical procedure are given in appendix 2.

Results of the Two-Layer Model

One result of the work with the two-layer model comes directly from the scale analysis. This is the smallness of $\frac{\Delta H_s}{H_s}$. In this model, the interface is not significantly deformed by the dynamical response of the system. From equations (93) and (94) we see that in order to have $\frac{\Delta H_s}{H_s}$ be of $\mathcal{O}(1)$ would require

an ageostrophic velocity component large enough to make $\frac{U_s}{\omega L} \sim O(1)$, or in the range of 0.5 m/sec to 1 m/sec. Such velocities are rarely found in the ocean except in the geostrophic components of important currents.

Observations of the Kamchatka Current by Reid (Reid, 1966; Scripps Institution of Oceanography, 1966) indicated that a major deformation of the interface may occur in this region. The observations were made in winter. In these reports it is stated that "the thickness of the mixed layer varied from less than 100 meters along the ridge separating the Kamchatka and Oyashio Currents from the waters offshore to about 200 meters along the coast of Kamchatka and at the entrance to the Okhotsk Sea" and also that "geostrophic balance requires a strong horizontal density gradient in that area: This is achieved by a thickening of the mixed layer ..." The Kamchatka Current is a boundary current, and in fact $\frac{U_s}{\omega L}$ can become of O(1) not only as a result of U_s becoming large, but also as a result of the appropriate length scale L becoming small. If the ageostrophic velocity component is on the order of 1 to 5 cm/sec, which is not unreasonable in this particular situation, a reduction of L to about 100 km, which is also reasonable, gives $\frac{U_s}{\omega L} \sim O(1)$. The Rossby radius of deformation corresponding to a depth of 100 meters, which is the depth of the mixed layer outside of the boundary region in this case, is $\frac{\sqrt{gh_1}}{f}$ 200 km. Since it is essentially the rotational constraint which keeps $\frac{\Delta H_s}{H_s}$ small in the present model, and the Rossby radius is often associated

with the length scale required for rotational effects to become dominant, these clues lead one to suspect that a length scale on the order of the Rossby radius or less may be the condition for substantial deformation of the interface to become possible. The further study of this example would be an interesting extension of the present work. Wind driving and the β effect are important in the case of the Kamchatka Current, but the representation of the mixed layer used here should be retained.

The numerical calculation was carried out with the initial conditions h_1 = 30 meters, h_2 = 170 meters (above an arbitrary reference level), S_1 = 30‰, S_2 = 34‰, U_1 = 0 and V_1 = 0. The width of the ocean L = 2000 km was divided into 40 grid intervals, with ΔX = 50 km. The forcing was

$$I = \frac{1}{2}\left\{1 - \mathrm{SIN}\left[\frac{\pi}{L}\left(x - \frac{1}{2}L\right)\right]\right\} I_o \quad ,$$

with I_o = 1 meter, divided into 100 steps of Δt = 2 days each. The results which are presented in table III confirm the prediction of the scale analysis that $\frac{\Delta H_s}{H_s}$ will be small, and also show that the change in free surface height is very nearly what is predicted from the steric variation in sea level. The latter is given in the second column of table III. This means that dynamical effects of the type studied here are not important in the problem of the seasonal variation in sea level.

Table IV shows U_1 and V_1 at the end of the season. U_1 is in the expected direction, toward the side where sea level is

depressed, and V_1 in the direction given by a deflection to the right of U_1. With the forcing function used here, the U_1 and V_1 fields are smooth and symmetrical, with maxima in the center of the ocean.

The results are illustrated in Fig. 23. The changes in the heights of the free surface and interface are greatly exaggerated.

TABLE III

x km	h_1 Without Dynamics m	h_1 With Dynamics m	h_2-H_2 With Dynamics 10^{-6}m	h-H With Dynamics 10^{-3}m
0	29.976	29.978	-548	-23
50	29.976	29.978	-540	-23
100	29.977	29.978	-532	-22
150	29.977	29.978	-524	-22
200	29.977	29.978	-516	-22
250	29.977	29.979	-505	-22
300	29.978	29.979	-493	-22
350	29.978	29.979	-479	-21
400	29.979	29.980	-463	-21
450	29.979	29.980	-445	-20
500	29.980	29.981	-426	-19
550	29.980	29.982	-405	-19
600	29.981	29.982	-383	-18
650	29.982	29.983	-359	-17
700	29.983	29.984	-335	-17
750	29.984	29.985	-309	-16
800	29.985	29.985	-282	-15
850	29.985	29.986	-255	-14
900	29.986	29.987	-227	-13
950	29.987	29.988	-198	-12
1000	29.988	29.989	-170	-11
1050	29.989	29.990	-141	-10
1100	29.990	29.991	-113	-10
1150	29.991	29.991	- 84	- 9
1200	29.992	29.992	- 57	- 8
1250	29.993	29.993	- 30	- 7
1300	29.994	29.994	- 3	- 6
1350	29.994	29.995	+ 22	- 5
1400	29.995	29.995	+ 46	- 5
1450	29.996	29.996	+ 69	- 4
1500	29.997	29.997	+ 90	- 3
1550	29.997	29.997	+109	- 3
1600	29.998	29.998	+127	- 2
1650	29.998	29.998	+143	- 2
1700	29.999	29.999	+157	- 1
1750	29.999	29.999	+168	- 1
1800	29.999	29.999	+178	- 1
1850	30.000	30.000	+185	0
1900	30.000	30.000	+190	0
1950	30.000	30.000	+190	0
2000	30.000	30.000	+190	0

TABLE IV

x	U_1 $10^{-8}\ \frac{m}{sec}$	V_1 $10^{-5}\ \frac{m}{sec}$	x	U_1 $10^{-8}\ \frac{m}{sec}$	V_1 $10^{-5}\ \frac{m}{sec}$
0	0	0	1050	-99.2	+120.0
50	- 5.9	+ 7.4	1100	-98.3	+118.9
100	-15.7	+ 18.9	1150	-96.9	+117.1
150	-23.3	+ 28.2	1200	-94.7	+114.5
200	-30.8	+ 37.2	1250	-92.0	+111.2
250	-38.1	+ 46.1	1300	-88.8	+107.3
300	-45.2	+ 54.7	1350	-84.9	+102.7
350	-52.1	+ 62.9	1400	-80.6	+ 97.4
400	-58.5	+ 70.7	1450	-75.7	+ 91.6
450	-64.6	+ 78.2	1500	-70.4	+ 85.2
500	-70.4	+ 85.1	1550	-64.7	+ 78.2
550	-75.6	+ 91.5	1600	-58.6	+ 70.8
600	-80.5	+ 97.4	1650	-52.1	+ 63.0
650	-84.8	+102.6	1700	-45.3	+ 54.7
700	-88.8	+107.2	1750	-38.1	+ 46.2
750	-91.9	+111.2	1800	-30.8	+ 37.3
800	-94.6	+114.4	1850	-23.3	+ 28.2
850	-96.8	+117.0	1900	-15.6	+ 18.9
900	-98.3	+118.9	1950	- 5.9	+ 7.1
950	-99.2	+120.0	2000	0	0
1000	-99.6	+120.4			

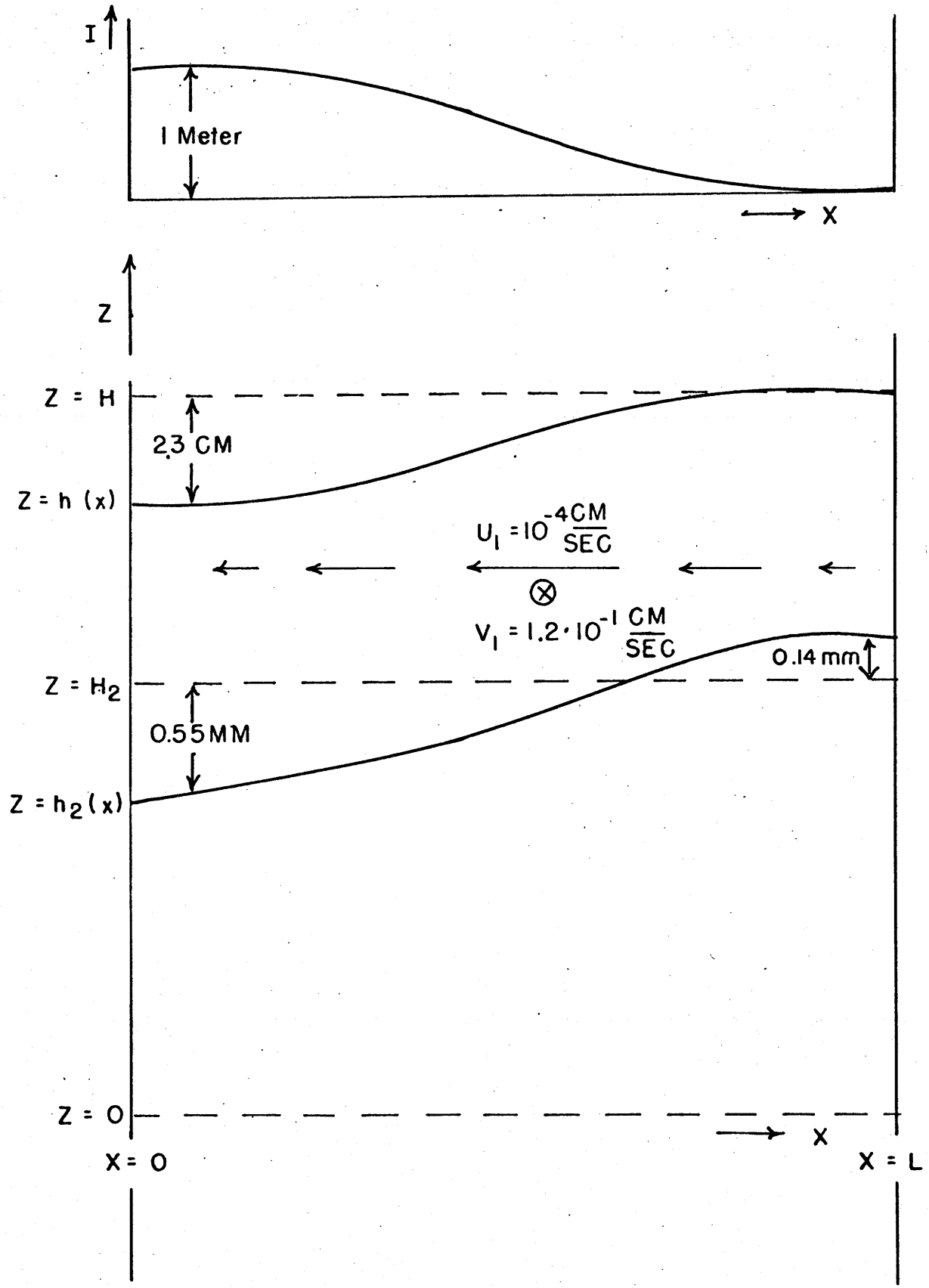

Figure 23 - Results of the two-layer model. The changes in the heights of the free surface and interface are greatly exaggerated. The forcing function is shown at the top.

Chapter 4

THE CONTINUOUSLY STRATIFIED DYNAMICAL MODEL

In this chapter we will investigate the baroclinic response in a more general way than is possible with a two-layer model. This is done with a model which in principle retains the actual continuous stratification that is found in the ocean. Actually, the "continuously stratified" model is many-layered, a finite difference approximation to a true continuously stratified model.

It is not practical to attempt to solve the quasigeostrophic equations simultaneously, as was done in the two-layer model, when the number of layers is large. Instead, it is necessary to leave the equations in their so-called primitive, or nongeostrophic, form, and integrate each equation separately at each time step. This has the disadvantage that the solutions of the system of equations now include gravity waves. If the top surface is free, these will include barotropic gravity waves, which, with their high propagation speed, require an extremely short time step for proper resolution. If the waves are not properly resolved numerical instability will result. If they are, so many of the short time steps will be required that the cost of the calculation becomes prohibitive. The usual way of resolving this dilemma, which is used here, is to impose a rigid lid, at which the large-scale vertical velocity is zero, at the boundary condition at the top surface. This, in turn, has the disadvantage of eliminating the barotropic mode, so that we

must rely on the two-layer model for information about the barotropic response of the ocean.

The rigid lid approximation makes it impossible to account for the detailed nature of the dynamics of the ice layer. Since the ice floats on top of the ocean, and its principal influence on the motion is through the pressure exerted by its weight, this influence is independent of Z (except within the thin layer of ice itself) and only affects the barotropic mode, which has already been eliminated. Therefore, there is no disadvantage in not being able to account for the ice dynamics beyond that which has already been incurred in losing the barotropic part of the motion.

As in the two-layer model, ice formation is calculated in steps which alternate with the dynamical steps. In this model advection of density can produce small local instabilities*. Since it is inconsistent with either the Zubov-Defant or Kraus-Turner-Ball mixing model to allow such instabilities to persist, a third step is added to the cycle to test for these instabilities and remove them through local mixing. The overall flow chart for each cycle is shown in Fig. 24.

The Ice Formation Step

The large number of steps involved in the dynamical cal-

*Could a similar process produce microstructure in the thermocline?

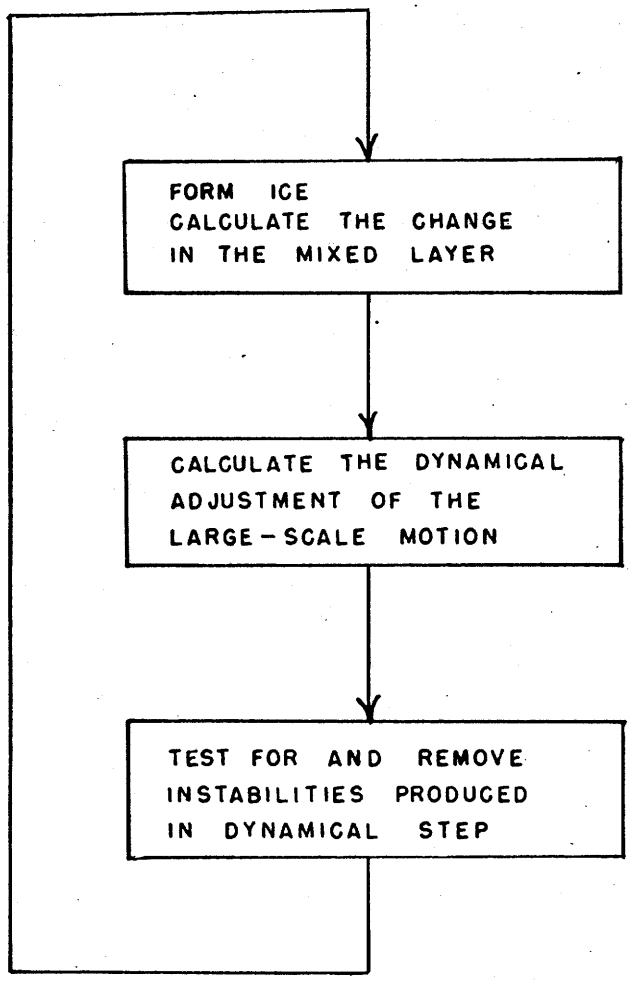

Figure 24 - Flow chart for the continously stratified dynamical model.

culation, and the shortness of the time step required for ~~dynamical~~ NUMERICAL stability, together with the storage requirements at a large number of grid points, made it impractical to use a 1-meter vertical grid spacing as was done with the numerical model in chapter 2. Layers several meters thick were the smallest that could be used. Therefore, the second of the numerical procedures presented for the Kraus-Turner-Ball model, which employs partial entrainment of the layer below the mixed layer in order to conserve potential energy exactly at each step, is used. (In fact, it was developed as a matter of necessity for use in the present dynamical model.) The mixed layer is taken to consist of those grid intervals (within each column) which have the same salinity as the uppermost grid interval; it could conceivably consist of as little as just the uppermost interval.

The mixing of horizontal momentum within the mixed layer and the entrainment of momentum carried by water entrained into the mixed layer from below are accounted for during this step. Assume that after the change in the salinity distribution has been calculated there is a mixed layer D meters deep, of salinity S_1' and density ρ_1', which would be another λ_B meters deep in a real stepwise-stratified ocean, as shown in Fig. 25. However, because the thickness ΔZ of the layers must remain fixed, the depth of the mixed layer is limited to D meters, and the entire layer below the mixed layer has its density reduced from ρ_2 to ρ_2'. The velocity of the layer below the mixed layer before mixing is V_2.

The momentum of the mixed layer before mixing, including that of the salt released by freezing, is $\rho_1 V_1$; This may actually have to be found as a sum of momenta of two or more layers if one or more layers is fully entrained during the mixing. It will be retained in the form $\rho_1 V_1$ in the present treatment for the sake of simplicity.

Following the notation in Fig. 25, the representation of the actual mixing by partial entrainment of a whole layer must conserve the mass within the layer of thickness Δz :

$$\rho_2' \Delta z = \rho_2 \lambda_A + \rho_1' \lambda_B \tag{102}$$

and of course the height is conserved:

$$\lambda_A + \lambda_B = \Delta z \tag{103}$$

(102) and (103) can be solved for λ_A and λ_B :

$$\lambda_A = \frac{\rho_2' - \rho_1'}{\rho_2 - \rho_1'} \Delta z \tag{104}$$

$$\lambda_B = \frac{\rho_2 - \rho_2'}{\rho_2 - \rho_1'} \Delta z \tag{105}$$

The representation must also conserve momentum:

$$\rho_2' V_2' \Delta z = \rho_2 V_2 \lambda_A + \rho_1' V_1' \lambda_B \tag{106}$$

The mixing process must conserve momentum in the mixed layer and the layer below it:

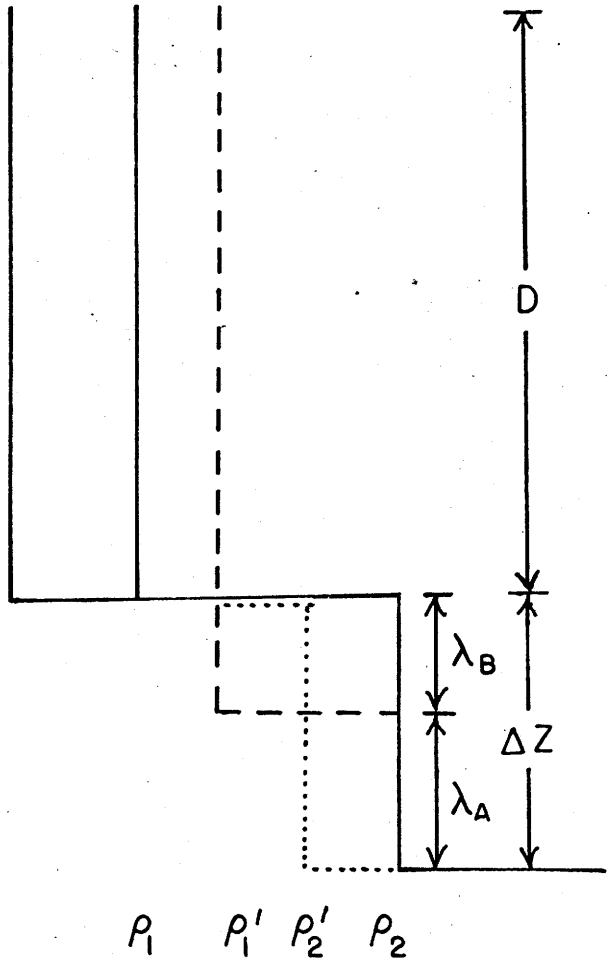

Figure 25 - Notation for the calculation of entrainment of momentum into the mixed layer. The solid line is the initial profile, the long-dashed line is the profile after Zubov-Defant mixing, the short-dashed line is the actual profile after Kraus-Turner-Ball mixing in a stepwise-stratified ocean and the dotted line is the representation of the actual profile in terms of a partially entrained layer of constant thickness.

$$(107)\quad \rho_1' V_1' D + \rho_2' V_2' \Delta Z = \rho_1 V_1 D + \rho_2 V_2 \Delta Z$$

(106) and (107) can be solved for V_1', the velocity in the mixed layer after entrainment, and V_2', the velocity in the partially entrained layer after entrainment:

$$(108)\quad V_1' = \frac{\rho_1 V_1 D + \rho_2 V_2 \lambda_B}{\rho_1' (D + \lambda_B)}$$

$$(109)\quad V_2' = \frac{\rho_1 V_1 D \lambda_B + \rho_2 V_2 (D\lambda_A + \Delta Z \lambda_B)}{\rho_2' \Delta Z (D + \lambda_B)}$$

Similar equations hold for U_1' and U_2' in terms of U_1 and U_2.

The Dynamical Step

After the completion of the ice formation step, the equations of motion are integrated for a time step Δt. These equations are, using the Boussinesq approximation:

$$(110)\quad \frac{\partial U}{\partial t} = -U\frac{\partial U}{\partial x} - W\frac{\partial U}{\partial z} - \frac{1}{\rho_0}\frac{\partial P}{\partial x} + fV \qquad \rho_0 = \text{CONSTANT}$$

$$(111)\quad \frac{\partial V}{\partial t} = -U\frac{\partial V}{\partial x} - W\frac{\partial V}{\partial z} - fU$$

$$(112)\quad \frac{\partial P}{\partial z} = -\rho g$$

$$(113)\quad \frac{\partial W}{\partial z} = -\frac{\partial U}{\partial x}$$

$$(114)\quad \frac{\partial \rho}{\partial t} = -u\frac{\partial \rho}{\partial x} - w\frac{\partial \rho}{\partial z}$$

(3) is also part of the system. These equations are integrated in steps, the right sides being calculated from known values, rather than solved simultaneously.

In solving (110) for U it is necessary to first substitute for P from (112) to obtain:

$$(115)\quad \frac{\partial u}{\partial t} = -u\frac{\partial u}{\partial x} - w\frac{\partial u}{\partial z} - \frac{1}{\rho_0}\frac{\partial P_0}{\partial x} - \frac{1}{\rho_0}\frac{\partial}{\partial x}\int_z^H \rho g\, dz' + fv$$

where the rigid lid is at Z = H, and the pressure at this lid is $P_0(x,t)$. It is necessary to use the boundary conditions to find $\frac{\partial P_0}{\partial x}$. Integrating (113) from top to bottom, gives

$$(116)\quad \frac{\partial \bar{u}}{\partial x} = 0\quad ,$$

where

$$(117)\quad \bar{\psi} = \frac{1}{H}\int_0^H \psi\, dz$$

for any variable ψ.

The boundary condition at either of the sidewalls then gives

$$\bar{U} = 0 \tag{118}$$

(118) restricts the solution to the baroclinic mode.

It is possible to integrate (115) vertically and apply (118) to obtain an equation for $\frac{\partial P_0}{\partial x}$. However, it is computationally simpler to avoid the direct calculation of $\frac{\partial P_0}{\partial x}$, and instead apply (118) directly to the U field. Adding $\frac{1}{\rho_0}\frac{\partial P_0}{\partial x}$ to both sides of (115) gives

$$\frac{\partial U'}{\partial t} = -U\frac{\partial U}{\partial x} - W\frac{\partial U}{\partial Z} - \frac{1}{\rho_0}\frac{\partial}{\partial x}\int_z^H \rho g\, dz' + fV \tag{119}$$

where

$$\frac{\partial U'}{\partial t} = \frac{\partial U}{\partial t} + \frac{1}{\rho_0}\frac{\partial P_0}{\partial x} \tag{120}$$

Integrating (119) vertically and applying (118) gives

$$\frac{\partial \bar{U'}}{\partial t} = \frac{1}{\rho_0}\frac{\partial P_0}{\partial x} \tag{121}$$

Substitution of (119) and (121) into (115) gives

$$\frac{\partial U}{\partial t} = \frac{\partial U'}{\partial t} - \frac{\partial \bar{U'}}{\partial t} \tag{122}$$

Since only $\frac{\partial U'}{\partial t}$ is given by (120), U' itself is arbitrary. It is convenient to let U' = U at the beginning of the time step, so that

$$U = U' - \bar{U'} \tag{123}$$

The procedure is to find U' from (119) and then U from (123); This is faster than finding $\frac{\partial \rho_o}{\partial x}$ and substituting its value in (115).

The important balance is expected to be between the terms which are retained in the usual small amplitude linearization:

$$(123)\quad \frac{\partial u}{\partial t} \approx -\frac{1}{\rho_o}\frac{\partial p}{\partial x} + fv$$

$$(124)\quad \frac{\partial v}{\partial t} \approx -fu$$

$$(113)\quad \frac{\partial w}{\partial z} \approx -\frac{\partial u}{\partial x}$$

$$(125)\quad \frac{\partial \rho}{\partial t} \approx -w\frac{d\rho_o(z)}{dz}$$

where $\rho_o(Z)$ is the density in the basic initial stratification. The calculations were actually done with the full equations including the nonlinear terms, but the location (in space and time) of points at which the variables are calculated is chosen in such a way that the derivatives in the important linear terms will be represented by centered differences in the finite difference equations. The locations at one typical grid point are shown in Fig. 26.

The non-linear advective terms are evaluated by using uncentered space derivatives evaluated in the upstream direction. The appropriate advecting velocities ($\hat{U}$, $\hat{W}$, $\tilde{U}$, $\tilde{W}$, $\mathring{U}$ and $\mathring{W}$ in the following equations) at the point at which the unknown quantity is being calculated are taken to be the average of values of U

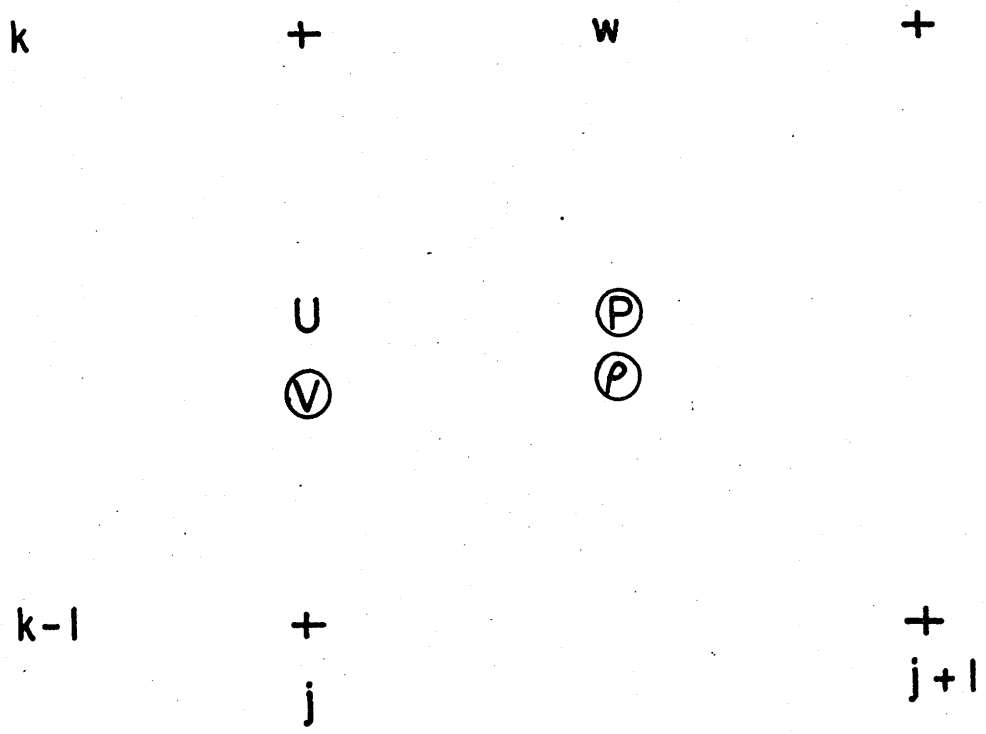

Figure 26 Locations in space-time of fluid variables assigned the grid point subscripts j, k, n, where $x = j\Delta x$, $z = k\Delta z$ and $t = n\Delta t$. Circled variables are calculated at $t = (n+1/2)\,\Delta t$; others are at $t = n\Delta t$.

(or W) at the nearest-neighboring points at which U (or W) is known. Referring to Fig. 26, we see that, for the calculation of U:

$$\hat{U}_{J,K,N} = U_{J,K,N-1} \tag{126}$$

$$\hat{W}_{J,K,N} = \frac{1}{4}\left(W_{J-1,K-1,N-1} + W_{J,K-1,N-1} + W_{J-1,K,N-1} + W_{J,K,N-1}\right) \tag{127}$$

for the calculation of V:

$$\tilde{U}_{J,K,N} = U_{J,K,N} \tag{128}$$

$$\tilde{W}_{J,K,N} = \frac{1}{4}\left(W_{J-1,K-1,N} + W_{J,K-1,N} + W_{J-1,K,N-1} + W_{J,K,N-1}\right) \tag{129}$$

and for the calculation of ρ (or S):

$$\mathring{U}_{J,K,N} = \frac{1}{2}\left(U_{J,K,N} + U_{J+1,K,N}\right) \tag{130}$$

$$\mathring{W}_{J,K,N} = \frac{1}{2}\left(W_{J,K,N} + W_{J,K-1,N}\right) \tag{131}$$

The difference equations for the case of non-negative advecting velocities are:

$$U'_{J,K,N} = U_{J,K,N-1} - \frac{\hat{U}_{J,K,N}\,\Delta t}{\Delta X}\left[U_{K,N-1}\right]_{J-1}^{J} - \frac{\hat{W}_{J,K,N}\,\Delta t}{\Delta Z}\left[U_{J,N-1}\right]_{K-1}^{K} - \frac{\Delta t}{\rho_0 \Delta X}\left[P'_{K,N}\right]_{J-1}^{J} + f\Delta t\, V_{J,K,N-1} \tag{132}$$

where P' is the x-variable part of the pressure due to the weight of the fluid column alone, without the pressure P_0 at the top lid:

$$\left[P'_{J,N}\right]_{K}^{K+1} = -\frac{g\Delta Z}{2}\left(\rho'_{J,K,N} + \rho'_{J,K+1,N}\right) \tag{133}$$

ρ' is the actual density minus the density at $z = k\Delta z$ at t = 0. It is used in place of the actual density in order to minimize the computer round-off error and retain accuracy to a greater number of places in the x-variable part of ρ. $P'_{J,KM,N} = 0$ where KM is the maximum value of k.

$$(134)\quad U_{J,K,N} = U'_{J,K,N} - \frac{1}{KM}\sum_{K=2}^{KM} U'_{J,K,N}$$

$$(135)\quad \left[W_{J,N}\right]_{K-1}^{K} = -\frac{\Delta Z}{\Delta X}\left[U_{K,N}\right]_{J}^{J+1}\ ;\ W_{J,1,N} = W_{J,KM,N} = 0$$

$$(136)\quad \left[V_{J,K}\right]_{N-1}^{N} = -\frac{\tilde{U}_{J,K,N}\Delta t}{\Delta X}\left[V_{K,N-1}\right]_{J-1}^{J} - \frac{\tilde{W}_{J,K,N}\Delta t}{\Delta Z}\left[V_{J,N-1}\right]_{K-1}^{K} - f\Delta t\, U_{J,K,N}$$

$$(137)\quad \left[\rho_{J,K}\right]_{N-1}^{N} = -\frac{\mathring{U}_{J,K,N}\Delta t}{\Delta X}\left[\rho_{K,N-1}\right]_{J-1}^{J} - \frac{\mathring{W}_{J,K,N}\Delta t}{\Delta Z}\left[\rho_{J,N-1}\right]_{K-1}^{K}$$

When $\hat{U}$ (or $\tilde{U}$ or $\mathring{U}$) is negative the horizontal advection difference is taken between j and j + 1, and similarly for negative $\hat{W}$ (or $\tilde{W}$ or $\mathring{W}$).

A time step of Δt = 7200 seconds = 2 hours was decided on after consideration of the computational stability criterion, which is covered in appendix 3.

This routine was tested by running it on the computer

alone, without the mixing steps. An internal gravity wave corresponding to an eigenfunction of the system, was specified as an initial condition, and its motion was followed for one complete period. The equations of the gravity wave are given for reference in appendix 4.

Removing Instabilities

The third step in each cycle is to test for any instabilities that may have been produced by advection during the dynamical step and to remove them by mixing. An instability is considered to exist when any value of salinity is lower than the value above it. The group of grid intervals in a vertical column for which the salinity decreases monotonically with depth is considered to form a mixed layer. The salinities in these intervals are averaged to find the salinity of the mixed layer. This is then compared with the layers above and below the mixed layer to see if an instability still exists, and additional layers are entrained, if necessary, until the instability is removed.

An attempt was made to extend this procedure to include entrainment into the mixing region but this had to be abandoned when it turned out that the routine was not fully reliable. The procedure for this is presented in appendix 5. It is believed that most of the instabilities removed by this routine were extremely small, resulting from weak advection and perhaps computer

round-off errors within the surface mixed layer, and that the omission of entrainment did not have a significant effect on the results. Momentum mixing was also included originally but was later deleted along with entrainment in order to keep the routine as simple and reliable as possible. This is also thought to have a negligible effect on the results, and is also discussed in appendix 5.

In practice this routine executed very few times, meaning that few instabilities were formed, near the beginning of the season, but toward the end of the season it executed often, about ten times every time step. Most of the instabilities that formed were within the surface mixed layer; the remaining ones were immediately below it.

Results from the Continuously Stratified Model

The full season's calculation was performed in an ocean 2000 kilometers wide. After examination of the data given by Mosby (1934) it was decided that a profile with S = 33.830‰ at the surface and S = 34.680‰ at the bottom would be a reasonable representation of the conditions in the Weddell Sea (although it must be pointed out that the "Norvegia" stations were taken somewhat to the east of the region where bottom water is believed to form). The actual profile used was not any of the specific observed profiles, but was calculated from the equation:

$$(138) \qquad S_0(z) = 34.68 - 0.85\, e^{-\frac{(H-21)-z}{50}}$$

There is a 21 meter deep mixed layer on top of the exponential profile.

With a scale height of 50 meters, it was decided to use a vertical grid interval of $\Delta Z = 3$ meters. Since 100 grid intervals is about the limit that could be used without requiring excessive computation time or storage space in memory, this meant that H, the depth of the ocean, was limited to 300 meters, although the Weddell Sea is over 1000 meters deep except on the Continental Shelf. The probable effect of this difference on the results will be discussed a bit later.

The forcing is given by the same sinusoidal forcing function that was used for the two-layer model, with a maximum ice formation of 1 meter at $X = 0$. The length of the freezing season was artificially shortened to 90 days, with the same total amount of ice formation, in order to save computer time. It is believed that this did not have a significant effect on the results since the Rossby number remains extremely small.

The instantaneous velocities generated were highly oscillatory in nature, the physical solution being masked by spurious numerical oscillations generated mainly by the discontinuous jumps in the depth of the bottom of the mixed layer. The oscillations are discussed in detail in appendix 1. Fortunately, the oscillations,

once generated, were well-behaved, and have a period (close to the inertial period) much shorter than that of the desired physical solution. Therefore, it was possible to extract some meaningful physical information from the solution by averaging. What was done was to take the time average, from t = 0, of U, V and W at selected points; this gave an estimate for the total distance traveled by fluid particles during the season. This required much less storage space than averaging over the period of the oscillations, and therefore could be done at a greater number of grid points. The averaged values themselves were oscillatory, but oscillated with a smaller amplitude than the instantaneous values; the value around which the average oscillated was estimated from a graph of the average value vs. time at the end of the season. Since the rate of increase of the averaged velocity components (and the amplitude of the oscillations) was roughly linear with time; the "instantaneous" average value is probably on the order of twice the actual average value, but this "hand-waving" cannot give more than a very crude estimate. Examples of the variation of the time-averaged U, V and W with time are shown in Figs. 27, 28 and 29.

The motions produced by this forcing are rather weak. The largest time-averaged U is about $5 \cdot 10^{-7}$ m/sec; V about $2 \cdot 10^{-4}$ m/sec and W about 10^{-9} m/sec. The horizontal motions tend to fit into a two-layer pattern. The time-averaged U, in the mixed layer, is negative (directed toward the region of strongest ice formation)

Figure 27. Instantaneous (left) and timeaveraged (right) V vs. time at the end of the season at one point in the mixed layer.

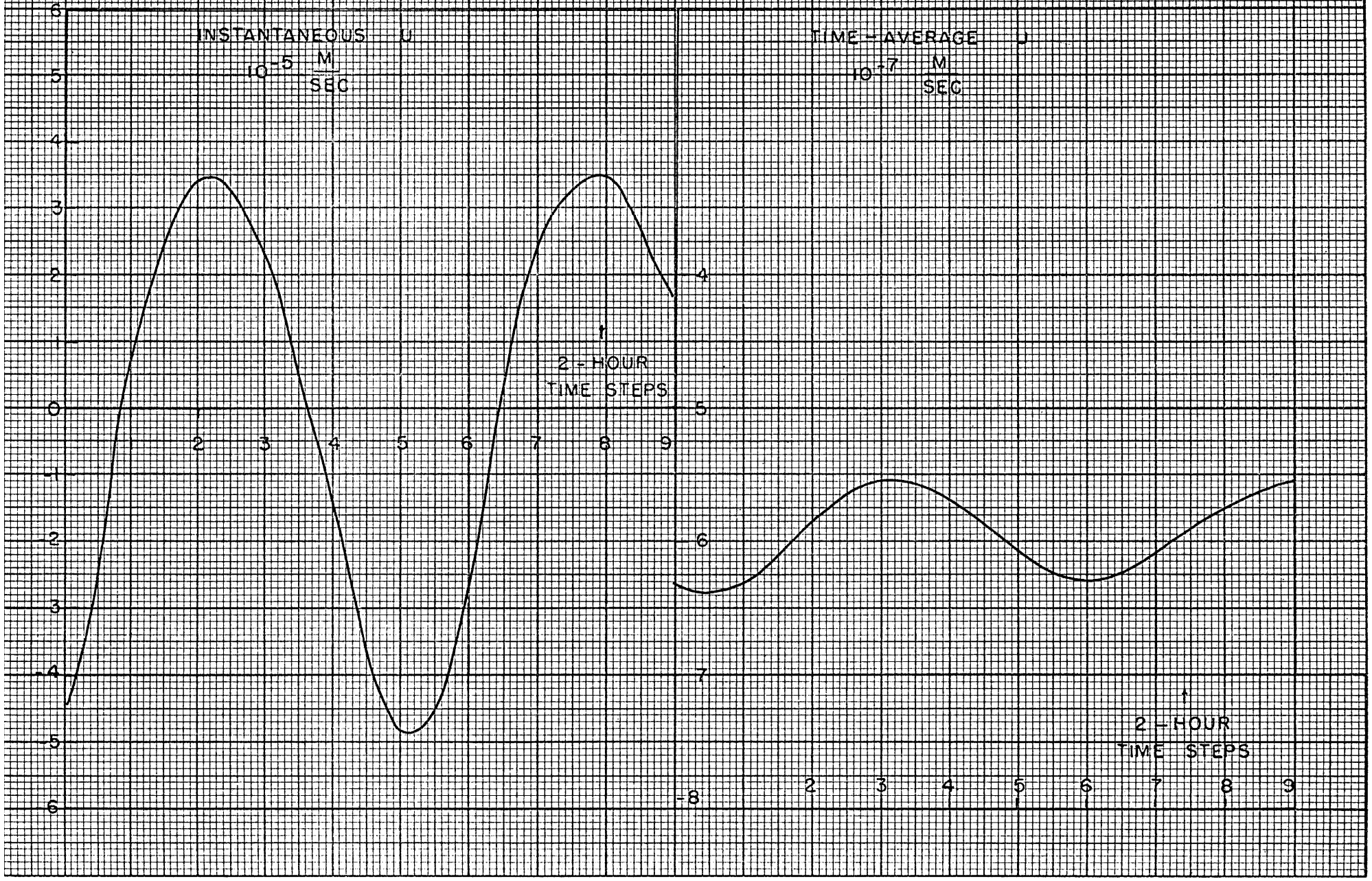

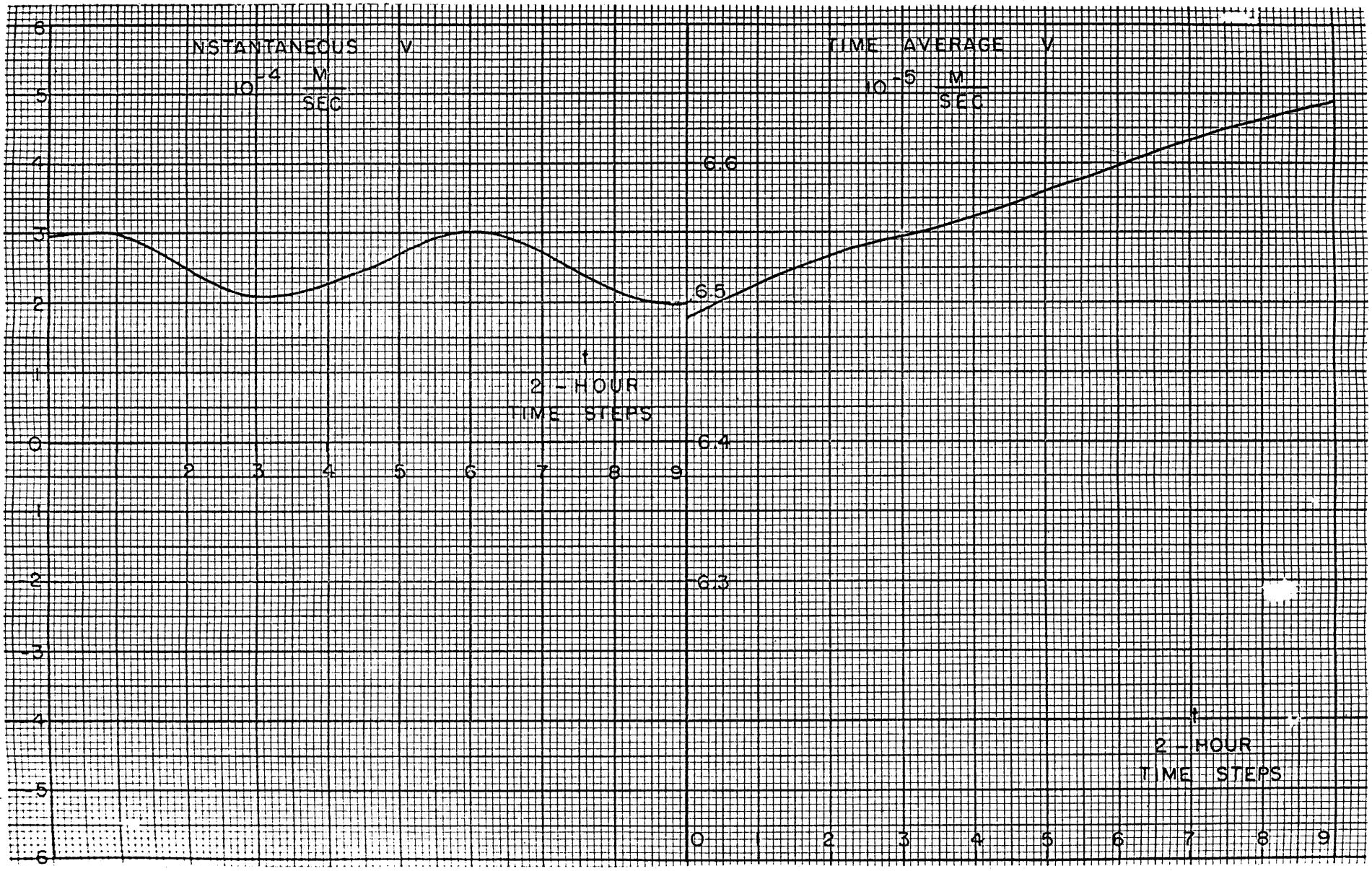

Figure 28 Instantaneous (left) and time averaged (right) V vs. time at the end of the season at one point in the mixed layer. Note how smooth the geostrophic velocity compared to the ageostrophic and vertical velocities.

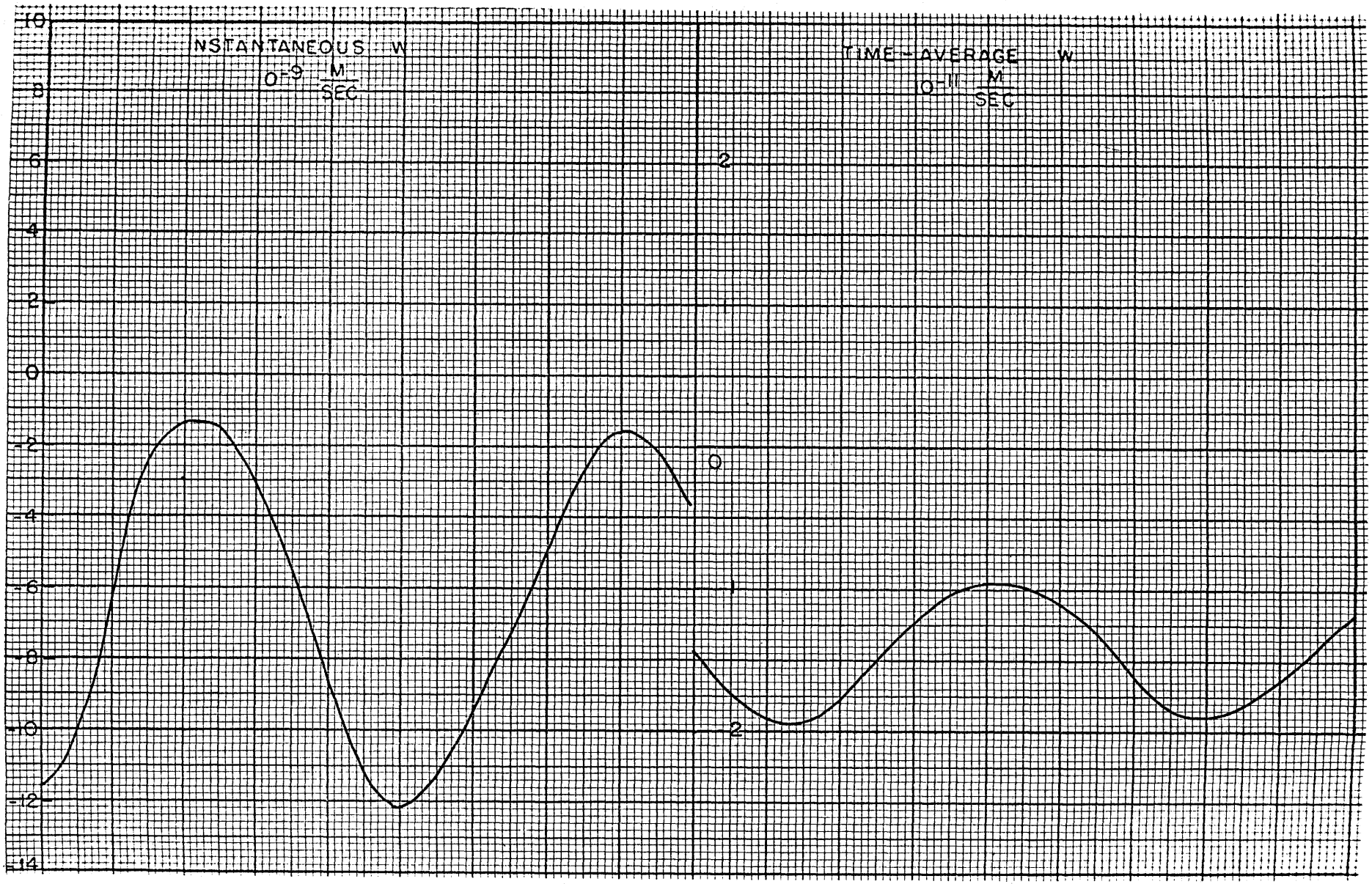

Figure 29 Instantaneous (left) and time averaged (right) W at one point in the mixed layer at the end of the season.

and positive below; the time-averaged V is to the right of U* - positive in the mixed layer and negative below. There is some "smearing" of the time-averaged U and V in the intermediate region which was not in the mixed layer at the beginning but became part of the mixed layer as the season progressed. The velocities in the mixed layer are roughly five times as strong as those in the deep water, corresponding to the depth ratio and the requirement of zero net transport across any plane X = constant. Therefore, it can be estimated that the main effect of using an ocean 300 meters deep instead of 1000 meters deep is to strengthen the deep currents by a factor of about four.

The time-averaged vertical velocity tends to oscillate with respect to X, being downward next to the wall at X = 25 km, upward at X = 75 km, downward again at X = 125 km, and so on. The W field appears to be complicated, and cannot automatically be considered to behave as part of a Hadley-like circulation. The strongest sinking motion is near the wall at X = 0. Note that U in the mixed layer is negative everywhere, but its magnitude fluctuates in X, as recirculating water alternately rises and sinks. The time-averaged circulation at the end of the season is shown in Figs. 30 and 31.

---

*The Coriolis parameter was taken to be positive in spite of the fact that this problem was partially motivated by the circulation in the Weddell Sea.

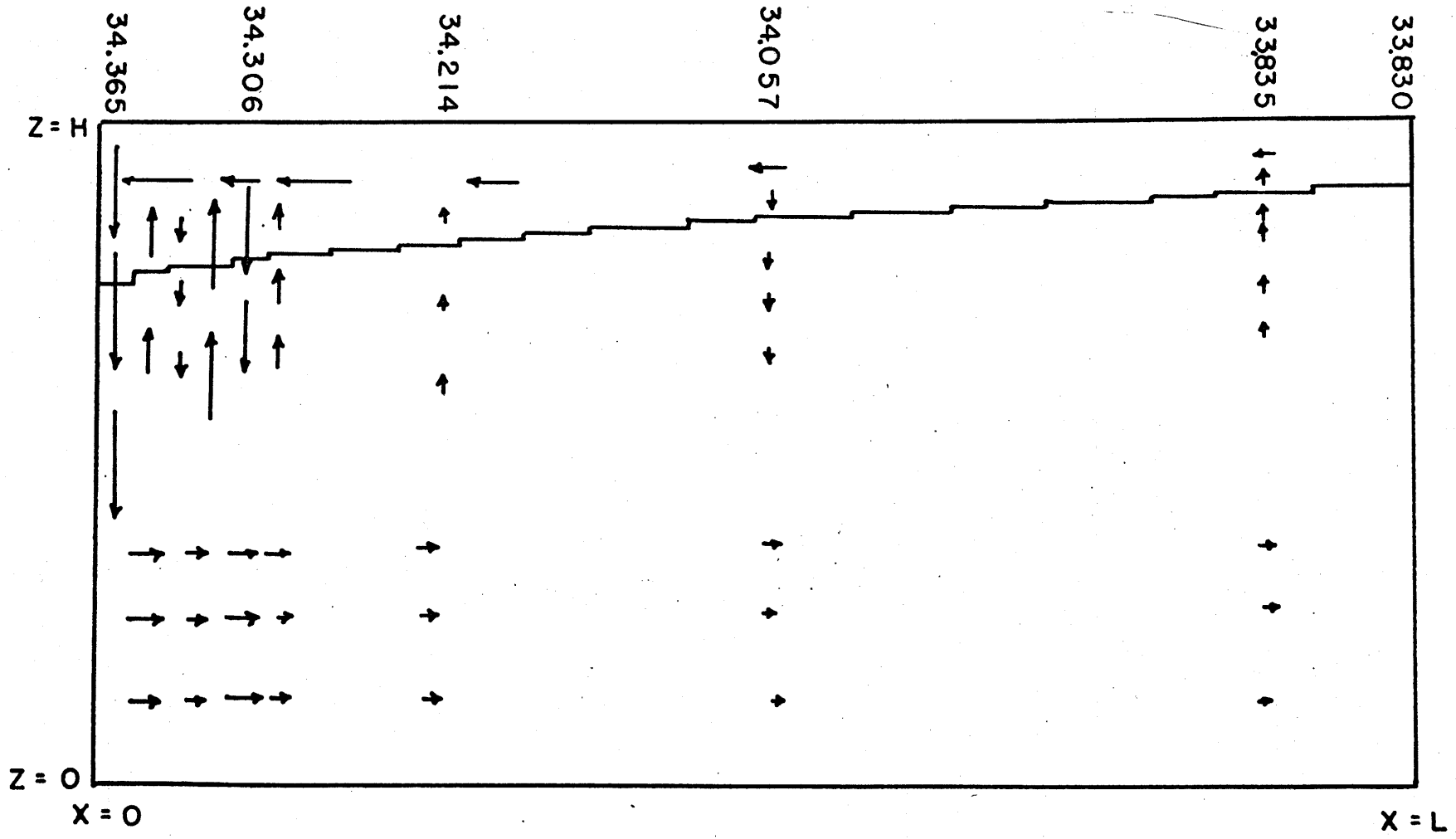

Figure 30. Time averaged vertical circulation and position of the interface at the end of the season. The vertical scale is 3 meters to 2 millimeter; the horizontal scale is 100 kilometers to 1 centimeter. The arrows are very roughly proportional to the velocity components; the vertical velocity is greatly exaggerated compared with the horizontal velocity. Values of the salinity in the mixed layer are shown at the top. Smaller velocities are somewhat exaggerated.

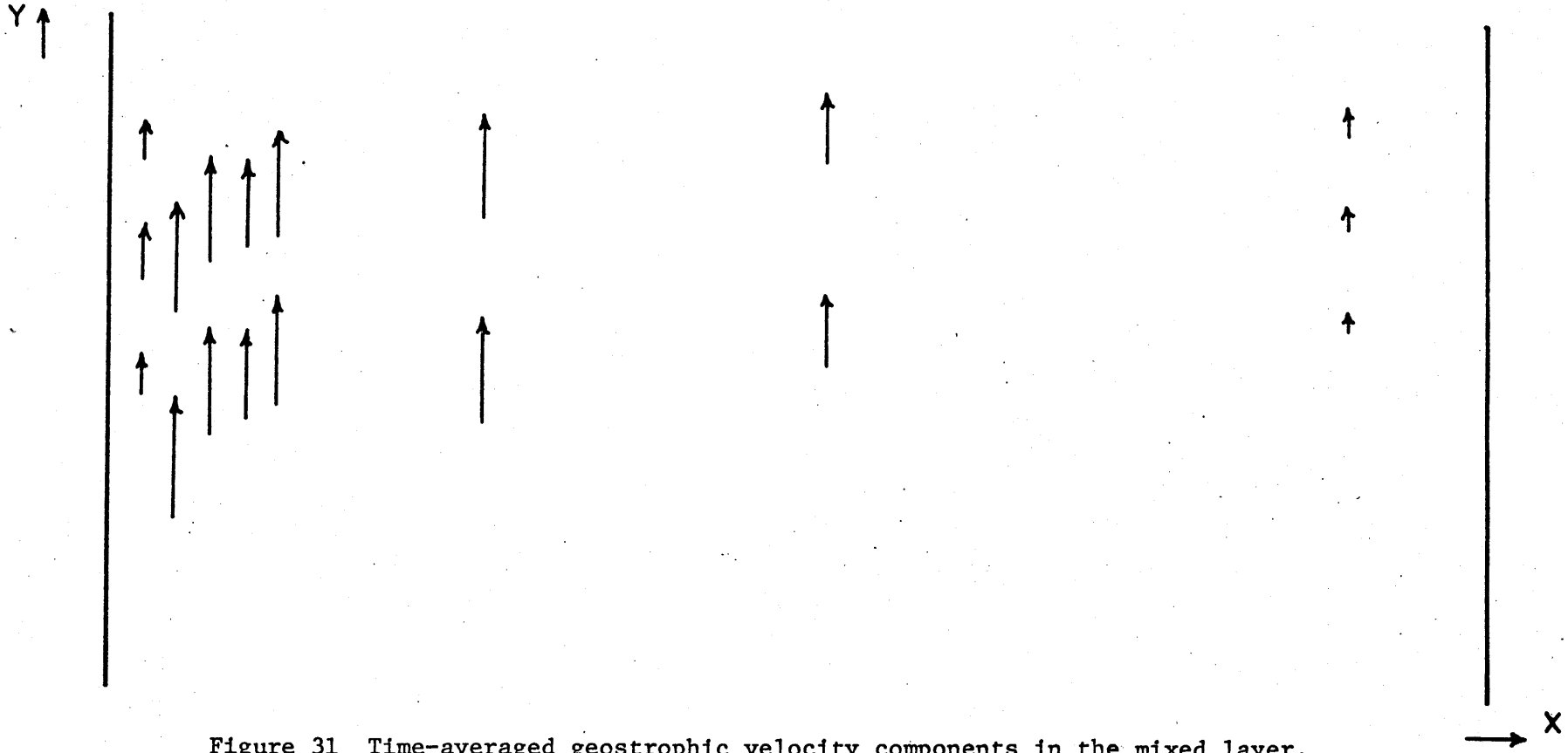

Figure 31 Time-averaged geostrophic velocity components in the mixed layer, drawn roughly to the scale of $10^4 \frac{M}{sec}$ to 1 cm. The geostrophic velocity below the interface is opposite to these and about 1/5 as great. The dirertion of v is given as for the northern hemisphere.

Significance for the Weddell Sea

The most recent estimate of the volume transport of the outflow of bottom water from the Weddell Sea (Gordon, personal communication, 1969) is 30 Sverdrups = 3 10^{+7} m^3/sec. This order of magnitude is consistent with earlier estimates by Stommel and Arons (1960) and Munk (1966). These estimates are based primarily on the supply of bottom water calculated to be necessary to account for the observed distribution of temperature, salinity and chemical tracers in the bottom water of the major ocean basins of the Southern Hemisphere, including the Antarctic region. This outflow must be replaced by an inflow of other types of Antarctic water at higher levels (Kort, 1962). Can this inflow and outflow circulation be driven by the seasonal formation of ice?

The western side of the Weddell Sea, where the formation of bottom water is thought to take place, is not a precisely defined region, but it is adequate for the present discussion to consider it to be about 500 kilometers on a side. The depth of the bottom water outflow current is assumed to be about 200 meters. We find from this that the transport estimated by Gordon requires an average sinking velocity (W) of about 10^{-2} cm/sec, and an average horizontal outflow velocity (U) of about 3 0 cm/sec. Both of these are larger than the velocity components calculated in the present theoretical model by a factor of about 10^5, so even allowing for reasonable error in the estimates, it is obvious that the

seasonal formation of ice cannot drive the necessary mean vertical circulation. The barotropic velocity which is excluded from the solution in this model is toward the region of strongest ice formation, so its absence does not affect this conclusion.

How, then, does the bottom water flow out? Here are several possibilities, not necessarily in any particular order:

1. The Palmer Peninsula could prevent the rotational constraint from operating as effectively as in the theoretical model. However, it must be noted that the inflow in the mixed layer, which produces the pressure gradient that drives the outflow, is deflected to the left, away from the Palmer Peninsula, so this is probably not the explanation.
2. It has been suggested by Gordon (personal communication, 1969) that considerably more than 1 meter of ice may form because of the constant breakup and outflow of the ice pack due to strong winds.
3. Bottom topography might play a role. The accumulation of dense saline water on the Continental Shelf could flow down the continental slope and in this way produce a stronger outflow than the same dense water in a mixed layer on top of a deep ocean. In this connection R. Beardsley (personal communication, 1968) has suggested that bottom friction might help to break the rotational constraint in a flow that is sufficiently close to the bottom.
4. The yearly freezing and melting cycle could produce a circulation

that drives some outflow of bottom water. Since the saline water produced by freezing mixes deeper than fresh melt water, the water at the bottom will eventually become more saline; the long-term steady state component of the resulting large-scale circulation will have to include removal of the saline bottom water by horizontal outflow. Note that this is not a Hadley-type circulation. The simplest model for such a circulation would have an ocean in which the surface is alternately melted and frozen at a horizontally varying rate, but the average net freezing is zero everywhere.

5. The vertical circulation may be forced by the inflow of the warm deep water at higher levels, which in turn is forced by the circulation in the region of the Antarctic circumpolar current. In a more general sense, in other regions of the ocean as well as in the Weddell Sea, it may well be that the formation and circulation of bottom water are virtually independent of each other. The water acquires its "bottom water" characteristics in areas where strong cooling or ice formation causes local convection to penetrate to the bottom, but its subsequent motion is controlled primarily by other types of forcing which are more effective in producing a large-scale deep circulation.

A preliminary investigation was made of the possibility that the large-scale dynamics affects the local mixing significantly. This is discussed in appendix 6.

Chapter 5

Conclusions

The conclusions which have been presented throughout this report are summarized here for the convenience of the reader.

1. Unstable surface convection due to ice formation (and cooling) entrains denser fluid from below, causing the mixed layer to penetrate deeper than the level at which its salinity equals that of the original profile. Its salinity is raised above that which would be produced by the formation of sea ice without entrainment, and a steep halocline is produced in the region from which the more saline water is entrained. In the Arctic Ocean, secondary mixing probably mainly due to the breaking of gravity waves which form on the interface, and upwelling are offered as a possible explanation for the observed rate of increase of salinity in the mixed layer and the failure of this layer to penetrate very deeply into the halocline.
2. Large-scale dynamical effects due to sea ice formation are generally weak, primarily because of the strong rotational constraint associated with a seasonal time scale. A change in sea level produced by the freezing of sea ice will not be affected by the very small dynamical effects which it produces. In the absence of entrainment, velocity fields are generally smooth and weak, and the deformation of the interface is very small. With entrainment, the velocity fields, while still weak, are more complicated, with alternating areas of rising and

sinking motion. The motion is strongest in the region of strongest ice formation.

3. The seasonal formation of ice cannot by itself drive the outflow of the tremendous volume of bottom water which has been estimated to flow out of the Weddell Sea in winter. A combination of ice formation with other factors, or perhaps a different mechanism altogether, must be found to account for this outflow. The velocities involved are quite large, even aside from the adequacy of ice formation as a driving force. In particular, the vertical velocity of 8 meters per day which is required to provide enough water for the estimated outflow of 30 Sverdrups is itself grounds for questioning whether this water is in fact supplied by the large-scale net sinking of water which entered the Weddell Sea at a different depth.

The continuously stratified dynamical model on which the conclusions concerning the Weddell Sea and the nature of the circulation with entrainment are based is the first attempt to include a well-mixed surface layer in an ocean circulation model. The finite difference representation of the mixing region produced numerical oscillations which were quite troublesome. The conclusions from this model are based on time-averaged, rather than instantaneous, motions.

Suggestions for Future Work

The present study overlaps several more or less distinct areas of research in oceanography and geophysical fluid dynamics. It is recommended that workers who wish to extend the present work concentrate on one of these areas at a time, until the area is understood thoroughly, rather than attempt to extend the work in several directions simultaneously.

1. Surface Mixing Processes and Seasonal Thermocline Theory

   The inclusion of cooling and evaporation to the local mixing model should enable it to be used in many areas where strong vertical convection takes place, such as the Mediterranean Sea, the North Pacific and North Atlantic Oceans and even the Weddell Sea. Observational work on the mixing of melt water in summer would be extremely valuable. The ultimate goal should be a predictive model for surface mixed layers, as well as more accurate parameterization of local mixing in large-scale dynamical models.

2. Numerical Techniques in Geophysical Fluid Dynamics

   Models similar to the continuously stratified model presented here should find wide application in a variety of atmospheric and oceanic problems if the troublesome oscillations can be eliminated. Suggestions for pursuing this work further are presented in appendix 1.

3. Formation of Antarctic Bottom Water

Much work is needed here, both theoretical models to test the possible mechanisms for driving the outflow listed in chapter 4, and observations of the outflow, of the vertical motion in the Weddell Sea and of the temperature and salinity under the ice pack.

4. Oceanography of the Arctic Ocean

The vertical motion, the nature of the erosion of the mixed layer and the large-scale dynamics of the sea ice are among the topics to be studied here. It would be especially interesting to see if a full year model with melting as well as freezing and some form of secondary mixing below the mixed layer can account for the structure of the halocline.

Appendix 1

The Numerical Oscillations

The development of the continuously stratified model with a mixed convective layer as a computational technique of geophysical fluid dynamics must be considered incomplete. As might have been expected with an untested numerical procedure (it now seems obvious), the new model has created difficult problems of its own. Extensive further work, probably in excess of the effort that was required to reach this point, will be required to study and refine the numerical methods that are used in solving this model. Only when the computational mathematics is much better understood than at present should an attempt be made to develop more realistic models, and models to be applied to a variety of different oceanographic problems.

The basic difficulty is that when the strong vertical mixing is performed on a grid which employs finite differences in both the horizontal and vertical directions, the height of the interface changes in quantum jumps rather than continuously. Where it jumps, the pressure gradient has a discontinuity; this produces a discontinuity in the variation of U, which in turn produces a strong, localized W, rather than a relatively weak w that is more uniformly distributed. Hence, spurious numerical oscillations in both U and W are generated.

The generation of these oscillations can be illustrated with a simple box model. Consider a model "box" ocean that is 7 units wide and 3 units deep (and infinitely long). For simplicity take $\Delta X=1$ and $\Delta Z=1$. Since only one time step will be calculated, V can be neglected, and so will stability criteria; we will simply take $\Delta t=1$. Numerical constants in the equations will also be neglected. If $U=0$ and $w=0$ initially, we can then find U and W. by applying these equations in succession (in finite difference form):

$$(A1) \quad U' = -\int_{z}^{z_{Top}} \frac{\partial S}{\partial x} dz$$

$$(A2) \quad U = U' - \int_{z_{Bottom}}^{z_{Top}} U' dz$$

$$(A3) \quad w = -\int_{z_{Bottom}}^{z} \frac{\partial u}{\partial x} dz'$$

First consider the initial condition shown in Fig. A1. The ocean is at rest, with a deep mixed layer on top of a more saline bottom layer. Add from 0 to 3 units of salt with a linear horizontal variation as shown, and assume that mixing takes place according to the Zubov-Defant theory. The mixed layer remains of uniform depth, and a reasonably simple circulation develops. Even

here, it must be noted that the use of finite differences effectively produces discontinuities which give rise to some numerical oscillations.

Next consider the initial condition shown in Fig. A2. Here the stratification extends through all three layers, so that when the salt is added, even with Zubov-Defant mixing, the interface jumps as shown. Where it jumps there is a small "spike" in W. The dynamical equations for the next step will propagate this spike as a wave.

Finally, consider the situation in Fig. A3, in which the salt is added to the same initial profile as in Fig. A2, but mixing produces entrainment according to the Ball theory. In this case the result is even more complicated, and more wave-like; there are two jumps in the interface height, with adjacent positive and negative values of W at two locations and even of U at one location. Therefore, we can expect U and W to be even more strongly oscillatory in this case.

In the full ocean model, it does not take many time steps before most or all of the columns have been the location of an interface discontinuity at least once. This, together with the horizontal propagation of these waves, produces a set of oscillations which cover the entire ocean and mask the physical solution. Some important relations between this oscillatory solution and the presumed correct physical solution can be gained from a careful examination of the simple box model:

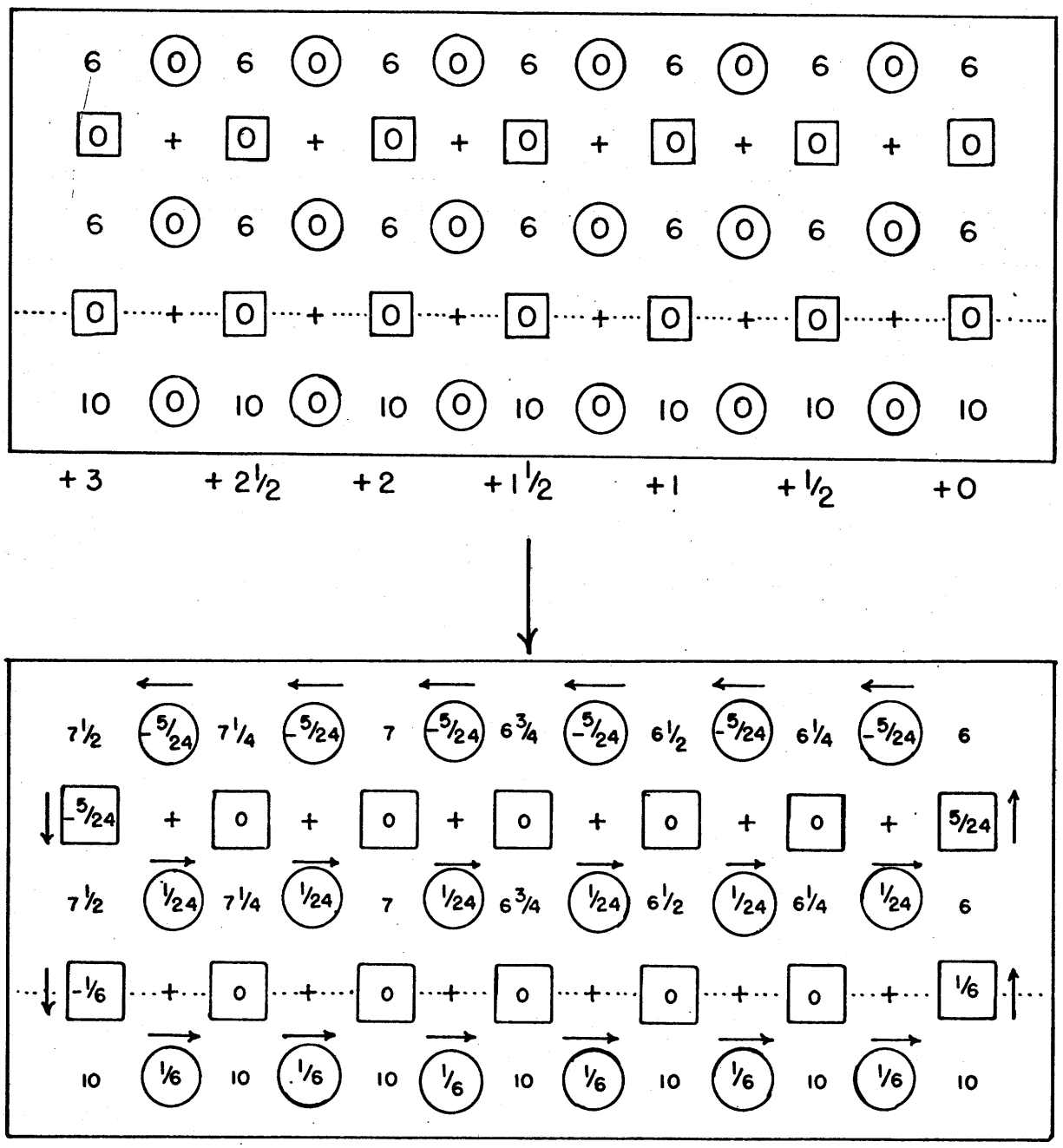

Figure A-1. Mixing by the Zubov-Defant model that does not produce a variation in the height of the interface. Values of U are enclosed in circles; values of W are in rectangles. The numbers that are not enclosed may be thought of as values of salinity in arbitrary units. Dots show the location of the interface.

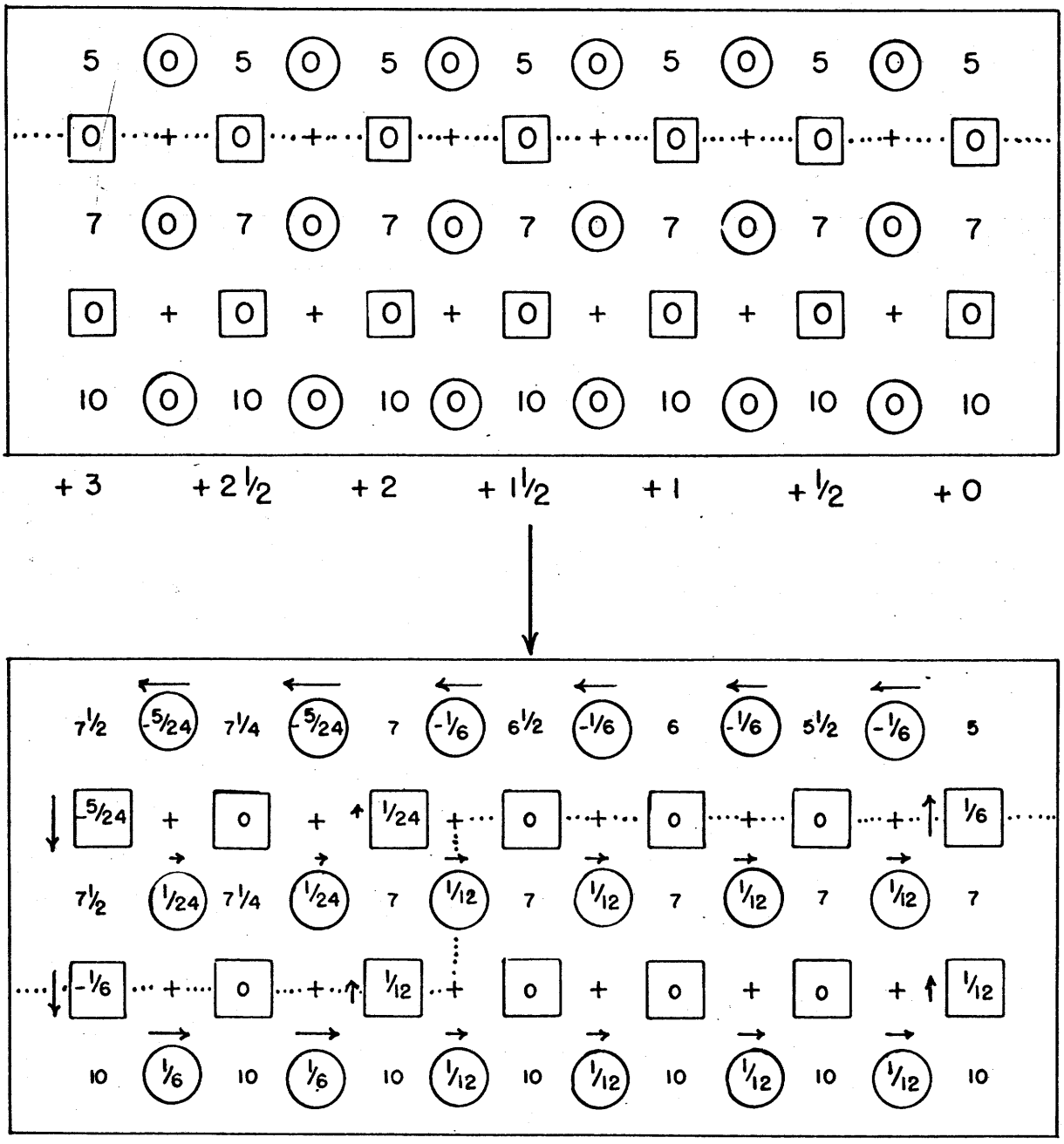

Figure A2 - Mixing by the Zubov-Defant Model that does Produce a Jump in the Interface. Note the "Spike" in w to the left of the Jump.

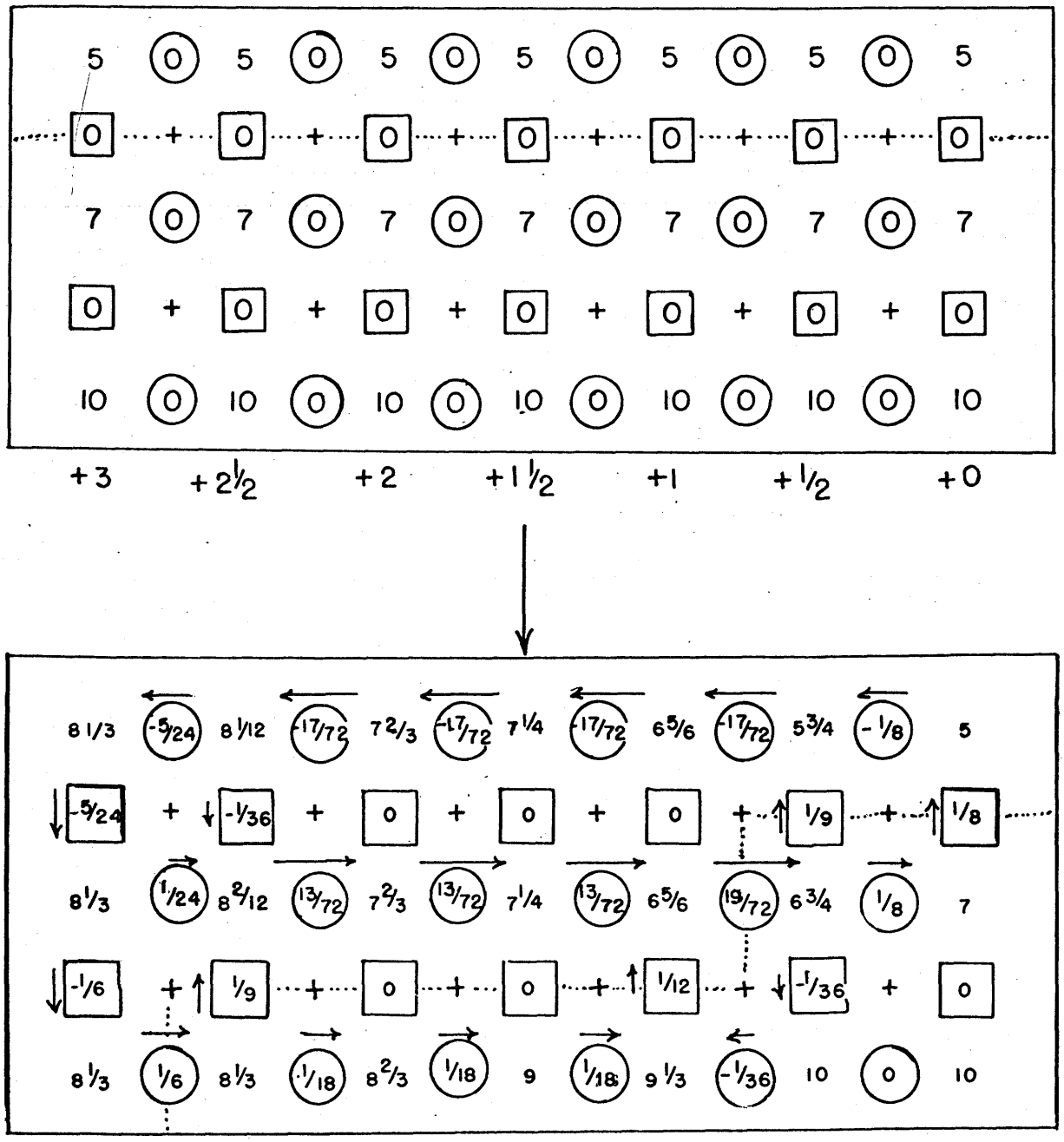

Figure A3 - Mixing by the Kraus-Turner-Ball model. The interface jumps twice, and oscillations in both U and W are generated.

1) The magnitude of U is not affected; the effect on U is that the variation of U occurs in quantum jumps rather than continuously. Once the oscillations have been generated and begin propagating, addition of waves could increase the amplitude by as much as a factor of 2 or so, but probably not by an order of magnitude.

2) W is concentrated where discontinuities in U take place. The instantaneous values of W are much larger than one would expect to find in the continuous physical solution.

In the case with entrainment, the basic (actual physical) circulation is more complicated than without entrainment because of the reversal of the density gradient at the level from which denser water is entrained upward.

When the oscillations are first generated, as in these simple box models, the irregularities could be "smoothed" in order to give one a general idea of what the physical solution ought to look like. However, after several time steps, oscillations have been generated at many points and have had a chance to propagate and to interact with each other. Then only the most general conclusions can be reached concerning the physical solution. If one of the velocity components is positive most of the time at a given point, the physical solution is probably positive at that point. Some reasonably accurate conclusions can be reached with regard to the order of magnitude of the motion. From the way that the oscil-

lations are generated it can be seen that the instantaneous values of W are larger than what one would expect as the physical solution. The values of U are on the order of the physical solution when generated. However, the oscillations are cumulative in their amplitude, and their short time scale prevents the growth of U from being as strongly controlled by rotation as it should be in the physical solution. This is consistent with the numerical results, which show that the instantaneous U is almost as large as the instantaneous V, but the time-averaged U is about two orders of magnitude smaller than the time-averaged V, in agreement with what would be expected from a scale analysis.

It should be noted that the mixing of salt alone is sufficient to produce the oscillations. Momentum mixing produces large values of W where the interface jumps; these undoubtedly add somewhat to the oscillations.

A few simple tests were run with the full-scale ocean model in an attempt to gain a better understanding of these oscillations. The amount of "waviness" was estimated subjectively by visual inspection of a printout of W at all values of x for one specified value of z near the top. Omission of momentum mixing did not visibly reduce the oscillatory character of the solution; neither did the introduction of the most elementary form of horizontal viscosity, a single second-order Laplacian with a constant coefficient. Little difference was noticed between otherwise identical cases in which

the vertical grid spacing was 3 meters (total depth 300 meters) in one and 10 meters (total depth 1000 meters) in the other. The 3-meter spacing was finally chosen on general principles, since the scale height of the initial profile is only 50 meters, but this much change in the grid spacing did not significantly reduce the waviness. The one thing that did significantly reduce the waviness was the use of a 2-layer initial profile, with Zubov-Defant mixing, so that the interface remained horizontal, with no jumps (corresponding to the box model in Fig. A1). Even here, some waviness eventually developed, probably due to the unavoidable discontinuities produced by the use of finite differences. There may also be some waviness in the physical solution, probably caused by adjustments needed to satisfy the boundary conditions.

How do the oscillations behave after they are generated? Fig. A4 is a graph of W and $\overline{W} = \frac{1}{N}\sum_{N=1}^{N} W_N$ vs. t for the first 60 time steps of one of the trial runs. Fig. A5 is a similar graph of U and $\bar{U}$ vs. t. Each is at one arbitrarily selected point in space (not the same in the two cases). It can be seen that the oscillations are reasonably regular, with a period just slightly shorter than the inertial period. The amplitude increases in a roughly linear way (except for one sudden jump, after which the increase is again linear, in Fig. A5) as the effects of repeated forcing accumulate, but never at an exponential rate. The results of all of the runs show that the amplitude remains highest in the

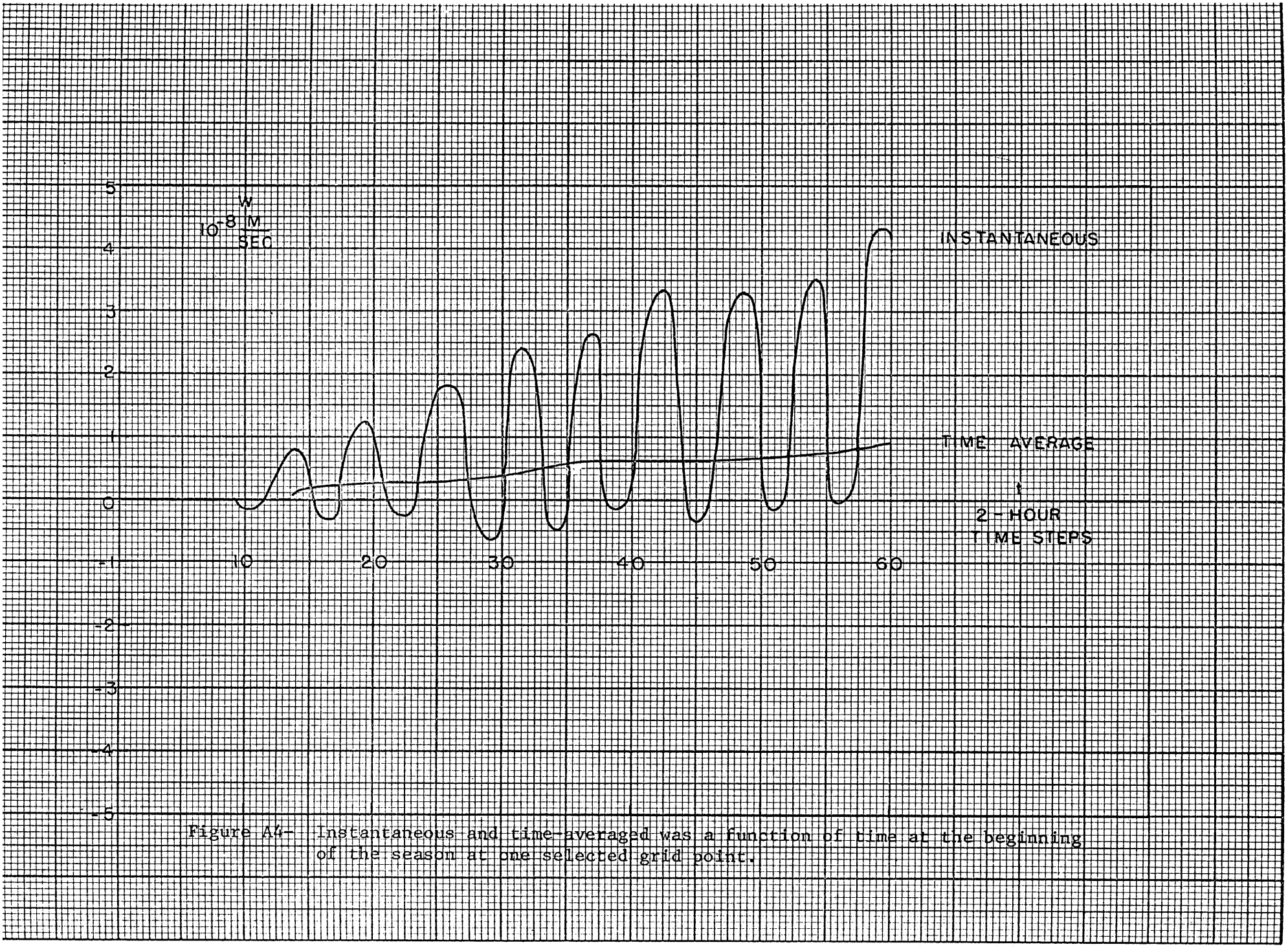

Figure A4- Instantaneous and time-averaged was a function of time at the beginning of the season at one selected grid point.

Figure A5 Instantaneous V vs. time for the rist 60 time steps at one selected grid point. The time-averaged v is nearly zero on this scale.

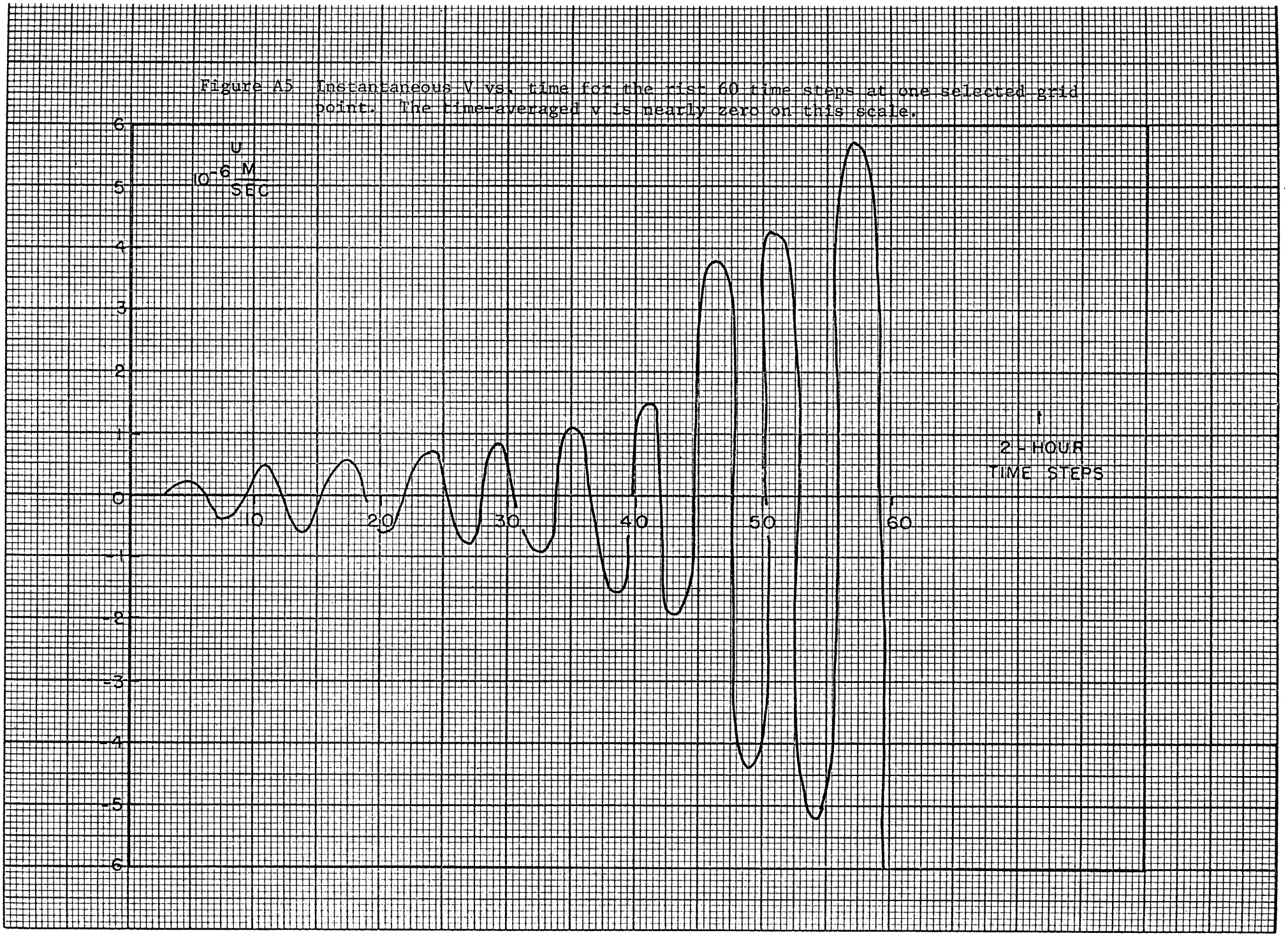

region of maximum forcing; the energy does not propagate very far. This evidence taken together would seem to indicate that the oscillations, once generated, behave as inertial oscillations, with frequency modified slightly by the stratification. In other words, they obey a physically meaningful solution to the dynamical equations; there is no evidence of an instability. If the forcing were stopped the waves already in the system would not grow with time. The printout of W at every x for one particular z (all values across the ocean in a horizontal line) indicates that the wavelength of the oscillations, while somewhat variable, is always longer than two grid spacings. Alternation of the sign at every grid spacing throughout the model, as happens with many numerical instabilities, does not occur.

Suggestions for Future Work on the Continuously Stratified Dynamical Model

A way will have to be found to control the oscillations described above before the inclusion of a mixed layer in a continously stratified model can be considered a reliable technique of numerical computation, and models developed to apply to other examples of density-driven flow. The problems involved here are somewhat different than those that are usually treated in work on finite difference methods, so that additional experience with this system will be required before they are solved. This work could

easily occupy the full-time attention of a research worker for a period of months or years during which no significant oceanographical results would be obtained. It is therefore probably best done by someone whose primary interest is in computational fluid dynamics rather than field oceanography.

The following suggestions are offered as possible approaches in pursuing this work further:

1) One obvious approach is to use a much finer grid; presumably this would reduce the magnitude of the oscillations compared to that of the physical motions. This approach will be expensive and will involve additional programming complications because the basic core memory will not be sufficient for storage of all of the fields.

2) If more can be learned about the nature of the secondary mixing process which is always eroding the mixed layer from the bottom, it is possible that the two can be combined into a single parameterized mixing process which does not have the abrupt discontinuity that the present model has. One possible form of such a mixing model would be a variable eddy viscosity, such as that used by Overstreet and Rattray (1969) in a local thermocline model. However, more research on the nature of the mixing process will have to be done before a really accurate representation of the mixing can be obtained.

3) In the special case of a two-layer initial profile,

with Zubov-Defant mixing and a sharp enough interface to keep the depth of the mixed layer uniform throughout the calculation, it might be possible to eliminate the oscillations by the use of an artificial horizontal viscosity. It is doubtful if this will work when the depth of the mixed layer varies in X, because the horizontal mixing at points where the interface jumps will generate still more oscillations. However, even this possibility is probably worth checking out just to make sure. The viscosity to be used here will probably have to contain a combination of terms of different order derivatives because the dominant wavelength of the oscillations is longer than the minimum that the grid can resolve.

4) An attempt could be made to retain an actual interface in the continuously stratified model, and to incorporate it into the model in such a way as to minimize the consequences of the coarse grid in producing oscillations. For example, in Fig. A6, W at point 3 would not be calculated on the basis of the difference in U between point 1 and point 2. Instead, the dynamics of the interface would enter into the calculation in some way. This would hopefully eliminate the effects of discontinuities between points inside and outside of the mixed layer in producing spurious oscillations.

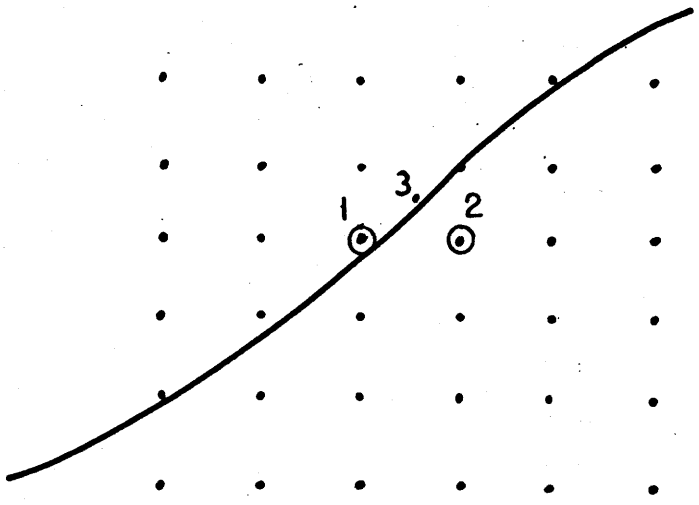

Figure A6

Appendix 2

DIFFERENCE EQUATIONS AND METHOD OF SOLUTION FOR THE TWO-LAYER MODEL

The finite difference form of the main governing equation, (100), is

$$(A4)\quad (\rho_2-\rho_{1\,J,N})\,\frac{(h_{1\,J+1,N+1}-2h_{1\,J,N+1}+h_{1\,J-1,N+1})-(h_{1\,J+1,N}-2h_{1\,J,N}+h_{1\,J-1,N})}{(\Delta x)^2\Delta t}$$

$$-\frac{f^2}{g h_{1\,J,N}}\,\rho_{1\,J,N}\,\frac{h_{1\,J,N+1}-h_{1\,J,N}}{\Delta t}=$$

$$=\frac{h_{1\,J,N}}{2}\,\frac{(\rho_{1\,J+1,N+1}-2\rho_{1\,J,N+1}+\rho_{1\,J-1,N+1})-(\rho_{1\,J+1,N}-2\rho_{1\,J,N}+\rho_{1\,J-1,N})}{(\Delta x)^2\Delta t}$$

where j is the index in the X-direction and N is the time index. The boundary condition, (101), becomes

$$(A5)\quad (\rho_2-\rho_{1\,J,N})\,\frac{(h_{1\,J+1,N+1}-h_{1\,J,N+1})-(h_{1\,J+1,N}-h_{1\,J,N})}{\Delta x\,\Delta t}$$

$$-\frac{h_{1\,J,N}}{2}\,\frac{(\rho_{1\,J+1,N+1}-\rho_{1\,J,N+1})-(\rho_{1\,J+1,N}-\rho_{1\,J,N})}{\Delta x\,\Delta t}=0$$

Since $(\Delta t)^{-1}$ is a common factor in all terms of (A4), linear computational stability is independent of the size of the time step, the relation between the space and time grid spacings and the type of difference scheme used.

(A4) can be written in the form of equation (8.15) of Richtmyer and Morton (1967); the method of solution given for the

latter equation will be used in the present problem. The unknowns are $h_{1\,J,N+1}$ AND $h_{1\,J+1,N+1}$.

Following the method of Richtmyer and Morton, Let

$$\gamma_J = 2 + \frac{f^2}{g h_{1\,J,N}} \frac{\rho_{1\,J,N}(\Delta x)^2}{\rho_2 - \rho_{1\,J,N}}$$

$$\eta_J = \frac{h_{1\,J,N}}{2(\rho_2 - \rho_{1\,J,N})}$$

Then (A4) has the form

$$(A6) \quad -A_J \phi_{J+1} + B_J \phi_J - C_J \phi_{J-1} = D_J$$

where

$$\phi_J = h_{1\,J,N+1}$$

$$A_J = -1$$

$$B_J = -\gamma_J$$

$$C_J = -1$$

$$D_J = +h_{1\,J+1,N} - \gamma_J h_{1\,J,N} + h_{1\,J-1,N} + \eta_J(\rho_{1\,J+1,N+1} - 2\rho_{1\,J,N+1} + \rho_{1\,J-1,N+1} - \rho_{1\,J+1,N} + 2\rho_{1\,J,N} - \rho_{1\,J-1,N})$$

The boundary condition is

$$(A7) \quad \phi_{J+1} - \phi_J = G_J \quad \text{FOR} \quad J=1 \text{ AND } J=JM-1$$

where JMis the maximum value of j and

$$G_J = \frac{h_{1\,J,N}}{2} \frac{\rho_{1\,J+1,N+1} - \rho_{1\,J,N+1} - \rho_{1\,J+1,N} + \rho_{1\,J,N}}{\rho_2 - \rho_{1\,J,N}}$$

(A6) is solved by looking for solutions of the form

$$(A8) \qquad \phi_J = E_J \phi_{J+1} + F_J$$

It is shown by Richtmyer and Morton that

$$(A9) \qquad E_J = \frac{A_J}{B_J - C_J E_{J-1}} \quad \text{AND} \quad F_J = \frac{D_J + C_J F_{J-1}}{B_J - C_J E_{J-1}}$$

At j = 1 we have

$$\phi_2 - \phi_1 = G_1$$
$$\phi_1 = E_1 \phi_2 + F_1$$

Eliminating ϕ_1 gives

$$\phi_2 = E_1 \phi_2 + (F_1 + G_1)$$

This must hold for all possible ϕ_2, so

$$E_1 = +1$$

$$F_1 = -G_1 \ (G_1 \text{ is known}).$$

All of the E_j's and F_j's can now be calculated, in increasing order of j, using (A9). Then

$$\phi_{JM} - \phi_{JM-1} = G_{JM-1}$$
$$\phi_{JM-1} = E_{JM-1} \phi_{JM} + F_{JM-1}$$

Eliminating ϕ_{JM-1} gives

$$(A10) \qquad \phi_{JM} = \frac{F_{JM-1} + G_{JM-1}}{1 - E_{JM-1}}$$

All quantities on the right side of (A10) are known, so we have ϕ_{JM}. Now all of the ϕ_j's can be calculated, in decreasing order of j, using (A8).

The next variable to be calculated is h_2. In finite difference form, (60) becomes

$$(A11)\quad \sum_{J=1}^{JM}(\rho_{1\,J,N+1}h_{1\,J,N+1}+\rho_2 h_{2\,J,N+1})(\Delta x)_J=\sum_{J=1}^{JM}(\rho_{1\,J,N}h_{1\,J,N}+\rho_2 h_{2\,J,N})(\Delta x)_J$$

Δx depends on j because the intervals are centered on points where ρ_1, h_1 and h_2 are known. Therefore the end intervals are only half as wide as the interior intervals.

Solved for the sum of the h_2's, this becomes

$$(A12)\quad \tfrac{1}{2}\left[h_{2\,1,N+1}+2(h_{2\,2,N+1}+\ldots+h_{2\,JM-1,N+1})+h_{2\,JM,N+1}\right]=$$
$$=\frac{1}{\rho_2}\left\{\left[\sum_{J=1}^{JM}(\rho_{1\,J,N}h_{1\,J,N}+\rho_2 h_{2\,J,N})\frac{(\Delta x)_J}{\Delta x}\right]-\sum_{J=1}^{JM}\rho_{1\,J,N+1}h_{1\,J,N+1}\frac{(\Delta x)_J}{\Delta x}\right\}$$

where Δx without a subscript is the interior grid spacing, and

$$\frac{(\Delta x)_J}{\Delta x}=\frac{2-(\delta_{J,1}+\delta_{J,JM})}{2}$$

The right side of (A12). will be called K :

$$(A13)\quad h_{2\,1,N+1}+2(h_{2\,2,N+1}+\ldots+h_{2\,JM-1,N+1})+h_{2\,JM,N+1}=2K$$

Let

$$(A14)\quad \nu_J=h_{2\,J+1,N+1}-h_{2\,J,N+1}$$

Then

$$h_{2\,2,N+1} + h_{2\,3,N+1} = 2h_{2\,2,N+1} + \nu_2 = 2h_{2\,1,N+1} + 2\nu_1 + \nu_2$$

$$h_{2\,2,N+1} + h_{2\,3,N+1} + h_{2\,4,N+1} = 3h_{2\,1,N+1} + 3\nu_1 + 2\nu_2 + \nu_3$$

This process can be continued until we obtain

$$\text{(A15)}\quad h_{2\,2,N+1} + \ldots + h_{2\,JM-1,N+1} = (JM-2)h_{2\,1,N+1} + (JM-2)\nu_1 + (JM-3)\nu_2 + \ldots + \nu_{JM-2}$$

Substitution of (112) and (113) into (111) eventually leads to:

$$\text{(A16)}\quad h_{2\,1,N+1} = \frac{2K - [(2JM-3)\nu_1 + (2JM-5)\nu_2 + \ldots + 3\nu_{JM-2} + \nu_{JM-1}]}{2JM-2}$$

The ν_J's can be found from the finite difference form of (59):

$$\text{(A17)}\quad \nu_J = -\frac{1}{\rho_2}\left(\rho_{1\,J+1,N+1}\, h_{1\,J+1,N+1} - \rho_{1\,J,N+1}\, h_{1\,J,N+1}\right)$$

After all of the ν_J's have been found from (A17), $h_{2\,1,N+1}$ can be found from (A16). Then the other $h_{2\,J,N+1}$'s can be found from (A14) in increasing order of j.

U_1 and V_1 can then be found from the finite difference forms of (99) and (98):

$$\text{(A18)}\quad U_{1\,J,N} = -\frac{g}{\rho_2 f^2 \Delta x \Delta t}\Big[(\rho_2 - \rho_{1\,J,N})(h_{1\,J+1,N+1} - h_{1\,J-1,N+1} - h_{1\,J-1,N+1} + h_{1\,J-1,N-1}) - \frac{h_{1\,J,N}}{2}(\rho_{1\,J+1,N+1} - \rho_{1\,J-1,N+1} - \rho_{1\,J+1,N-1} + \rho_{1\,J-1,N-1})\Big]$$

$$\text{(A19)}\quad V_{1\,J,N} = +\frac{g}{\rho_2 f \Delta x}\Big[(\rho_2 - \rho_{1\,J,N})(h_{1\,J+1,N} - h_{1\,J-1,N}) - \frac{h_{1\,J,N}}{2}(\rho_{1\,J+1,N} - \rho_{1\,J-1,N})\Big]$$

Appendix 3

THE NUMERICAL STABILITY CRITERION

The computational stability criterion for the set of equations (132), (133), (134), (135), (136) and (137) [or, better, with the finite difference form of (110) replacing (132) and (134)], can be investigated, and then only partially, by determining the "von Neumann necessary condition". The objective is to place a limit on the size of the time step so that small perturbations will not grow exponentially with time. Since the growth rate of the perturbations varies with their wavelength, we start by taking the Fourier transforms (in space) of the difference equations. The nonlinear terms are "linearized" with the advecting velocities $\breve{U}$ and $\breve{W}$ considered to be constant.

$$\text{(A20)}\quad \hat{U}_{J,K,N} = \Lambda \hat{U}_{J,K,N-1} - 2i\frac{\Delta t}{\rho_o \Delta x}\,\mathrm{SIN}\left(\tfrac{1}{2}\xi x\right)\hat{P}_{J,K,N-\frac{1}{2}} + f\Delta t \hat{V}_{J,K,N-\frac{1}{2}}$$

$$\text{(A21)}\quad \hat{V}_{J,K,N+\frac{1}{2}} = \Lambda \hat{V}_{J,K,N-\frac{1}{2}} - f\Delta t \hat{U}_{J,K,N}$$

$$\text{(A22)}\quad \hat{\rho}_{J,K,N+\frac{1}{2}} = \Lambda \hat{\rho}_{J,K,N-\frac{1}{2}} - \Delta t \frac{d\rho_o}{dz}\hat{W}_{J,K,N}$$

$$\text{(A23)}\quad \hat{P}_{J,K,N-\frac{1}{2}} = +\frac{\frac{1}{2}ig\Delta z}{\mathrm{SIN}\left(\frac{1}{2}\eta\Delta z\right)}\hat{\rho}_{J,K,N-\frac{1}{2}}$$

$$\text{(A24)}\quad \hat{W}_{J,K,N} = -\frac{\Delta z}{\Delta x}\frac{\mathrm{SIN}\left(\frac{1}{2}\xi\Delta x\right)}{\mathrm{SIN}\left(\frac{1}{2}\eta\Delta z\right)}\hat{U}_{J,K,N}$$

where $\Lambda = 1 - \frac{\breve{U}\Delta t}{\Delta x}(1-e^{-i\xi\Delta x}) - \frac{\breve{W}\Delta t}{\Delta z}(1-e^{-i\eta\Delta z})$, $i=\sqrt{-1}$, ξ and η are the x and z Fourier wave numbers, respectively, and $\hat{\psi}$ is the Fourier transform of ψ for each variable.

Substituting $\hat{P}$ and $\hat{W}$ from (A23) and (A24) into (A20), (A21) and (A22) gives:

$$\text{(A25)}\quad \hat{U}_{J,K,N} = \Lambda \hat{U}_{J,K,N-1} + \frac{g\Delta z\Delta t}{\rho_o \Delta x}\frac{d\rho_o}{dz}\frac{\text{SIN}(\frac{1}{2}\xi\Delta x)}{\text{SIN}(\frac{1}{2}\eta\Delta z)}\hat{\rho}_{J,K,N-1/2} + f\Delta t\,\hat{V}_{J,K,N-1/2}$$

$$\text{(A26)}\quad \hat{V}_{J,K,N+1/2} + f\Delta t\,\hat{U}_{J,K,N} = \Lambda \hat{V}_{J,K,N-1/2}$$

$$\text{(A27)}\quad \hat{\rho}_{J,K,N+1/2} - \frac{\Delta z\Delta t}{\Delta x}\frac{d\rho_o}{dz}\frac{\text{SIN}(\frac{1}{2}\xi\Delta x)}{\text{SIN}(\frac{1}{2}\eta\Delta z)}\hat{U}_{J,K,N} = \Lambda \hat{\rho}_{J,K,N-1/2}$$

Writing these in matrix form and multiplying both sides by the inverse of the coefficient matrix on the left side leads to:

$$\text{(A28)}\quad \begin{bmatrix} \hat{U}_{J,K,N} \\ \hat{V}_{J,K,N+1/2} \\ \hat{\rho}_{J,K,N+1/2} \end{bmatrix} = \begin{bmatrix} \Lambda & +f\Delta t & +\frac{g\zeta}{\rho_o} \\ -f\Delta t\Lambda & \Lambda - f^2(\Delta t)^2 & -f\frac{g\zeta}{\rho_o}\Delta t \\ +\Lambda\zeta\frac{d\rho_o}{dz} & +f\Delta t\zeta\frac{d\rho_o}{dz} & \Lambda + \frac{g}{\rho_o}\frac{d\rho_o}{dz}\zeta^2 \end{bmatrix}\begin{bmatrix} \hat{U}_{J,K,N-1} \\ \hat{V}_{J,K,N-1/2} \\ \hat{\rho}_{J,K,N-1/2} \end{bmatrix}$$

where

$$\zeta = \frac{\Delta z\Delta t}{\Delta x}\,\frac{\text{SIN}(\frac{1}{2}\xi\Delta x)}{\text{SIN}(\frac{1}{2}\eta\Delta z)}$$

The 3x3 matrix on the right side is the amplification matrix $\underline{A}'$, which determines the amplification of the (ξ,η) Fourier component of the solution vector in a single time step. The von Neumann necessary condition for computational stability is $\|\underline{A}'(\omega)\| \leq 1$. In practice this is usually used as the stability criterion, without proof of sufficiency except for the computation itself. This criterion is satisfied if and only if all of the eigenvalues of A are ≤ 1. The eigenvalues are found from the characteristic equation:

$$|\lambda I - A'| = 0 \tag{A29}$$

OR

$$(\lambda-\Lambda)\left\{(\lambda-\Lambda)^2 + \left[f^2(\Delta t)^2 - \frac{g}{\rho_0}\zeta^2\Gamma\right]\lambda\right\} = 0 \tag{A30}$$

where the λ's are the eigenvalues and $\Gamma = \frac{d\rho_0}{dz}$.

The three eigenvalues are:

$$\lambda_1 = \Lambda \tag{A31}$$

$$\lambda_2 = -\frac{1}{2}\left[f^2(\Delta t)^2 - \frac{g}{\rho_0}\zeta^2\Gamma - 2\Lambda\right] + \frac{1}{2}\sqrt{\left[f^2(\Delta t)^2 - \frac{g}{\rho_0}\zeta^2\Gamma - 2\Lambda\right]^2 - 4\Lambda^2} \tag{A32}$$

$$\lambda_3 = -\frac{1}{2}\left[f^2(\Delta t)^2 - \frac{g}{\rho_0}\zeta^2\Gamma - 2\Lambda\right] - \frac{1}{2}\sqrt{\left[f^2(\Delta t)^2 - \frac{g}{\rho_0}\zeta^2\Gamma - 2\Lambda\right]^2 - 4\Lambda^2} \tag{A33}$$

First consider the condition for λ_1.

$$|\lambda_1|^2 = 1 - 4\Psi \tag{A34}$$

where

$$(A35)\quad \Psi = \frac{\breve{u}\Delta t}{\Delta x}\left(1-\frac{\breve{u}\Delta t}{\Delta x}\right)\mathrm{SIN}^2\left(\tfrac{1}{2}\xi\Delta x\right) + \frac{\breve{w}\Delta t}{\Delta z}\left(1-\frac{\breve{w}\Delta t}{\Delta z}\right)\mathrm{SIN}^2\left(\tfrac{1}{2}\eta\Delta z\right) - 2\frac{\breve{u}\Delta t}{\Delta x}\frac{\breve{w}\Delta t}{\Delta z}\mathrm{SIN}\left(\tfrac{1}{2}\xi\Delta x\right)\mathrm{SIN}\left(\tfrac{1}{2}\eta\Delta z\right)\cos\left[\tfrac{1}{2}(\xi\Delta x-\eta\Delta z)\right]$$

(A35) can be rewritten as:

$$(A36)\quad \Psi = \left[\frac{\breve{u}\Delta t}{\Delta x}\mathrm{SIN}^2\left(\tfrac{1}{2}\xi\Delta x\right)+\frac{\breve{w}\Delta t}{\Delta z}\mathrm{SIN}^2\left(\tfrac{1}{2}\eta\Delta z\right)\right]\left(1-\frac{\breve{u}\Delta t}{\Delta x}-\frac{\breve{w}\Delta t}{\Delta z}\right) + \frac{\breve{u}\Delta t}{\Delta x}\frac{\breve{w}\Delta t}{\Delta z}\mathrm{SIN}^2\left[\tfrac{1}{2}(\xi\Delta x-\eta\Delta z)\right]$$

The condition

$$(A37)\quad \frac{\breve{u}\Delta t}{\Delta x}+\frac{\breve{w}\Delta t}{\Delta z}\leq 1$$

is necessary and sufficient to insure $\Psi \geq 0$ and $|\lambda_1|^2 \leq 1$.

The condition on λ_2 and λ_3, which arises from the propagation of internal gravity waves in the system, turns out to be a far more stringent restriction on Δt than the condition on λ_1. To investigate this condition, let

$$(A38)\quad A = \frac{\breve{u}\Delta t}{\Delta x}\left[1-\cos\left(\xi\Delta x\right)\right]+\frac{\breve{w}\Delta t}{\Delta z}\left[1-\cos\left(\eta\Delta z\right)\right]$$

$$(A39)\quad B = \frac{\breve{u}\Delta t}{\Delta x}\mathrm{SIN}\left(\xi\Delta x\right)+\frac{\breve{w}\Delta t}{\Delta z}\mathrm{SIN}\left(\eta\Delta z\right)$$

$$(A40)\quad \ell = f^2(\Delta t)^2 - \frac{g}{\rho_0}\zeta^2\Gamma$$

Then

$$\text{(A41)}\quad \lambda_{\frac{2}{3}} = 1-(A+iB)-\tfrac{1}{2}\ell \pm \tfrac{1}{2}\sqrt{\ell[\ell-4+4(A+iB)]}$$

$$\text{(A42)}\quad |\lambda_{\frac{2}{3}}|^2 \approx 1+4\frac{A^2+B^2}{4-\ell}+2A\mp B\left(2+\ell\sqrt{\frac{\ell}{4-\ell}}\right)\pm B\sqrt{\ell(4-\ell)} \qquad 0<\ell<+4$$

$$\text{(A43)}\quad |\lambda_{\frac{2}{3}}|^2 \approx -\left(1+A\mp\sqrt{2\left(A+\sqrt{A^2+B^2}\right)}\right)^2+B^2\left(1\mp\sqrt{\frac{2}{A+\sqrt{A^2+B^2}}}\right)^2 \qquad \ell=+4$$

$$\text{(A44)}\quad |\lambda_{\frac{2}{3}}|^2 \approx 1+\tfrac{1}{2}\ell^2+(A^2+B^2)\left(1\mp\sqrt{\frac{\ell}{\ell-4}}\right)^2+A(2-\ell)\left(1\mp\sqrt{\frac{\ell}{\ell-4}}\right)$$
$$\pm\sqrt{\ell(\ell-4)}\left[1-\tfrac{1}{2}\ell+A\left(1-\sqrt{\frac{\ell}{\ell-4}}\right)\right] \qquad \ell<0;\ \ell>+4$$

$$\text{(A45)}\quad |\lambda_{\frac{2}{3}}|^2 \approx A^2+B^2 \qquad \ell=0$$

(A43), (A44) and (A45) are approximate formulas derived from

$$\text{(A46)}\quad \lambda_{\frac{2}{3}} \approx 1-(A+iB)-\tfrac{1}{2}\ell\pm\tfrac{1}{2}\sqrt{\ell(\ell-4)}\pm(A+iB)\sqrt{\frac{\ell}{\ell-4}}\quad ,$$

which is obtained from (A3-22) when $4(A + iB) \ll \ell - 4$. It will be seen that this approximation holds for all ℓ for which the condition on λ_2 and λ_3 is satisfied.

The case $\ell = 0$ is equivalent to the eigenvalue λ_1.

For the cases $\ell < 0$ and $\ell > +4$ it is sufficient to consider the special case in which A = 0 and B = 0. In this special case it is possible to work directly with (A41), without making the approximation (A46):

$$\lambda_{\frac{2}{3}} = 1 - \tfrac{1}{2}\ell \pm \tfrac{1}{2}\sqrt{\ell(\ell-4)}$$
$$= 1 - \tfrac{1}{2}\ell \pm \sqrt{(1-\tfrac{1}{2}\ell)^2 - 1}$$

so that

$$\lambda_{\frac{2}{3}} = e^{\pm i\theta} \tag{A48}$$

where

$$\cos\theta = 1 - \tfrac{1}{2}\ell \tag{A49}$$

Then

$$|\lambda_{\frac{2}{3}}|^2 = \cos^2\theta + \sin^2\theta \tag{A50}$$

If $\ell < 0$ or $\ell > +4$, $\cos\theta > 1$ (corresponding to an imaginary θ), and $|\lambda_{\frac{2}{3}}|^2 > 1$, which implies instability.

For the case $\ell = +4$, considering first the special case B = 0, we have

$$|\lambda_{\frac{2}{3}}|^2 = (1 \mp \sqrt{A})^4 \tag{A51}$$

One of these will always be greater than 1 except when A = 0, so that A ≠ 0 implies instability. Next consider the special case A = 0. Then

$$|\lambda_{\frac{2}{3}}|^2 = (1 \pm \sqrt{B})^4 + 2B \tag{A52}$$

One of these will always be greater than 1 except when B = 0. Therefore B ≠ 0 also implies instability, and the only

stable case is when A = 0 and B = 0. From (A38) and (A39) we see that this is the trivial case when no motion develops in the system.

This leaves $0 \leqq \ell < +4$ as the only range within which stability is possible. A rigorous derivation of the stability criterion in this case would be extremely complicated, if it is in fact possible, when $U \neq 0$ and $W \neq 0$ since, as must be done with the von Neumann condition, all values of ξ and η must be considered. An estimate of the condition is derived below on the assumption that, as often happens, the worst case occurs for the shortest wavelength which can be resolved by the finite difference grid, which is $2\Delta x$ ($2\Delta z$ in the vertical). The condition obtained in this way is $\Delta t \leqq 7205$ seconds. Since $\Delta t = 7200$ seconds (2 hours) was used and the computations were stable, it is likely that this was in fact the worst case, since Δt was so close to the limit that if there were a worse case an instability would have probably occurred.

To examine the case $0 < \ell \leqq +4$, it proved convenient to start from an exact equation derived from (A41) rather than the approximate form (A42):

$$(A53)\quad |\lambda_{\frac{2}{3}}|^2 = 1 + (A^2+B^2) + \frac{1}{4}\ell^2 + \frac{1}{4}\ell\mu - 2A - \ell + A\ell \pm \sqrt{2\ell}\,\sqrt{-\tau+\mu}\,\left(A - \tfrac{1}{2} + \tfrac{1}{4}\ell - \tfrac{1}{2}B\right)$$

where

$$(A54)\quad \tau = 4 - \ell - 4A$$

and

$$(A55)\quad \mu = \sqrt{\tau^2 + 16B^2}$$

Assume that a result derived for $\breve{U} > 0$ and $\breve{W} > 0$ is valid

in the general case. From (A3-19) and (A3-20), if $\frac{\breve{w}}{\Delta z} \sim \frac{\breve{u}}{\Delta x}$,

(A56) $$A \lesssim 4\frac{\breve{u}\Delta t}{\Delta x}$$

(A57) $$B \lesssim 2\frac{\breve{u}\Delta t}{\Delta x}$$

It is not necessarily rigorously true that the worst case is obtained when both A and B have these maximum values, because of the phase relationships of the sines and cosines, but an approximate upper bound is obtained by using them. Since A and B are relatively small this point is probably not very critical. In the same way we obtain roughly

(A58) $$A^2+B^2 \lesssim 2\frac{\breve{u}\Delta t}{\Delta x}\left[1-\cos\left(\tfrac{1}{2}\xi\Delta x\right)\right]+2\frac{\breve{w}\Delta t}{\Delta z}\left[1-\cos\left(\tfrac{1}{2}\eta\Delta z\right)\right] \lesssim 8\frac{\breve{u}\Delta t}{\Delta x}$$

Taking an upper bound for $\breve{U}$ to be 10^{-2} m/sec, we have

$A = 8\cdot10^{-7}\,\Delta t$

$B = 4\cdot10^{-7}\,\Delta t$

$A^2 + B^2 = 3.2\cdot10^{-13}\,(\Delta t)^2$

$\frac{\sin^2\left(\frac{1}{2}\xi\Delta x\right)}{\sin^2\left(\frac{1}{2}\eta\Delta z\right)}$ is maximized by giving $\sin^2\left(\frac{1}{2}\xi\Delta x\right)$ its maximum possible value, 1, and $\sin^2\left(\frac{1}{2}\eta\Delta z\right)$ its minimum, which is $\approx \frac{1}{2}\eta\Delta z = \frac{1}{2}\frac{2\pi}{2H}\Delta z = \frac{\pi\Delta z}{2H}$

This gives

$$\ell = \left[f^2 - \left(\frac{2H}{\pi\Delta x}\right)^2\frac{g}{\rho_0}\frac{d\rho_0}{dz}\right](\Delta t)^2 = +5.3064\cdot10^{-8}(\Delta t)^2 ,$$

taking

$H = 10^{+3}$ m. Since we already know $0 < \ell < +4$, $\ell = \mathcal{O}(1)$, which implies $\Delta t \sim 10^{+4}$ seconds; A, B and $A^2 + B^2$ are much less than 1. Using this, we find that

$$r \sim \mathcal{O}(1)$$

$$\mu = \sqrt{r^2 + 16B^2} \approx r\left(1 + 8\frac{B^2}{r^2}\right)$$

$$\sqrt{-r+\mu} \approx 2\sqrt{2}\frac{B}{r}$$

Then

$$(A59)\quad |\lambda_{\frac{2}{3}}|^2 \approx 1 + \tfrac{1}{4}\ell^2 + \tfrac{1}{4}\ell\mu - 2A - \ell + A\ell \pm \sqrt{2\ell}\, 2\sqrt{2}\frac{B}{r}\left(A - \tfrac{1}{2} + \tfrac{1}{4}\ell - \tfrac{1}{2}B\right)$$

Neglecting terms of $\mathcal{O}(AB)$ and $\mathcal{O}(B^2)$,

$$(A60)\quad |\lambda_{\frac{2}{3}}|^2 \approx 1 + \tfrac{1}{4}\ell^2 + \tfrac{1}{4}\ell\mu - 2A - \ell + A\ell \pm \sqrt{\ell}\frac{B}{r}(\ell - 2)$$

At this point we can simplify further by taking $r \approx \mu$. This could not be done previously because $\sqrt{-r+\mu}$ would have reduced to 0.

$$(A61)\quad |\lambda_{\frac{2}{3}}|^2 \approx 1 + \tfrac{1}{4}\ell^2 + \tfrac{1}{4}\ell r - 2A - \ell + A\ell \pm \sqrt{\ell}\frac{B}{r}(\ell - 2)$$

From (A54),

$$(A62)\quad \frac{1}{r} \approx \frac{1}{4-\ell}\left(1 + \frac{4A}{4-\ell}\right)$$

Substituting (A62) into (A61) and neglecting the term of $\mathcal{O}(AB)$,

$$(A63)\quad |\lambda_{\frac{2}{3}}|^2 \approx 1 - 2A \mp \sqrt{\ell}\,\frac{\ell-2}{\ell-4}B$$

so that $|\lambda_{\frac{2}{3}}|^2 \leq 1$ reduces to

$$(A64)\quad -2A \mp \sqrt{\ell}\,\frac{\ell-2}{\ell-4}B \leq 0$$

It should be noted that (A64) is independent of $\breve{U}$, as long as the order of magnitude approximations are satisfied, if the upper bounds given in (A56) and (A57) are used for A and B.

Call the left side of (A64) $\psi_{\mp}(\Delta t)$ and substitute for A, B and ℓ in terms of Δt.

Then:

For $0 < \ell \leqq +2$ we have $\psi_{+}(\Delta t) < 0$ and $\psi_{-}(\Delta t) < 0$, so the scheme is stable in this region.

For $+2 < \ell < +4$ $\psi_{+}(\Delta t) < 0$, but $\psi_{-}(\Delta t) \rightarrow +\infty$ as $\ell \uparrow +4$, so $\psi_{-}(\Delta t)$ must be 0 somewhere in this region. Solving the cubic equation for $\psi_{-}(\Delta t)$, we find that $\psi_{-}(\Delta t) = 0$ at $\Delta t = 7205$ seconds. This is the crude estimate of the stability criterion which was referred to above.

Appendix 4

GRAVITY WAVE EQUATIONS FOR TESTING THE DYNAMICAL ROUTINE

The basic equations for internal gravity wave motion were obtained from the paper by Fjeldstad (1935). His notation is used throughout this appendix. The subscript 1 refers to perturbations (of P and ρ) associated with the wave motion. Fjeldstad defines

$$\lambda^2 = \frac{k^2}{\sigma^2 - 4\omega^2} \tag{A65}$$

where k is the horizontal wave number, σ is the frequency and ω is the local normal component of the earth's rotation. If $\phi = -\frac{1}{\bar{\rho}}\frac{d\bar{\rho}}{dz}$ is the reciprocal scale height of the undisturbed exponential density distribution,

$$w = -A \sin[\gamma(H-z)] e^{-\frac{\phi}{2}(H-z)} \cos(kx) \cos(\sigma t) \tag{A66}$$

$$u = +\frac{A}{k}\left\{\frac{\phi}{2}\sin[\gamma(H-z)] - \gamma\cos[\gamma(H-z)]\right\} e^{-\frac{\phi}{2}(H-z)} \sin(kx) \cos(\sigma t) \tag{A67}$$

$$v = +\frac{fA}{\sigma k}\left\{\frac{\phi}{2}\sin[\gamma(H-z)] - \gamma\cos[\gamma(H-z)]\right\} e^{-\frac{\phi}{2}(H-z)} \sin(kx) \sin(\sigma t) \tag{A68}$$

With a rigid top

$$\gamma_N = \frac{N\pi}{h} \tag{A69}$$

Fjeldstad also gives

$$\gamma_N = \lambda_N^2(g\phi - \sigma_N^2) - \frac{\phi^2}{4} \tag{A70}$$

and

$$k_N = \frac{N\sigma\pi}{\sqrt{gh}}\frac{1}{\sqrt{\phi h}} \tag{A71}$$

In the present problem h = 10^{+3} meters, $\omega = 7.29 \cdot 10^{-5}$ sec^{-1} and g = 9.81 m/sec^2. We will take n = 1 and allow k to have the longest possible wavelength, 2L, where L = 2000 km. This gives $k = 1.57\ 10^{-6}\ m^{-1}$. The initial density distribution is

$$\bar{\rho} = 1027.336 - 3.216 e^{-\frac{1000-z}{1000}},$$

corresponding to S = 30‰ at the top and 34‰ at the bottom. Then $\phi = 10^{-2}\ m^{-1}$, $\sigma = 1.461\ 10^{-4}\ sec^{-1}$ and the period is 42980 seconds. With Δt taken to be 4298 seconds for purposes of the test, it was found that the numerical solution does in fact oscillate with this period, confirming that the dynamical routine (without mixing) is working properly.

Appendix 5

EXTENSION OF THE PROCEDURE FOR MIXING INSTABILITIES TO INCLUDE ENTRAINMENT AND MOMENTUM MIXING

The computer program for the step that tests for instabilities and removes them by mixing was originally written to include entrainment and momentum mixing, in the belief that it would be appropriate to keep the mixing theory as consistent as possible with that used for the surface mixing that takes place as a result of ice formation. This routine seemed to work satisfactorily in tests, and during the first part of the calculation with the full program, when relatively few instabilities were formed. However, toward the end of the season's run, when this routine had to execute thousands of times, there were occasionally situations in which a stable profile was not produced until the routine had mixed a much greater depth than one would expect to be mixed by a very small instability, and reduced the salinity by an unreasonably large amount in the layer above the resulting mixed layer. It is believed, although not definitely known, that the cause of this problem is some very subtle effect which makes it difficult to arrive at a stable profile when there is simultaneous entrainment from both above and below the mixed layer. At this point it was decided that the inclusion of entrainment is not really essential, the entrainment calculations were removed from the routine and their further debugging shelved until after the completion of this thesis.

The momentum mixing, although it did not seem to be giving any trouble, was also removed in order to make the routine as simple and reliable as possible.

In the equations that follow the subscript m refers to the mixed layer, 1 to the layer above it and 2 to the layer below it. The mixed layer is initially formed by averaging the salinity in N_m layers of thickness Δz. $\overline{Z_i}$ is the average height of layer i. Since the changes in salinity are small, the actual density of salt $10^{-3}\rho S$ can be replaced by S itself to a good approximation. Entrainment is represented by partial entrainment from layers of fixed thickness Δz.

First consider the case where the mixed layer is next to the ocean bottom. The equations of conservation of salt and potential energy are:

$$N_m S_m + S_1 = \Sigma S \tag{A72}$$

$$N_m \overline{Z_m} S_m + \overline{Z_1} S_1 = \Sigma E \tag{A73}$$

ΣE refers to the sum of $\overline{Z_k} S_k$ over the layers before mixing, not to the actual potential energy.

The solution is:

$$S_m = \frac{\overline{Z_1}\Sigma S - \Sigma E}{N_m(\overline{Z_1} - \overline{Z_m})} \tag{A74}$$

$$S_1 = \frac{\Sigma E - \overline{Z_m}\Sigma S}{\overline{Z_1} - \overline{Z_m}} \tag{A75}$$

If the mixed layer is adjacent to the top, the solution is similar:

$$(A76)\quad S_M = \frac{\sum E - \bar{Z}_2 \sum S}{N_M(\bar{Z}_M - \bar{Z}_2)}$$

$$(A77)\quad S_2 = \frac{\bar{Z}_M \sum S - \sum E}{\bar{Z}_M - \bar{Z}_2}$$

The difficulty comes when the layer is not adjacent to either the top or the bottom. Then entrainment takes place from two layers simultaneously. It was arbitrarily assumed that the energy transfer at each interface of the mixed layer is the same, so that the net effect of the entrainment is to transfer energy from the lower layer to the upper layer, without affecting the mixed layer. The equations are:

$$(A78)\quad S_1 + N_M S_M + S_2 = \sum S$$

$$(A79)\quad \bar{Z}_1 S_1 + N_M \bar{Z}_M S_M + \bar{Z}_2 S_2 = \sum E$$

$$(A80)\quad \bar{Z}_1 S_1 + \bar{Z}_2 S_2 = \sum' E$$

where $\sum' E$ is the sum of the potential energies in the upper and lower layers before mixing. The solution is:

$$(A81)\quad S_1 = \frac{-\bar{Z}_2 \bar{Z}_M \sum S + \bar{Z}_2 \sum E + (\bar{Z}_M - \bar{Z}_2)\sum' E}{\bar{Z}_M(\bar{Z}_1 - \bar{Z}_2)}$$

$$(A82)\quad S_M = S_M \text{ BEFORE ENTRAINMENT}$$

$$(A83)\quad S_2 = \frac{+\bar{Z}_1 \bar{Z}_M \sum S - \bar{Z}_1 \sum E + (\bar{Z}_1 - \bar{Z}_M)\sum' E}{\bar{Z}_M(\bar{Z}_1 - \bar{Z}_2)}$$

After the entrainment calculation, the resulting profile must of course be tested to see if it is stable, and additional layers entrained if necessary. This procedure seemed to work well most of the time, but in less than one per cent of the cases it did not give a stable profile until a great depth of water had been mixed. Further work will be needed, first to thoroughly debug the computer program, and, if this is insufficient, the theory (especially as it concerns simultaneous entrainment from two layers) will have to be re-examined.

If entrainment is not accounted for, the mixing of momentum simply involves averaging the velocities within the mixed layer. If there is entrainment between a mixed layer and one other layer, equations (102) through (109) in chapter 4 can be used.

If there is simultaneous entrainment from two layers, the representation of the "actual" profile by partially entrained layers is as is shown in Fig. A7. $\lambda_A, \lambda_B, \lambda_C$ and λ_D can be found from equations (102) through (105). Then using primes to denote velocities after mixing and making use of the Boussinesq approximation, the momentum equations are:

(A84) $$\Delta z V_1' = \lambda_A V_1 + \lambda_B V_m'$$

(A85) $$\Delta z V_2' = \lambda_D V_2 + \lambda_C V_m'$$

(A86) $$V_1' + N_m V_m' + V_2' = \Sigma V$$

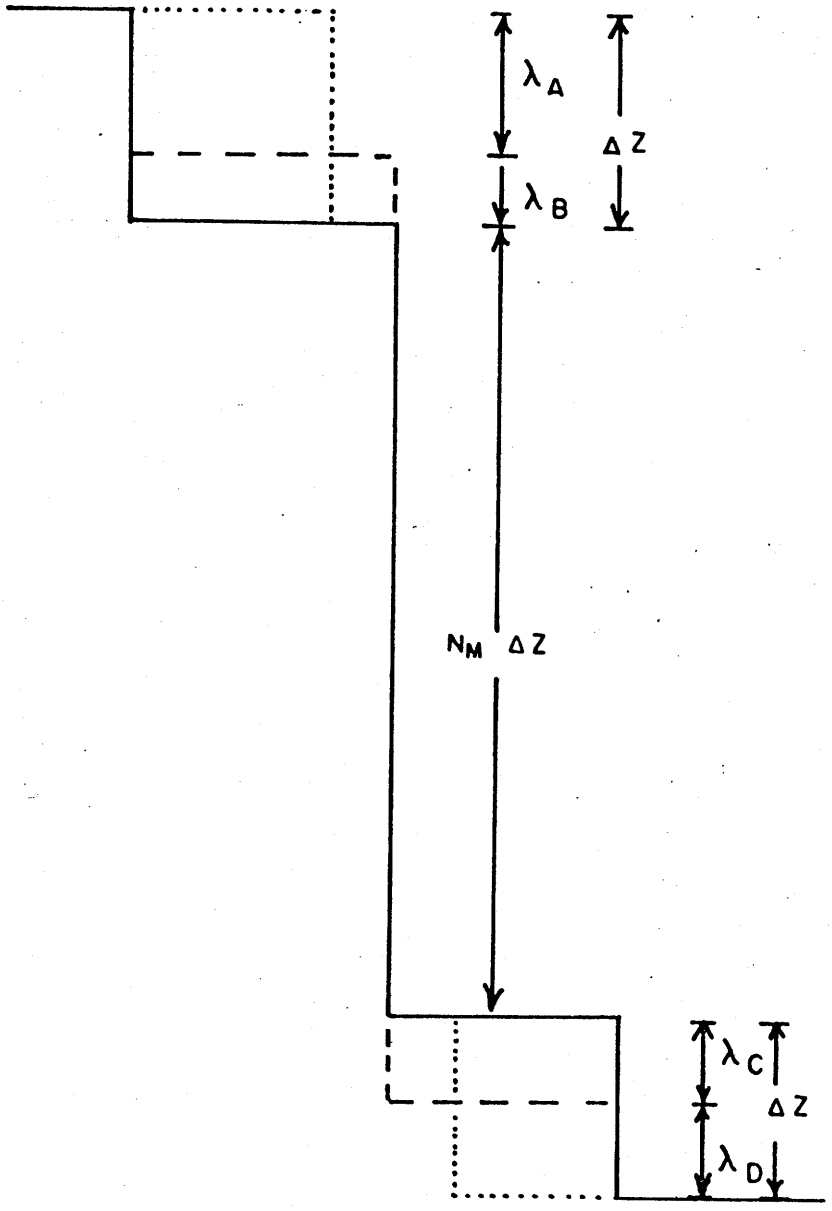

Figure A7 Simultaneous momentum entrainment from two layers. The dashed lines indicate the "actual" profile after entrainment takes place; the dotted line shows the representation in terms of partial entrainment from layers of fixed thickness. ρ

where ΣV is the sum of all of the velocities, including those in the partially entrained layers, before mixing.

The solution is:

$$V_1' = \frac{-\lambda_A \lambda_C V_1 - \lambda_B \Delta Z \Sigma V + \lambda_A N_M \Delta Z V_1 + \lambda_B \lambda_D V_2}{\Delta Z (\lambda_B - \lambda_C + N_M \Delta Z)} \quad (A87)$$

$$V_M' = \frac{+\lambda_D V_2 - \lambda_A V_1 + \Delta Z \Sigma V}{\lambda_B - \lambda_C + N_M \Delta Z} \quad (A88)$$

$$V_2' = \frac{-\lambda_C \Delta Z \Sigma V - \lambda_B \lambda_D V_2 + \lambda_A \lambda_C V_1 - \lambda_D N_M \Delta Z V_2}{\Delta Z (\lambda_B - \lambda_C + N_M \Delta Z)} \quad (A89)$$

Appendix 6

EFFECT OF THE DYNAMICS ON THE LOCAL MIXING

A preliminary investigation of the possibility that the large-scale dynamical motion has some kind of a feedback effect on the local mixing was made at the end of this work. The program was run with the dynamical routine bypassed in what was thought would be a routine check, but it turned out that there are subtle effects in the program which will require considerable additional work to investigate thoroughly. What happened is that the mixed layer was somewhat deeper and more saline at the end of a full season without dynamics than at the end of a season with dynamics. The difference was too large to be explained by horizontal advection, which would tend to decrease rather than increase the salinity even if large enough, or by vertical advection, which, at any rate, would tend to lower rather than raise the interface. in the column next to the wall at $X = 0$, where the comparison was made. The actual explanation must await a detailed (and time-consuming) tracing of the computer calculations. On the basis of experience with this program, the two most likely causes are thought to be:

1. Round-Off Error due to the use of Single-Precision Numbers.
   A correction, based on the difference between the profile in the column nearest $X = L$, where practically no ice forms, and the initial profile, which was stored in double precision, was added to all of the salinity profiles at each time step

in order to compensate for losses due to round-off error in the computer. This worked correctly in the full dynamical program; after 1080 time steps the salinity values in the deep part of the ocean were the same as those in the initial profile to 8 significant figures (all that was printed out). Without this correction the cumulative round-off error (more than .00002% per time step) would have resulted in a decrease in salinity values that would have been significant everywhere and would have resulted in a net decrease of salinity (in spite of the ice formation) in the five or six columns near $x = L$. When the dynamical routine was bypassed, the salinity values in the deep ocean, which should not have changed at all, increased in a random way; this indicates that perhaps the correction is over-correcting since the computer no longer operating on the salinity values as many times as previously. In any case, the changes in values that should not change, and do not change when the dynamical routine operates, indicates that something is not quite right when the dynamical routine is bypassed.

2. The Oscillations.

There may be advective effects associated with the numerical oscillations described in chapter 1 which interact with the mixing process in a subtle way to delay the penetration of the mixed layer. The difficulty of looking for an explanation in this way is shown by Fig. A8, which shows the stream function field of the instantaneous solution (including the oscillations)

at the end of the season.

In conclusion, it is thought that the discrepancy will turn out to be primarily due to numerical causes, but the possibility of a real dynamical effect cannot be totally discounted yet.

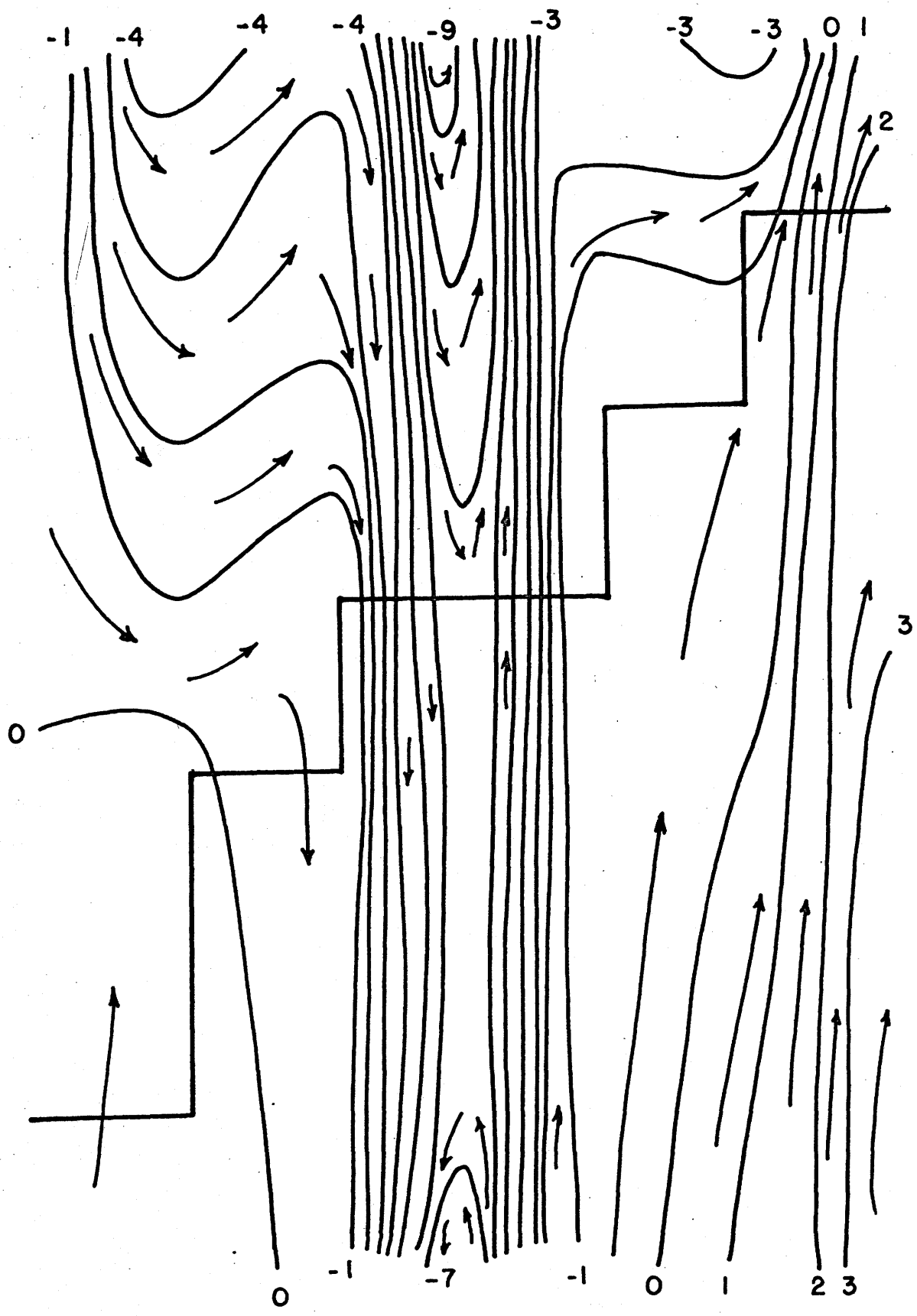

Figure A8 Stream function for the instantaneous motion at the end of the season, in the region where the interface intersects the wall at x = 0.

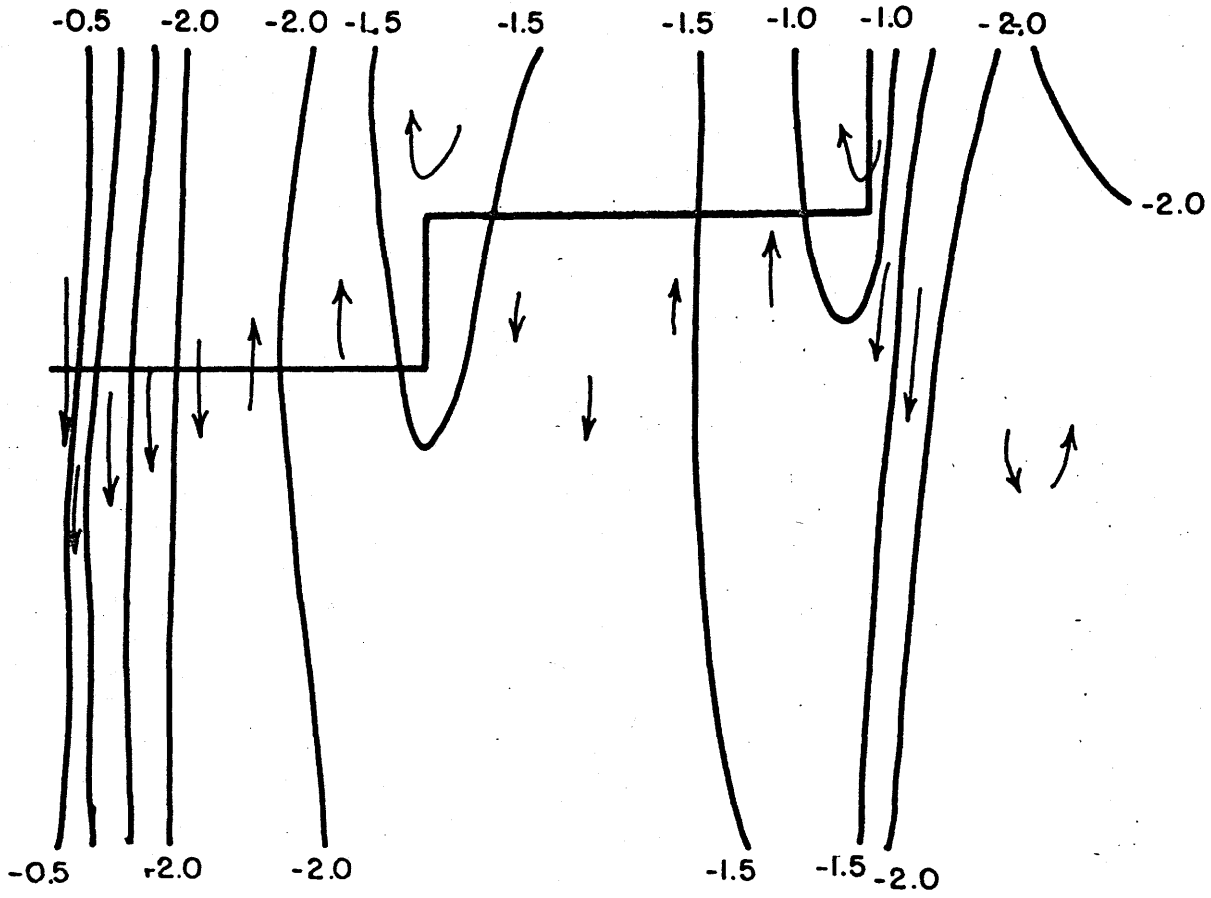

Figure A9 Time-average streams function at the end of the season in the vicinity of the wall at x = 0, w
Since the motion increases in a roughly linear way, this can be thought of as vaguely resembling the actual motion at the end of half of the season. The interface at the end of half of the season is shown.

BIBLIOGRAPHY

Ball, F. K., 1960: Control of inversion height by surface heating. Quarterly Journal of the Royal Meteorological Society, 86, 483.

Beal, M. Allan, 1968: The seasonal variation in sea level at Barrow, Alaska. Arctic Drifting Stations. A report on activities supported by the Office of Naval Research coordinated by John E. Sater. Proceedings of the Symposium at Warrenton, Virginia, April, 1966. Arctic Institute of North America.

Brennecke, Wilhelm, 1921: Die ozeanographischen arbeiten der Deutschen Antarktischen Expedition, 1911-1912 (Deutschland), [The oceanographic work of the German Antarctic Expedition, 1911-1912 (Deutschland)]. Aus dem Arkiv der Deutschen Seewarte XXXIX, No. 1, Hamburg.

Brayton, G.E., 1962: Station Arlis-I Oceanography (parts I and II). University of Washington, Department of Meteorology and Climatology. Scientific Report of the Office of Naval Research contract 477 (NR 307-252).

Bruce, John G., Jr, and Henry Charnock, 1965: Studies of winter sinking of cold water in the Aegean Sea. Extrait des Rapports et Proces-Verbeaux des Reunions de la C.I.E.S. M.M.

Bulgakov, N. P., 1962: Study of convection and of the autumn cooling process in the sea. Contributions to Physical Oceanology, 60, Edited by V. N. Stepanov, Published for the U.S. Department of Commerce and the National Science Foundation by the Israel Program for Scientific Translations, Jerusalem, 1967.

Cabaniss, G. H. (Editor), 1962: Geophysical Data from U.S. Arctic Ocean Drift Stations, 1957-1960. Air Force Cambridge Research Laboratories, Research Note AFCRL-62-683, Project 7628, 234 pp.

Campbell, William J., 1964: On the Steady-State Flow of Sea Ice. Doctoral dissertation, Department of Atmospheric Sciences, University of Washington, 167 pp., Published as Office of Naval Research Scientific Report NR 307-252, University of Washington.

_____, 1965: The wind-driven circulation of ice and water in a polar ocean. Journal of Geophysical Research, 70, 3279.

Coachman, Laurence K., 1966: Production of supercooled water during sea ice formation. Proceedings of the Symposium of the Arctic Heat Budget and Atmospheric Circulation, edited by Joseph O. Fletcher, The Rand Corporation, p 497.

Coachman, Laurence K. and C. A. Barnes, 1961: The contribution of Bering Sea water to the Arctic Ocean. Arctic 14, 147.

Collin, A. E., 1963: The waters of the Canadian Arctic Archipelago. Proceedings of the Arctic Basin Symposium, October 1967, Arctic Institute of North America, p 128.

Cromwell, Townsend, 1960: Pycnoclines created by mixing in an aquarium tank. Journal of Marine Research 18, 73.

Cromwell, Townsend and Joseph L. Reid, Jr., 1956: A study of oceanographic fronts. Tellus 8, 94.

Deacon, G. E. R., 1963: The southern ocean. The Sea, edited by M. N. Hill Interscience publisher, Division of John Wiley and Sons.

Deardorff, J. W., G. E. Willis and D. K. Lilly, 1969: Laboratory investigation of non-steady penetrative convection. Journal of Fluid Mechanics, 35, 7.

Defant, Albert, 1949: Konvektion und eisbereitschaft in polaren schelfmeeren (Convection and ice potential in polar shelf seas). Geografiska Annaler 31, 25.

Drogaitsev, D. A., 1958: Wind currents in the Arctic Ocean. Problems of the North 2, 5-15, 1-12.

Farmer, Harlow G., 1966: Long-period time-dependent motion in a polar ocean. Proceedings of the Symposium on the Arctic Heat Budget and Atmospheric Circulation, edited by Joseph O. Fletcher, The Rand Corporation, p. 531.

Felzenbaum, A. I., 1958: The theory of the steady drift of ice and the calculation of the long period mean drift in the central part of the Arctic Basin. Problems of the North 2, 5-15, p 13-44.

Fjeldstad, Jonas Ekman, 1933: Interne wellen (internal waves). Geofysiske Publikasjoner 10, no. 6.

Fofonoff, Nicholas P., 1936: Some properties of sea water influencing the formation of Antarctic bottom water. Deep-Sea Research 4, 32.

Foster, Theodore D., 1968: Haline convection induced by the freezing of sea water. Journal of Geophysical Research 73, 1933.

Francis, J. R. D. and Henry Stommel, 1953: How much does a gale mix the surface layers of the ocean? Quarterly Journal of the Royal Meteorological Society 79, 534.

Fujino, Kazuo, 1966: 氷島アリースIIに於ける海洋観測 (Oceanographic observations on the drifting station Arlis II, June-November, 1964). Teion Kagaku (Low Temperature Science) Series A 24, 283.

Gudkovich, Z. M., 1954: Results of a preliminary analysis of the deep-water hydrological observations. Observational Data of the Scientific Research Drifting Station of 1950-1951, edited by M. M. Somov, translation, American Meteorological Society, 170 pp.

_____, 1962: On the nature of the Pacific current in Bering Strait and the causes of its seasonal variations. Deep-Sea Research 9, 507, translation from Океанология 1, 608 (1961).

Hori, Sadakiyo, 1966: 極地海洋学シンポジウム：物理 (Polar Oceanography Symposium: Physical Oceanography). Journal of the Oceanographical Society of Japan 22 (5), 41-42.

Hunkins, Kenneth, 1966: Ekman drift currents in the Arctic Ocean. Deep-Sea Research 13, 607.

Kort, V. G., 1962: The Antarctic Ocean. Scientific American 207, 113.

Kraus, Eric B. and J. Stuart Turner, 1967: A one-dimensional model of the seasonal thermocline II. The general theory and its consequences. Tellus 19, 98.

Kusunoki, Kou, 1955: Observations on the horizontal and vertical distribution of the chlorinity of sea ice. Journal of the Oceanographical Society of Japan 12, 179.

_____, 1962: On the hydrography of the Arctic Ocean with special reference to the Beaufort Sea. Teion Kagaku (Low Temperature Science) Series A No. 17. 1.

_____, 1963: 氷島の漂流について (On the drift of ice islands in the Arctic Ocean). Teion Kagaku (Low Temperature Science) Series A, No. 21, 159.

Kusunoki, Kou, Takashi Minoda, Kazuo Fujino and Akito Kawamura, 1967a: Description of Oceanographic Observations at Drift Station Arlis II in 1964-1965. Arctic Institute of North America.

_____, 1967b: Data from Oceanographic Observations at Drift Station Arlis II in 1964-1965. Arctic Institute of North America.

Kusunoki, Kou, J. Muguruma and K. Higuchi, 1962: Oceanographic Observations at Fletcher's Ice Island (T-3) in the Arctic Ocean in 1959-1960. Arctic Institute of North America, Research Paper No. 22, 110 pp.

LeBlond, Paul H., 1964: Planetary waves in a symmetrical polar basin. Tellus 16, 503.

Ledenyov, V. G., 1966: South ocean bottom water formation. Proceedings of the 11th Pacific Science Congress 2, Science Council of Japan, abstract only. Xerox copies available from the author of this thesis.

Lilly, D. K., 1968: Models of cloud-topped mixed layers under a strong inversion. Quarterly Journal of the Royal Meteorological Society 94, 292.

Metcalf, W. G., 1960: A note on the water movement in the Greenland-Norwegian Sea. Deep-Sea Research 7, 190.

Mosby, Hakon, 1934: The waters of the Atlantic Antarctic Ocean. Scientific Results of the Norwegian Antarctic Expeditions 1927-1928 et Sqq., Instituted and financed by Consul Lars Christensen No. 11, Oslo.

_____, 1959a: La topographie et la geologie des profondeurs oceaniques. (Topography and geology of the oceanic depths.) Colloques Internationaux du Centre National de la Recherche Scientifique, Paris.

_____, 1959b: Deep water in the Norwegian Sea. Geofysiske Publikasjoner XXI, No. 3, Oslo.

_____, 1961: Veines et arteres de la mer (Veins and arteries of the sea). Bulletin de l'Institut Oceanographique, Monaco.

_____, 1962: Water, salt and heat balance of the North Polar Sea and of the Norwegian Sea. Geofysiske Publikasjoner No 11, Oslo.

_____, 1967: Bunnvannsdannelse i havet. Fridtjof Nansen Minneforelesningen (Bottom water formation in the sea, Fridtjof Nansen Memorial Lecture). Universitets Forlaget, Oslo.

Munk, Walter H., 1966: Abyssal recipes. Deep-Sea Research 13, 707.

Ooyama, Katsuyuki, 1963a: A Dynamical Model for the Study of Tropical Cyclone Development. Text prepared for the 43rd Annual Meeting of the American Meteorological Society in New York, January 21-24, 1963.

_____, 1963b: A dynamical model for the study of tropical cyclone development. Geofisica Internacional 4, 187.

_____, 1967: Numerical Simulation of the Life Cycle of Tropical Cyclones. New York University, Department of Meteorology and Oceanography, Geophysical Sciences Laboratory Report No. TR 67-9.

_____, 1969: Numerical simulation of the life cycle of tropical cyclones. Journal of the Atmospheric Sciences 26, 3.

Overstreet, Roy and Maurice Rattray, Jr., 1969: On the roles of vertical velocity and eddy conductivity in maintaining a thermocline. Journal of Marine Research 27, 172.

Pattullo, June, 1963: Seasonal changes in sea level. The Sea, edited by M. N. Hill Interscience publishers, Division of John Wiley and Sons.

Pattullo, June, Walter Munk, Roger Revelle and Elizabeth Strong, 1955: The seasonal oscillation in sea level. Journal of Marine Research 14, 88.

Phillips, Owen M., 1966: On turbulent convection currents and the circulation of the Red Sea. Deep-Sea Research 13, 1149.

Rattray, Maurice, Jr., 1962: Interpolation errors and oceanographic sampling. Deep-Sea Research 9, 25.

Reed, Richard J. and William J. Campbell, 1960: Theory and Observations of the Drift of Ice Station Alpha. O.N.R. Final Report, Task Number NR 307-250, 255 pp., University of Washington.

_____, 1962: The equilibrium drift of Ice Station Alpha. Journal of Geophysical Research 57, 281.

Reid, Joseph L., Jr., 1966: Zetes Expedition. Transactions, American Geophysical Union 47, 555.

Richtmyer, Robert D. and K. W. Morton, 1967: Difference Methods for Initial-Value Problems. Second edition, Interscience publishers, Division of John Wiley and Sons.

Rossby, C. G. and R. B. Montgomery, 1935: The layer of frictional influence in wind and ocean currents. M.I.T.-W.H.O.I. Papers in Oceanography and Meteorology 3, 1.

Rouse, H. and J. Dodu, 1955: Diffusion turbulente a traverse une discontinuite de densite (Turbulent diffusion across a discontinuity of density). La Houille Blanche 10, 522 (Text in French and English).

Ruzin, M. I., 1959: The wind drift of ice in a heteorogeneous pressure field. Arkticheskii i Antarkticheskii Nauchno-Issued, Inst. Trudy, 226, 123.

Scripps Institution of Oceanography, 1966: Boreas Expedition Data Report, Physical and Chemical Data. SIO Reference 66-24.

Sheppard, P. A., 1958: Transfer across the earth's surface and through the air above. Quarterly Journal of the Royal Meteorological Society 84, 205.

Shuleikin, V. V., 1938: The drift of ice-fields. Compt. Rend. (Doklady) Acad. Sci. USSR 19, 589.

Stewart, R. W., 1963: Some aspects of turbulence in the Arctic. Proceedings of the Arctic Basin Symposium of October, 1962, Arctic Institute of North America, p 122.

Stommel, Henry, 1962: On the smallness of the sinking regions in the ocean. Proceedings of the National Academy of Sciences 48, 766.

Stommel, Henry and A. B. Arons, 1960: On the abyssal circulation of the world ocean-II. Deep-Sea Research 6, 217.

Stone, Peter H., 1968: Some properties of Hadley regimes on rotating and non-rotating planes. Journal of the Atmospheric Sciences 25, 644.

Sverdrup, H. U., 1928: The wind-drift of the ice on the North Siberian Shelf. The Norwegian North Polar Expedition with the "Maud", 1918-1925, Scientific Results 4, 1.

Sverdrup, H. U., Martin W. Johnson and Richard H. Fleming, 1942: The Oceans. Prentice-Hall, Inc. 1087 pp.

Turner, J. Stuart and Eric B. Kraus, 1967: A one-dimensional model of the seasonal thermocline I. A laboratory experiment and its interpretation. Tellus 19, 88.

Untersteiner, Norbert, 1968: Natural desalination and equilibrium salinity profile of perennial sea ice. Journal of Geophysical Research 73, 1251.

Worthington, L. Valentine, 1953: Oceanographic results of project Skijump I and Skijump II in the polar sea, 1951-1952. Transactions, American Geophysical Union 34, 543, 1953.

Zore-Armanda, Mira, 1969: Water exchange between the Adriatic and the eastern Mediterranean. Deep-Sea Research 16, 171.

Zubov, N. N., 1943: Arctic Ice. Translation by the United States Naval Oceanographic Office and the American Meteorological Society, published by the United States Navy Electronics Laboratory, San Diego, 491 pp.

ACKNOWLEDGEMENTS

It is a pleasure to acknowledge the helpful guidance of my thesis advisor, Professor Norman Phillips; he has taken an active interest in an area of research related to this thesis and has devoted far more time than is normally expected to thoughtful criticism of this work. I also owe a great deal of appreciation to Professor Claës Rooth of the Institute of Marine Science, University of Miami. He suggested that I look into the seasonal cycle of surface density changes as a promising area in which to find a thesis topic on the Arctic Ocean. He was a member of the thesis committee before leaving Woods Hole Oceanographic Institution.

Many other individuals have been of assistance in this work; unfortunately any list contains the danger of omission. Mr. L. Valentine Worthington of Woods Hole Oceanographic Institution helped to introduce me to the literature on the Arctic Ocean. This thesis would not have been possible without the assistance of many individuals in obtaining arctic data. These include Worthington; Dr. Waldo Lyon and Dr. M. Allen Beal of the Arctic Sciences and Technology Division, United States Navy Undersea Research and Development Center; Professor Laurence Coachman, Mr. Richard Tripp and Professor Norbert Untersteiner of the University of Washington; Dr. Kou Kusunoki of the Department of

of Polar Science, National Science Museum (Tokyo) and Dr. Kazuo Fujino of the Institute of Low Temperature Science, Hokkaido University. Valuable discusssions on some aspects of the work were provided by Worthington, Untersteiner, Dr. Isidoro Orlanski of the ESSA Geophysical Fluid Dynamics Laboratory; Professor Eric Kraus of the Institute of Marine Science, University of Miami; Dr. J. Stuart Turner of Cambridge University and Professor Walter Munk and Mr. Joseph L. Reid, Jr. of the Scripps Institution of Oceanography.

Many individuals in the M.I.T. Department of Meteorology assisted me during the inevitable last minute rush to finish the thesis. Miss Diane Lippincott did most of the typing, and Miss Isabel Kole prepared all of the illustrations and graphs, in both cases in spite of a heavy work schedule. Mrs. Karen MacQueen Mrs. Jane McNabb and Miss Louise Harris also helped with the typing. Mr. Peter Webster, Mr. James Sullivan, Mr. Robert Knox, Miss DianaLees and Mrs. Eugenia K. DeRivas helped put the copies together.

The author's graduate studies were supported partly by a Ford Foundation Fellowship in the Atmospheric Sciences, partly by a research assistantship under N.S.F. Grant GA402X and partly by a loan. The computations were prepared on the I.B.M. 360/65 at the information processing service center of the Massachusetts Institute of Technology. Computer time was purchased partly with

funds from the Department of Meteorology and partly with funds from N.S.F. Grant GA402X.

BIOGRAPHICAL NOTE

The author of this thesis was born in Burbank, California on April 30, 1942. He grew up in Inglewood, California, where he attended public schools, graduating from Morningside High School in 1959. He received his first introduction to marine science in the marine biology course of the Los Angeles County Museum Science Workshop during his senior year. He then attended the Massachusetts Institute of Technology, receiving a B.S. in physics in 1963 after completion of a B.S. thesis on detection of neutrons which, it was believed, might be produced in solar flares. He then entered the Department of Meteorology to begin the graduate study which led to the present degree. During this period he has participated in a Summer Institute in Planetary Physics at U.C.L.A. (for two summers), in two research cruises on board RV Atlantis II and worked one summer in the Arctic Sciences and Technology Division of the United States Navy Electronics Laboratory (now the Undersea Research and Development Center).